The Dissertation Committee for Aurore Yvonne Joelle Mercelat Certifies that this is the approved version of the following dissertation:

Fundamental Study of Hydrophobic Microporous Membrane Contactors for the Recovery of Insoluble Oil from Oil-Water Mixtures

Committee:

Lynn E. Katz, Supervisor

A. Frank Seibert, Co-Supervisor

Kerry A. Kinney, Co-Supervisor

Benny D. Freeman

Desmond F. Lawler

Fundamental Study of Hydrophobic Microporous Membrane Contactors for the Recovery of Insoluble Oil from Oil-Water Mixtures

by

Aurore Yvonne Joelle Mercelat, M.S.E, M.E

Dissertation

Presented to the Faculty of the Graduate School of

The University of Texas at Austin

in Partial Fulfillment

of the Requirements

for the Degree of

Doctor of Philosophy

The University of Texas at Austin

May 2016

Dedication

A ma très chère famille ; Maman, Papa et Hélène, sans qui ce travail n'aurait été possible.

Acknowledgements

During my time as a doctoral student, people often asked me what kept me going all this time in school and when I would be ready to start my "real" life. The truth is all the years spent here have been one of the most formative and exciting times of my life. Learning every day in the lab, in classes, about a new country and culture, and experiencing life in this hidden-gem city has been amazing. But most importantly, the people I have met here made this an incredible and gratifying journey and carried me through this adventure. I could not be more thankful.

I want to thank my three advisors: Dr. Katz, Dr. Kinney and Dr. Seibert for their mentorship through this experience. It's been quite a venture to coordinate our work together but I am very grateful as each of you brought something unique to our collaboration. Dr. Seibert, thank you for your day-to-day support, I truly enjoyed all of our technical brainstorming sessions. Dr. Katz, I was continually impressed with your lucid and on point advice. Dr. Kinney, thank you for always recognizing when I needed a pep-talk and bringing out the best in my work. I would also like to acknowledge my committee members Dr. Freeman and Dr. Lawler for supporting me along this path. A special thanks to Dr. Lawler who was the first to believe in me and played a major role in my coming to UT.

Little did I know when I went to a local membrane conference three years ago that it would change the fate of my doctoral project. There, I met Anne Bréhant, Flavia Zraick, and Reynald Bonnard for the first time. We shared a meal and there was the start of my collaboration with Suez. Later, I worked closer with Emilie Sutton-Sharp and Anne Bréhant. I want to thank all of them for supporting this work financially and technically through Suez as well as believing in my project and work all along this PhD.

I also want to thank Membrana (3M) and, in particular, Paul Peterson for supporting this work by providing the membrane contactors. Working with such industrial partners has been truly rewarding.

I also want to acknowledge the work accomplished behind the scenes by the great staff at SRP: Steve Briggs and Robert Montgomery. I learned so much about electrical wires, nuts and bolts and inch/cm wrenches thanks to you. Also, thank you to my lab helpers, Nash and Meagan, for teaching me how to tutor and delegate during my project.

Upon arrival here, international students often think: “Americans are so nice yet so hard to become friends with”. Well, I also learnt that amazing friendships can be found if you persist. Anne, how can I do justice to the incredible years we spent as roommates and the bond we created for life? You helped me build a second home here and every day I looked forward to our evening life debriefs. From the bottom of my heart thank you to the dinner club: Anne, Catherine, Cédric, Elena, Clément, Natalia and Fernando. Life felt so comfortable with you around. Also, thanks to all the EWRE people that came and went every two or three years; I could not have hoped for a more fun and social department. Special thanks to my officemates who brightened my week days: Soyoon, Farith, Celina, Ijung, Shahana and Ray. Thank you Justin for concurrently going through the PhD experiences with me and Arielle for bringing some of France with you. Lastly, I could not have gone through those years without my amazing volleyball partners: Wil, Maggie, Chase, and Clément. I already miss our early Sunday morning meetups at Zilker; they always helped me recharge for the week. Thank you Bryant and Dave, my two favorite dance partners who constantly added to the Texas fun.

Finally, I want to thank my dear family; Maman, Papa, and Hélène. You were always there for me, ready to pick up the phone to hear about the good or bad news of the

day. Your unconditional love and unfailing support for all my endeavors has allowed me to explore the world knowing there was always a home somewhere for me.

Fundamental Study of Hydrophobic Microporous Membrane Contactors for the Recovery of Insoluble Oil from Oil-Water Mixtures

Aurore Yvonne Joelle Mercelat, Ph.D.

The University of Texas at Austin, 2016

Supervisors: Lynn E. Katz, A. Frank Seibert, Kerry A. Kinney

Insoluble oil and water mixtures occur in many industries such as food, metallurgical, or biofuel production. In particular, as we strive to meet global energy demands, the associated risks and waste management of the oil and gas industry must be addressed. Technologies capable of separating oil and water efficiently are needed for the treatment of highly variable oil and gas streams such as produced and flowback waters or oil spills. The goal of this doctoral work was to advance the understanding of a membrane contactor process for the recovery of insoluble oil from water. The hydrophobic hollow fiber membrane had been successfully tested in our laboratories for oil recovery from algae slurries. However, a thorough study to understand the fundamental mechanisms of the separation process was necessary for engineering design and process optimization. First, pure oil experiments were performed to define baseline performance attainable with the studied membrane contactors. Then, oil-water separation experiments were conducted to quantify the effect of key operating parameters. Two relevant ranges of oil feed concentration were identified. For high oil feed concentration, increases in transmembrane pressure and influent flow rate were confirmed to increase oil flux, while higher viscosity lowered oil permeation across the fiber walls. However, an important finding was that, for dilute mixtures, decreases in transmembrane pressure and

higher viscosity increased oil permeation. The results of this research support the conclusion that oil separation within the particular geometry and design of the membrane contactor is due to both internal coalescence of oil droplets and selective permeation of oil over water. The stability of an oil film on the fibers was critical to enhance effective surface area of the membrane contactor. In addition, the technology showed great promise for long-term high oil removal with no signs of viscous fouling as often observed in hydrophilic membranes. Finally, a model describing the process was developed and can be used as a guideline for membrane sizing and process engineering design.

Table of Contents

List of Tables

List of Figures

Chapter 1: Introduction

PROBLEM STATEMENT

Insoluble oil-water mixtures are present as waste or valuable products in numerous industries. Many industries such as metallurgical, petroleum and petrochemical refineries, food manufacturers, or metal finishing industries produce oil-water mixtures as end products that require disposal. The oil and gas industry is particularly concerned since oil-water mixtures are found in the refining and production sectors. In the United States, the wastewater associated with oil and gas extraction (produced water) is generated at an estimated rate of 5.3 barrels for every barrel of oil produced (*1*), which in 2012 represented a production of approximately 28 billions barrels per year (*2*). This water has been traditionally treated as waste in need of disposal or re-injection (*3*), but rising concerns are leading towards beneficial handling and reuse. First, increasing production of produced water leads to an increase in disposal costs. Re-injection is a viable option for many locations but is highly dependent on availability and accessibility of wells. Second, water is a scarce resource, and the large volumes of produced wastewater generated may be suitable for water reuse applications if properly treated (*4-6*). The separation of oil from water is a first step for reuse, and will allow the simultaneous recovery of oil, a valuable product.

Oil-water separation is also a key step for many other industries. Biofuel production from microalgae is one example for which the challenge lies in recovering lipids from a lysed cell mixture (*7*). Similarly, oil-water separation is of interest in biocatalytic desulfurization where specific bacteria remove organically bound sulfur from petroleum allowing the collection of high quality biofuel (*8*). In these applications, the recovery of the insoluble oil from water defines the success of the process.

In the case of oil spills in natural waters, oil-water separation is critical to remove oily pollutants, restore ecosystems, and protect habitats from harm. Recent events have

shown the primary importance of finding treatment solutions; BP had to pay an unprecedented fine to compensate for the disastrous effects of the 2010 oil spill in the Gulf of Louisiana. Such events have serious environmental, social, and financial consequences and demonstrate the need to develop effective countermeasures to mitigate the consequences of oil-contaminated waters.

In this context, research across many fields has been conducted to provide technologies for cost effective oil-water separation. The research described in this dissertation focuses mainly on produced water treatment for the petroleum industry, but it should be recognized that the oil-water separation technology under development has the potential to be more broadly implemented for the treatment of other types of oil-water mixtures. Due to a long-term recognition that additional research in the produced water field is needed, many technologies have been investigated to identify processes that are cost-effective and reliable. These technologies have focused on breaking down emulsions and separating oil and water using hydrocyclones (*9*), gravity settlers (*10*) or coalescing filters (*11-14*). However, common limitations associated with these technologies include low efficiency for small oil droplets, lack of flexibility, large surface footprints, and high costs. Membrane technologies represent a good alternative and complement to existing technologies. However, past research has focused primarily on hydrophilic membrane systems, which have demonstrated limited success due to progressive viscous fouling.

OBJECTIVES

This research investigates a membrane technology new to the field of oil-water separation. The membrane contactor, originally developed for liquid-liquid extraction, has significant commercial applications associated with de-gassing of liquids such as the oxygen removal from water in the microelectronic industry (*15*). This microporous hydrophobic hollow fiber membrane contactor was initially tested in our laboratories to

recover nonpolar oil from concentrated and lysed algal slurries (*16*). The membrane contactor extracted the majority of the available nonpolar oil for most of the feedstocks. The work was supported by OpenAlgae LLC at the Separations Research Program (UT-Austin) and resulted in a patent issued in 2013 (*17-19*). Additional experiments conducted over multiple days confirmed the promising results observed with saltwater and freshwater micro-organisms slurries (*20*). Backed by this success, the application of the membrane contactor to produced water treatment was only logical. These initial data, while important, did not provide sufficient understanding to reliably design and engineer an optimized oil recovery system that could be applied to biological and petroleum based oils. This work focuses on understanding the fundamental mechanisms of oil-water separation with the membrane contactor, identifying the effects of key operating parameters on oil-water separation efficiency, and developing a model that enables engineering design and process optimization for a range of source waters. To this end, the main objectives of this research were to:

- Characterize the effect of operating parameters such as oil concentration, viscosity, transmembrane pressure, and influent flow rate on membrane performance including oil permeation rate and recoveries
- Understand the effect of membrane characteristics such as surface area, module size, porosity, and wall thickness on membrane performance
- Assess the potential of the system for oil-removal overtime
- Develop a model for preliminary assessment and engineering design of a membrane contactor system.

DISSERTATION STRUCTURE

This dissertation is divided into chapters organized as follow:

Chapter 2: Background

This chapter includes a review of existing produced water treatment challenges and technologies including membrane systems.

Chapter 3: Materials and Methods

This section gives an overview of the approach, chemicals, and equipment used to conduct the experimental work for all of the research described in Chapters 4-8. Some of this information is repeated and described in more detail in individual chapters.

Chapter 4: Pure oil experiments

This chapter presents the baseline performance of the membrane contactor obtained when the membrane is used with pure oil feed. Under such feed conditions, maximum oil flux can be evaluated and compared to permeation models including important operating parameters such as transmembrane pressure, viscosity, and membrane characteristics. The findings are used as a comparative baseline to characterize system performance of subsequent oil-water mixtures experiments.

Chapter 5: Oil-Water separation experiments

This chapter details the effects of operating parameters and membrane characteristics on system performance, including oil flux and recoveries, when oil-water mixtures are processed with the membrane contactor. Long-term operation behavior and separation mechanisms are discussed.

Chapter 6: Modeling for engineering design

This chapter introduces the concept of effective surface area in the membrane contactor. A model predicting oil flux is developed and relates system performance observed with pure oil feed and oil-water feeds. The model includes the effect of all parameters studied in previous chapters on the membrane contactor performance. Use of the model is shown

through example calculations for membrane surface area sizing and selection of optimal operating parameters.

Chapter 7: Practical membrane considerations

This chapter addresses the possible biological fouling of the membrane contactor, the cleaning procedures undertaken, and the restoration of membrane performance.

Chapter 7: Membrane contactor start-up and operating configurations

This chapter highlights early stage operation and provides recommendations for optimized steady-state system operation.

Chapter 8: Conclusions and recommendations

This chapter provides a summary of the key findings and recommendations for future efforts to further develop and implement the technology.

Chapter 2: Background

One of the most promising areas for application of the hydrophobic hollow-fiber membrane contactor is in the area of produced water treatment. In 2007, the total volume of produced water was estimated to be about 21 billion barrels, making it the largest waste stream produced by the oil and gas industry. For every barrel of oil produced an average of 5.3 barrels of water are produced in the United States for both onshore and off-shore operations (*1*). There are two main incentives for the treatment of produced water in the United States. First, the EPA strictly regulates oil and gas extraction effluents for deep injection wells (*21*) or for release in the environment (*22*). Second, there is a financial interest in recovering oil contained in produced water. One of the key challenges associated with developing treatment technologies for produced water is the complexity and variability of produced water compositions.

OIL-WATER MIXTURE CHARACTERISTICS

Different types of oil-water emulsions exist and two categories can be identified: water-in-oil emulsions that contain less than 30% water (oil is the continuous phase) and oil-in-water emulsions that contain more than 30% water (water is the continuous phase). Oil droplets found in those emulsions have different physical states: free, dispersed, emulsified or dissolved. Emulsions with "free oil" are characterized by large droplets size (≥ 150μm) allowing the oil to easily rise to the surface. Dispersed oil is composed of droplets that are 20-150μm, while emulsified oil presents smaller droplets (≤ 20μm) that can remain stable naturally for long periods of time or with the addition of emulsifiers such as surfactants. Finally, dissolved oil can also be present in water and cannot be observed as an independent phase (*23*).

Produced water often contains additional constituents (other than oil and water) that present treatment challenges. The composition of produced water is highly variable

depending on the geographical origin and production process (shale gas, coal bed methane, conventional oil wells). Typical constituents are oil and grease compounds, dissolved formation minerals (anions and cations, heavy metals, and radioactive materials), production chemical compounds (corrosion inhibitors, biocides, emulsion breakers among others), solids (formation solids, precipitated solids, biological materials…), and dissolved gases (*24*). The concentration of those constituents may vary greatly; for instance, oil concentrations can range from 10 ppmv to 200,000 ppmv depending on the source of the produced water (*24-27*). An important class of components with respect to separation processes is emulsifiers such as surfactants that help stabilize emulsions, which make oil and water separation difficult (*9, 10, 23, 28*).

CONVENTIONAL PRODUCED WATER TREATMENT TECHNOLOGIES

Produced water treatment can be divided in three steps: primary, secondary and tertiary treatment depending on the type of oil or contaminants to be removed.

Primary treatment consists of removal of free oil (droplets size ≥ 150 μm) and coarse solids. There are mainly two treatment techniques used for primary treatment: gravity and centrifugal separations. Gravity separation techniques include gravity settlers (*10*), such as API (American Petroleum Institute) separators (*9, 29*), and plate coalescers (*9*). In gravity separators the oil, which is the lighter phase rises to the top while the water sinks to the bottom of the separator (*3, 29*). The success of this operation lies in the ability of the oil droplets to coalesce during ascension, which increases the separation rate. However, droplets smaller than 150 μm can decrease process efficiency. In that case, the effluent requires further downstream treatment (*29*). Plate coalescers are an improvement over traditional gravity separators with the addition of inclined parallel plates in the tanks. This configuration only requires droplets to rise a small distance before contacting the plates, which improves coalescence. The enlarged droplets are then

redirected to the top of the tank (*30, 31*). However, an additional downstream treatment is often needed to remove the smaller oil droplets not captured by the gravity system.

Centrifugal separations, such as centrifuges (*32, 33*) and hydrocyclones (*9*), enable the separation of solids and oil from water by applying a centrifugal force on the mixture. Centrifuges are composed of a central moving part and the rotor that generates a circular motion of the liquids and increases centrifugal force. The oil, which is the lighter phase, remains at the center of the rotation while the water, which is the heavier phase, is propelled to the outer surface of the mixture leading to emulsion separation. In the presence of solids, an additional stream is also recovered (*34*). Hydrocyclones differ from centrifuges in that there are no moving parts, and the centrifugal force is induced by tangential pumping into a conical tank (*35*). Centrifuges and hydrocyclones lower the required space for the equipment and reduce the operation time compared to gravity settlers. In addition, for larger volumes of water treated, the capital and operational costs are also lower (*32*). The disadvantages of those separation techniques are the lack of flexibility when the influent composition varies (*36*) and a decrease in removal efficiency of smaller oil droplets (*37*).

Secondary treatment consists in breaking up the oil-water emulsions and removing the dispersed oil (droplets size of 20-150 μm) present in the wastewater. Chemicals reducing the electrostatic repulsion between oil droplets can be used to trigger coagulation of the oil droplets. Induced air flotation (*38*) or dissolved air flotation (*39*) can then be used to mechanically separate the enlarged oil droplets by purging gas bubbles into the wastewater. The gas bubbles adhere to the oil droplets and allowing them to rise to the top where the viscous layer is skimmed off. The main drawback to this technique is the highly turbulent flow generated by the mixing of the gas bubbles, causing re-dispersion of oil into smaller droplets, which are harder to capture (*40*).

Other separation techniques consist of a combination of oil droplet coalescence and adsorption to fibrous or granular supports (i.e. filters). A wide array of such filters

have been investigated such as peat beds (*41*), sawdust deep-bed filters (*11*), fibrous and granular beds (*12*), glass fiber media (*13, 14*) as well as specific oil adsorbent media (*42*). Once the oil is adsorbed onto the media, it has to be discarded and typically cannot be reused (*11, 41*). When the only operative mechanism is coalescence, the water/oil mixture needs an additional separation treatment (*12*).

The technologies detailed so far are used successfully as primary and secondary treatment solutions. However, small droplet size is one of the main challenges that typically reduces the efficiency of these treatment techniques. Membrane technologies allow the removal of micron sizes droplets not captured by conventional treatment systems. Membranes also have the advantages of allowing high purification levels, are a rather inexpensive and flexible technology, and minimize the process area footprint and weight for offshore applications (*43, 44*). Microfiltration and ultrafiltration are typically implemented to remove emulsified oil remaining after primary treatment, while reverse osmosis is used to remove dissolved solids (*23, 45*) and complete the treatment of produced water before water reuse or discharge. As a result, much research has been undertaken to understand oil-water separation mechanisms with membranes (*46-48*).

MEMBRANE TECHNOLOGIES

Many types of membrane systems have been investigated for oil-water separation including microfiltration (*46, 49-51*), ultrafiltration (*52-54*), and nanofiltration (*45*); and a broad range of hydrophilic (*43, 46, 47, 55*) and hydrophobic (*8, 56-60*) materials have been tested. Within the realm of hydrophilic and hydrophobic membranes, systems have been used for either direct oil-water separation or as coalescing devices.

Direct Oil-Water Separation

Hydrophilic Membranes

Many hydrophilic materials have been investigated for the design of membranes for oil-water separation, including cellulose, ceramic, sulfonated polysulfone, hydrophilized PVDF (polyvinylidene fluoride), or polycarbonate.

Typically hydrophilic membranes are used for direct separation where water permeates the porous surface while oil is retained (*53, 61-63*). Many researchers, including Mueller et al. (*61*), Chakrabarty et al. (*63*) and Padaki et al. (*64*), identified the key operating parameters as transmembrane pressure (TMP), cross flow velocity, temperature, pH, and oil concentration. Increasing TMP and cross flow velocity were shown to increase water flux through the membrane. On the contrary, higher oil concentrations in the emulsion lead to lower water permeation across the membrane wall. Many researchers highlighted the build-up of a fouling viscous layer at the membrane surface ultimately decreasing water flux. The oil layer acts as a hydrophobic barrier, preventing water from approaching the membrane surface. Masoudnia et al. (*50*) showed that a combination of higher TMP and cross flow velocity improved oil permeation by disrupting the formation of the oil layer. Abadi et al. (*65*) showed that increasing temperature increased water flux by reducing the viscosity of the fouling layer on the membrane surface as well. Huang et al. (*66*) pointed out that increasing TMP leads to an increase in steady-state flux only to a certain point, after which an increase in TMP did not significantly improve the system performance due to the pore being blocked by the oil layer. Many studies focused on characterizing and modeling of the fouling behavior in hydrophilic membrane systems (*50, 54, 55, 67, 68*). Masoudnia et al. (*50*) identified the type of blocking mechanisms occurring at the membrane surface ranging from cake formation to intermediate pore blocking and standard pore blocking with increasing TMP. Additional work has focused on improving operating techniques to reduce the buildup of the viscous layer by employing backflushing (*69, 70*) or through the addition

of vibration during filtration (*71-73*). Other approaches consisted of changing the membrane surface by adding corrugations (*57*) or modifying the material surface chemistry (*74*).

Extensive work has also been conducted to understand breakthrough pressures and oil rejection by hydrophilic membranes. Nazzal (23), Cumming (*75, 76*), and Darvishzadeh (*77*) developed detailed models that include membrane characteristics, oil droplet geometry and oil-water interfacial tension to estimate critical pressures derived from the Young Laplace equation. Operating at TMPs below the oil breakthrough pressure allows a high quality water effluent. For cross-flow filtrations, Darvishzadeh (*77*) showed that the permeation of oil droplets results from a balance between a tangential shear force, created by cross flow, and the normal force applied on a droplet through transmembrane pressure. As a result, Darvishzadeh (*77*) proposed a diagram showing zones of rejection, permeation, and breakup of oil droplets depending on shear rate and transmembrane pressure.

Modeling of permeation behavior of hydrophilic systems has typically been the result of an analogy between typical solid particles and oil droplets filtrations. Oil droplets are analogous to solid particles that progressively block the pores or form a layer at the membrane surface leading to a reduced steady state liquid flux across the membrane. Huang et al. (*66*) developed a mechanistic model describing the limiting permeation of water in a highly hydrophilic UF membrane system. Fouling behavior was shown to follow Hermia's models and water flux was proven to become pressure independent over time. Viscosity, oil concentration and shear rate were confirmed as important parameters affecting water flux across the hydrophilic membranes. Other studies have compared experimental data collected from hydrophilic systems to the typical transport models used for microfiltration such as Brownian diffusion, shear-induced diffusion, or inertial lift (*78*). Singh et al. (*47*) combined both Brownian and shear-induced diffusion models to obtain good agreement between predicted and

measured steady state flux data in a hydrophilic microfiltration system treating industrial oily wastewater.

Finally, hydrophilic membrane systems are technologies already being implemented in the field for oil-water separation. Among others, Pall Corporation proposes the use of Membralox® a ceramic tubular membrane; Osmonics developed the M-series UltraFilic®, a set of hydrophilic membranes advertised to reduce viscous fouling; Orelis Environnement offers the KleanSep™ ceramic membrane; and HTI Water Divisions commercializes SepraMem™, a set of spiral wound membrane modules promoted as solutions for oil-water separation.

While hydrophilic systems have been studied extensively and much research has focused on reducing fouling behaviors, hydrophobic membranes are viable alternatives for oil-water separation. In hydrophobic systems, oil permeates the porous surface rather than water, which presents great promise in preventing typical viscous fouling experienced by hydrophilic membranes.

Hydrophobic Membranes

A few materials can be used to obtain a hydrophobic membrane surface; some examples are PET (polyethylene terephthalate) (*59*), PP (polypropylene) (*79*), PTFE (polytetrafluoroethylene) (*80*) also known as Teflon, and PVDF (polyvinylidene fluoride) (*74*).

Early research on direct oil-water separation with hydrophobic membranes was conducted by Unno et al. (*80*) in 1986 and Ueyama et al. (*81*) in 1987. These researchers demonstrated the possible use of specific membrane characteristics to selectively permeate oil. The penetration of oil through the membrane was only enhanced by gravity and shear forces applied by a propeller in the operation tank. Oil concentration, viscosity, and droplet size were identified as key parameters for process improvement. Ueyama et

al. (*81*) showed that increased stirring enhanced the flux across the membrane. One significant study for the successful use of hydrophobic membranes was the work conducted by Tirmizi et al. (*59*). Various hollow fiber hydrophobic and hydrophilic membranes were studied and compared for separation of oil and water. The performance of the hydrophobic membranes were first studied with a pure oil feed and oil flux was compared to the Hagen-Poiseuille model seen in Equation 2-1.

$$Q = nq = \frac{n \cdot \Delta P \cdot \pi \cdot r^4}{8 \cdot \tau \cdot \mu \cdot L} \qquad \text{(Eq. 2-1)}$$

With Q is the permeate flux

n: the number of pores per unit area

q: the volumetric flow rate through each pore

ΔP: the transmembrane pressure

r: is the pore radius, μ the fluid viscosity

τ: the tortuosity of the pores

L: the pore length.

As predicted by the model, TMP was seen to linearly enhance oil permeation. Oil-water mixtures were also tested and high quality permeate was obtained. Transmembrane pressures applied up to 0.3 bar were shown to improve oil permeation as well. Oil mixtures at a concentration of 80% and 1% tetradecane were tested. The filtration of both emulsions proved to be successful; and Tirmizi et al. concluded that the viability of using hydrophobic membranes for oil-water separations was confirmed. Oil/water/surfactant mixtures were also tested with the hydrophobic membranes and temporary limiting flux behavior was observed and could be reversed with backflushing. The work of Tirmizi et al. (*59*) showed promising results for the separation of oil and water with hydrophobic membranes. Pure oil permeate could be recovered along with high effluent water quality

mixtures. Since then, only a few researchers have investigated the use of hydrophobic membranes for the permeation of oil and rejection of water (*8, 56*). Ezzati et al. (*56*) studied the effect of various operating parameters with the Taguchi method on the separation of an oil/water/surfactant emulsion, with oil concentrations ranging from 80 to 95% oil (v/v). Increasing temperature was shown to lead to increasing oil permeation rate by reducing viscosity. Transmembrane pressure was shown to improve oil flux for low-pressure values. For very high pressures, a decrease in flux was observed due to the compression of micelle and water onto the pores; and increasing amounts of water were detected in the permeate. Longer residence time was shown to impair oil permeation due to micelles fouling the membrane surface. The study confirmed the possible use of hydrophobic membranes for the recovery of oil from emulsions, but was conducted on a limited flat sheet section and was focused on feeds with high oil concentrations.

Membrane Coalescence

Similar to the coalescence filters mentioned earlier in this review, membranes have also been employed as coalescing devices. Hydrophilic and hydrophobic membranes have been used to demulsify water-in-oil emulsions (*82-84*). The technique consists of forcing the complete oil-water emulsion through the membrane pores to enhance droplet size by coalescence on the membrane material. This mechanism has been described in several studies (*82-85*). Subsequent gravity separation is enhanced by the enlarged size of the oil droplets. To elucidate the oil droplet coalescence mechanisms, researchers have used see-through micro-channels to simulate membrane pores. Kawakatsu et al. (*86*) observed the coalescing and phase inversion mechanisms of triolein droplets in water while permeating a hydrophobic PTFE pore (Figure 2-1).

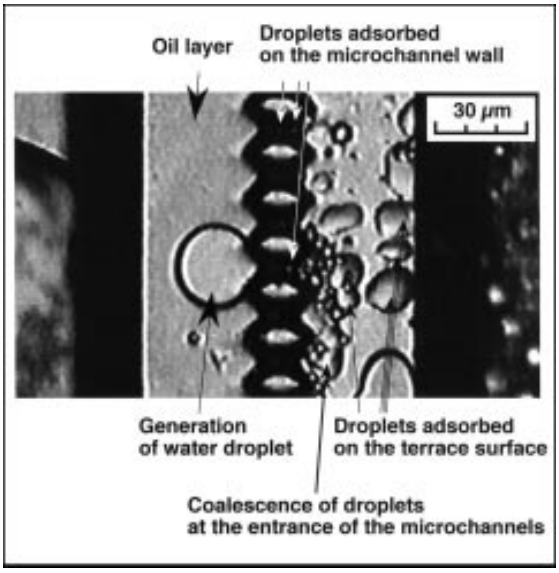

Figure 2-1: Magnified image around microchannels in demulsification of O/W emulsions (triolein/water containing 0.1 wt % SDS) (*86*).

The results demonstrated that larger oil droplets are created in the mixture, facilitating subsequent oil-water separation by gravity separation. Many researchers investigated the use of hydrophobic membranes as coalescing devices. Hoffman and Nitsch (*60*) forced an isododecane/water emulsion through a microporous PTFE membrane and demonstrated the subsequent enhanced settling and separation of the water and oil phases. Daiminger et al. (*87*) tested diverse membrane materials for coalescence and replaced the settling phase by a direct separation process conducted with an additional membrane. Hlavacek (*88*) also demonstrated the increase in droplet size after permeation of a polypropylene membrane. Several parameters were evaluated for their importance to successful coalescence such as pressure and temperature. The results suggested that the cross-flow velocity did not significantly affect the permeation or the settleability of the oil-water mixture. A higher transmembrane pressure (TMP) increased permeation rates and improved effectiveness and time of settling, while an increase in temperature allowed higher permeation and better separation efficiency. Furthermore, Kawakatsu (*86*), Hoffman (*60*), and Hong (*89*) emphasized the importance of relative

droplet to pore size ratio to achieve successful coalescence. The pore should be small enough for the oil droplets to contact the membrane surface but not so small as to re-disperse the emulsion. An oil droplet significantly smaller than the pore size may also flow out of the channel without contacting the membrane walls. Figure 2-2 summarizes these coalescing mechanisms.

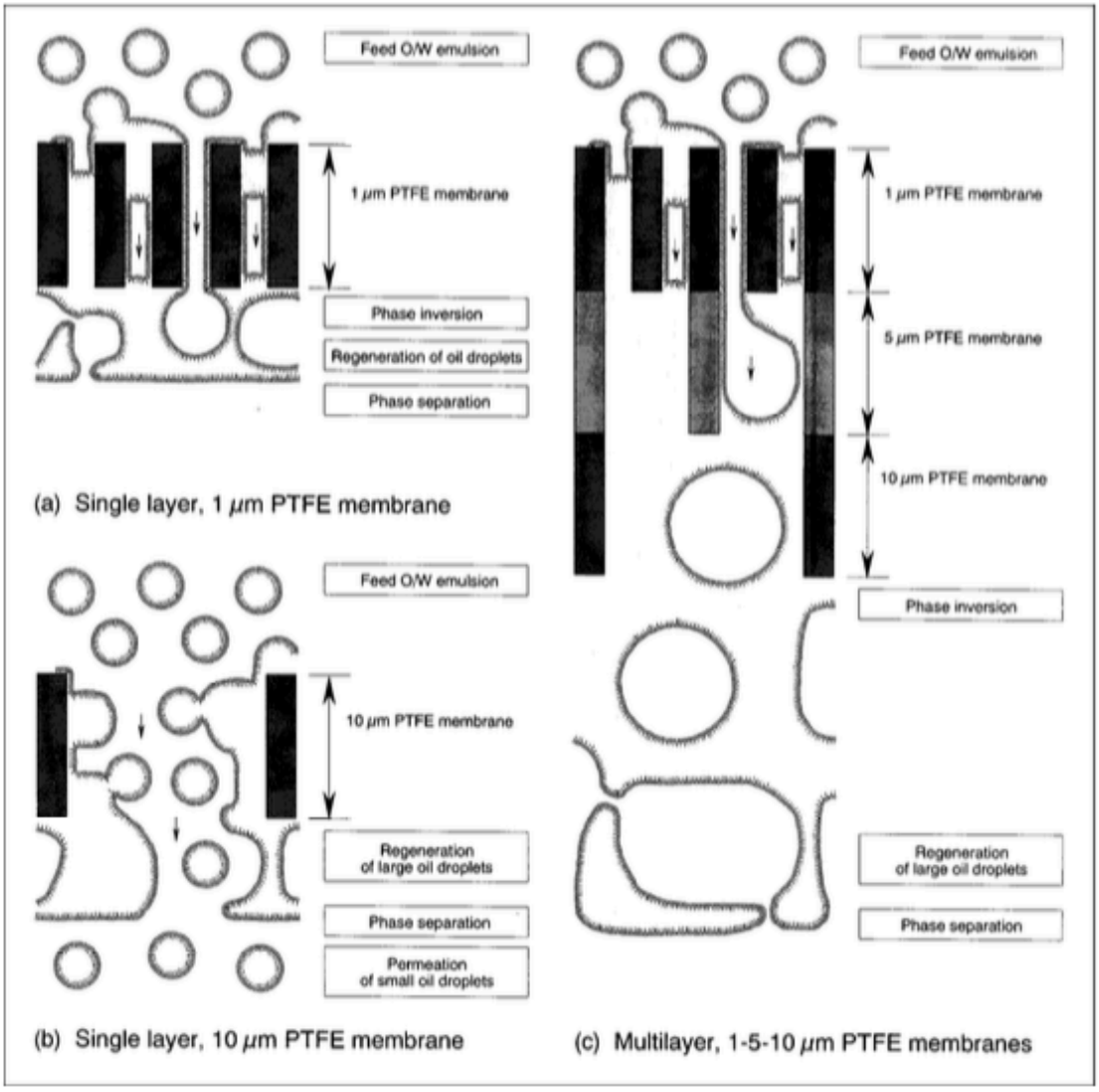

Figure 2-2: Phase inversion and separation mechanism of O/W emulsion permeating through single layer (a, b) and multilayer (c) PTFE membranes. (Kawakatsu et al. (*86*))

Hydrophobic Hollow Fiber Microporous Membrane Contactor

The membrane technology examined in this dissertation is a hydrophobic hollow fiber microporous membrane contactor manufactured by Membrana and known as the Liqui-Cel® Extra Flow modules. The technology is commercially available and used extensively for degassing applications (*15*). In early studies, the technology tested for the removal of non-polar lipids from microalgae slurries was licensed by the University of Texas to OpenAlgae LLC. Research conducted at the Separations Research Program (UT-Austin) on various saltwater and freshwater microorganisms slurries led to IP work (*17-19*). Simulated feedstocks were also tested and showed successful operations for up to two weeks with increasing oil recovery above 95% (*20*). These initial data, while important, did not provide sufficient understanding to reliably design and engineer an optimized oil recovery system that could be applied to biological and petroleum based oils. It is believed that the hollow fiber geometry of the membrane module allows internal coalescence of oil droplets between fibers combined with selective permeation of oil through the membrane.

The technology represents a promising solution for oil-water separation without the typical fouling observed for hydrophilic systems. Hydrophobic membranes for the permeation of oil have not been investigated extensively and more research is necessary to understand the fundamental mechanisms of such systems. Even though early research conducted on hydrophobic membrane systems appears promising, the module sizes and the operating parameter ranges such as transmembrane pressure, oil concentration, or influent flow rates have not been studied sufficiently. An in-depth understanding of the hydrophobic membrane contactor will allow optimized implementation and use of this technology in the field.

Chapter 3: Materials and Methods

The system of interest in this work is a hollow fiber microporous membrane contactor presently manufactured for degassing applications by Membrana (USA) and successfully tested in our laboratories for the new applications of oil and water separation. The membrane contactor has polypropylene hydrophobic fibers allowing selective permeation of oil while water is rejected and presents the potential for long-term operation without the typical viscous fouling observed in hydrophilic systems. In this chapter, the membrane contactor characteristics provided by the manufacturer are detailed and additional results obtained in our laboratory are presented. The oil used for this study is also described. The experimental systems used in this work to test the membrane performance are described. First, the pure oil feed experimental setup used for determination of the maximum baseline oil flux is detailed. Then, the oil-water mixture apparatus is detailed, and the associated data acquisition system is presented. Finally, cleaning procedures used in the occurrence of biological fouling are listed.

Some chapters of this dissertation will be submitted directly for publication; therefore, some of the material presented here will be repeated as necessary in subsequent chapters.

MEMBRANE CONTACTORS

The membranes used in this study are manufactured by Liqui-Cel® (Membrana, USA) and commercially available under the name Liqui-Cel® Extra Flow. The modules are composed of hydrophobic microporous hollow-fibers with a central baffle to eliminate shell side bypassing (*90*) and evenly distribute fluid perpendicularly to the fibers. Modules with different intrinsic characteristics were investigated and are detailed in Table 3-1. A precision contact angle goniometer (Ramé-hart Instrument Co., USA) was used to estimate the contact angle of water on a sample of the hollow-fiber sheet

used in the membrane contactor. The contact angle of water in air on the membrane surface was approximatively 120° confirming the hydrophobicity of the membrane material.

Table 3-1: Membrane contactor characteristics

Membrane Module name	Module size (diameter x length) (inch)	Fiber Type	Surface area (m^2)	Porosity (%)	Wall thickness (µm)
A	2.5x8	X50	1.4	40	40
B	2.5x8	X50	0.7	40	40
C	2.5x8	X40	1.4	25	50
D	4x28	X50	20	40	40

Membrane B is not commercially available and was specifically manufactured for the purpose of this study. All membranes had the same design, which is a hollow-fiber flat sheet rolled into a cylindrical casing allowing a pseudo cross-flow filtration. The membrane geometry is presented in Figure 3-1.

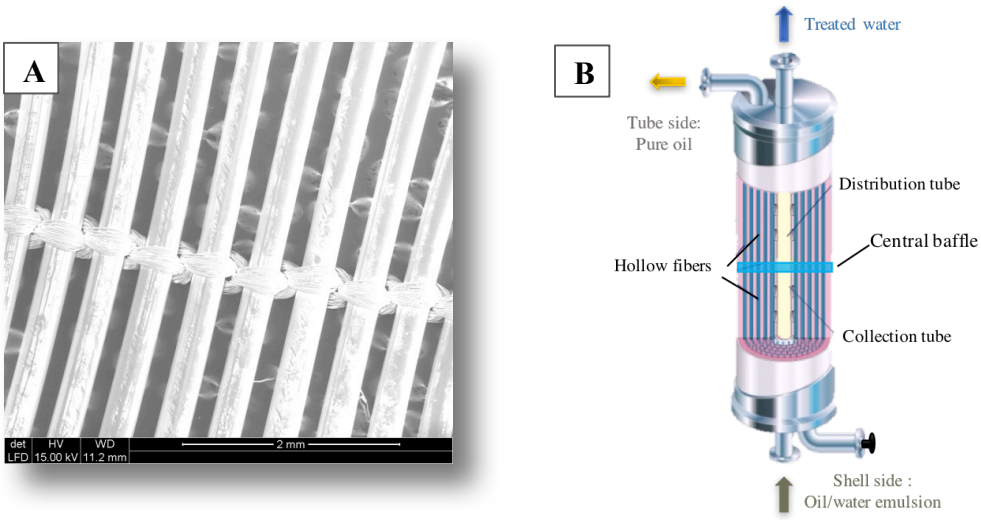

Figure 3-1: Liqui-Cel® Extra flow design. A) SEM picture of hollow-fiber sheet with prior gold and palladium sample coating. B) Drawing adapted from Liqui-Cel®.

The region outside of the fibers is referred to as the "shell side", while the volume inside is the "tube side". Four ports allow the distribution of the fluid in and out of the module; two ports for each side. The manufacturer advertises an average pore size of 0.04 μm for the X50 fiber and 0.03 μm for the X40 fiber. The pore size distribution of the X50 fiber was determined in this research with scanning electron microscopy (Hitachi S5500 SEM/STEM, USA). Image analysis of the SEM picture seen in Figure 3-2 was conducted using the open source program ImageJ (developed by the National Institutes of Health, USA). As can be seen in Figure 3-2, there is variability in the pore size and the range extends up to 0.12 μm. The average pore size calculated from the measurements was 0.047 μm, which compares nicely to the provided pore size from the manufacturer.

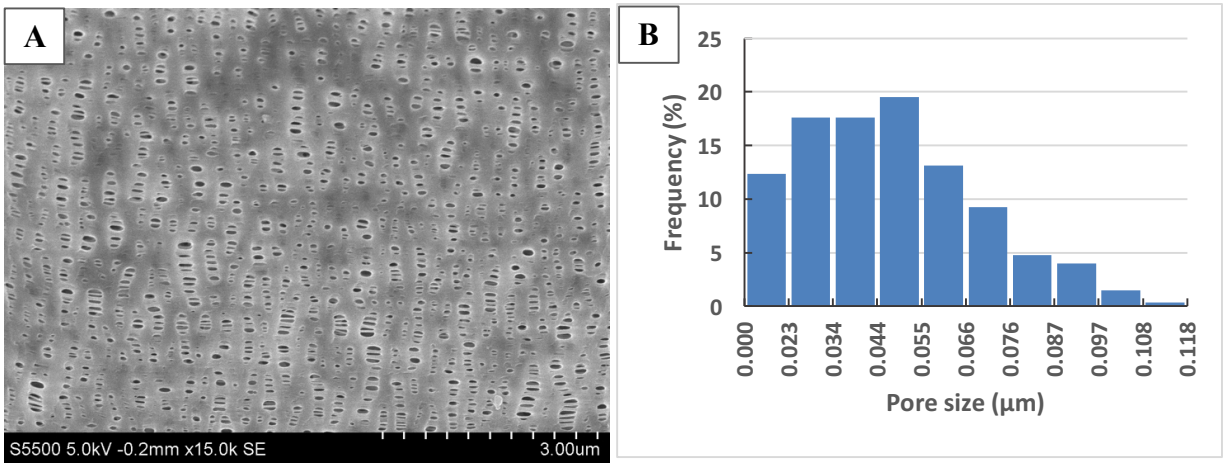

Figure 3-2: Pore size analysis. A) SEM picture with prior gold and palladium sample coating, B) Pore size distribution obtained with ImageJ analysis of the SEM in A.

SYNTHETIC OIL

The synthetic oil used in this study is a controlled mixture of paraffinic compounds called Isopar™ and manufactured by ExxonMobil. Isopar™ oil can be purchased in various grades with different viscosities as seen in Table 3-2. Isopar™ oils are relatively safe to use and the mixture of compounds used is well-controlled, which make them a good choice for experimental repeatability.

Table 3-2: Viscosities at 25°C of Isopar™ grades used for the study.

Isopar™ grade	Viscosity (cP)
Isopar™ L	1.5
Isopar™ M	3.5
Isopar™ V	10.7

The effect of temperature on viscosity was measured for all three grades of Isopar™ with a modular compact rheometer Paar Physica MCR300 (USA). The results presented in Figure 3-3 show that the dependency of viscosity on temperature varies among the Isopar™ mixtures. The exponential correlations developed are useful to estimate oil viscosity when temperatures vary either due to seasonality or heat build-up in the system (*91*).

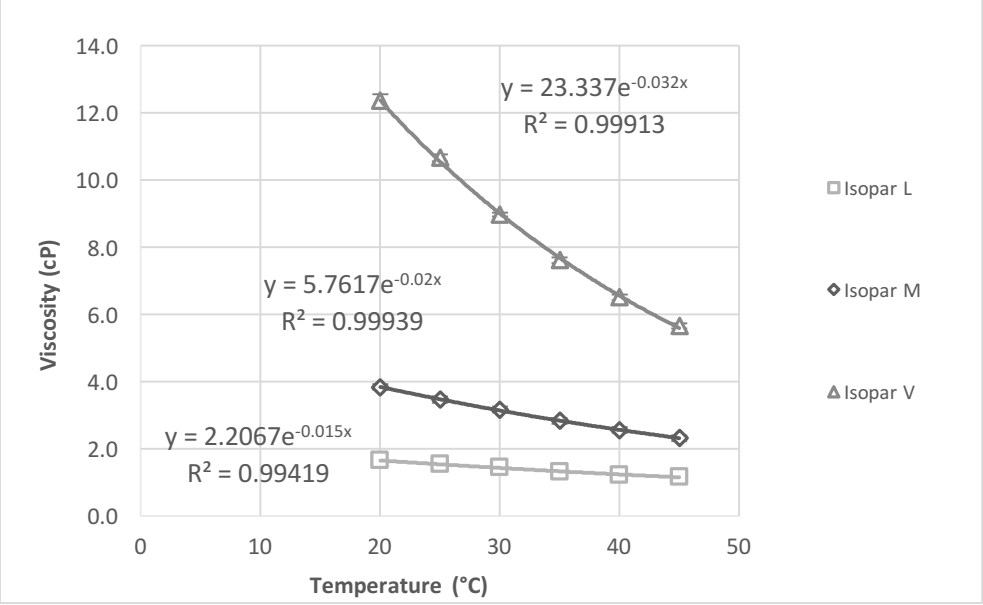

Figure 3-3 : Viscosity vs temperature for three Isopar™ grades.

The interfacial tensions of the three Isopar™ grades and water were measured with a precision goniometer (ramé-hart instrument co., USA). The pendant drop method was used in combination with the ramé-hart DROPimage software to determine an interfacial tension of 52 dynes/cm for all three Isopar™ grades with water.

EXPERIMENTAL SETUP

A system integrating the membrane contactor was built on a vertical structure that could be used to support tubing and instruments in a 3D configuration seen in Figure 3-4. The membrane setup was placed in a containment area for any spill occurrences. The system was situated in a floor-to-ceiling hood with constant ventilation. Such laboratory conditions allowed safe operation of the hollow fiber membrane contactor for long periods of time and without 24-hour human surveillance. Two membrane systems were used; a setup for pure oil feed experiments and a setup for oil-water mixtures experiments.

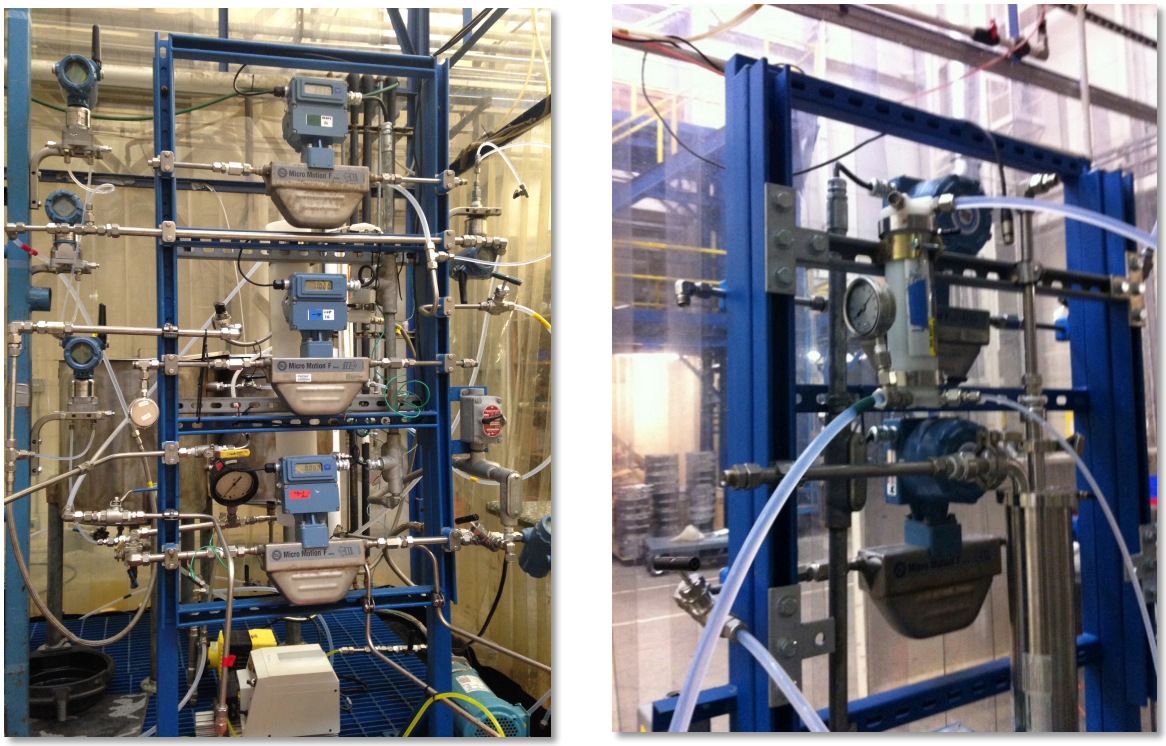

Figure 3-4: Experimental apparatus and laboratory environment.

Pure Oil Feed Experimental Setup

Safety Note

Operating the membrane system under pure oil conditions can present risks. After running for a few months, a clicking noise was detected during an experiment with Isopar V, which is the highest viscosity Isopar™ oil. The noise was identified as static discharge in the system. Friction along the fibers with elevated influent flow rate and lack of conductive material in the membrane contactor resulted in the build up of an electrical charge released periodically through a spark. In an environment with hydrocarbons, a spark could have led to a fire. However, the lack of oxygen in the closed system helped avoid such occurrence. Even though all metallic parts of the system were grounded, the noise could still be detected from the membrane module, where no conductive material is present. Salt was tentatively added to the Isopar™ to increase conductivity, but the low solubility of the salt in the oil made this solution inefficient. An acceptable solution was to add ppmv levels of water to the oil, thereby, adding conductivity to the system. An alternative idea would be to run a thin metal filament through the membrane module allowing electrical discharge to the ground. However, this approach was not tested in this research. The observed static charging phenomenon is unlikely to happen in field applications since the process is designed to separate oil and water. The presence of water provides constant electrical conductivity to the ground.

Experimental Apparatus

Figure 3-5 shows the schematic of the membrane system operated with a single pure phase. The feed was distributed through the system with a high shear pump (MTH pump, USA) and entered the membrane from the shell-side bottom port. The retentate was sent back to the feed tank, while the permeate was collected in a graduated glass cylinder for quantification. The needle valve located downstream of the membrane

module was used in conjunction with the pump variable speed drive to control transmembrane pressure and influent flow rate. The transmembrane pressure was calculated from the reading of two two pressure gauges (Solfrunt, USA). No pressure gauge was used on the membrane tube side since it was left open to atmospheric conditions and oil exited the system by gravity. The influent flow rate was measured with a MicroMotion flow meter (Emerson, USA). Temperatures were obtained using a Rosemount RTD sensor (Emerson, USA).

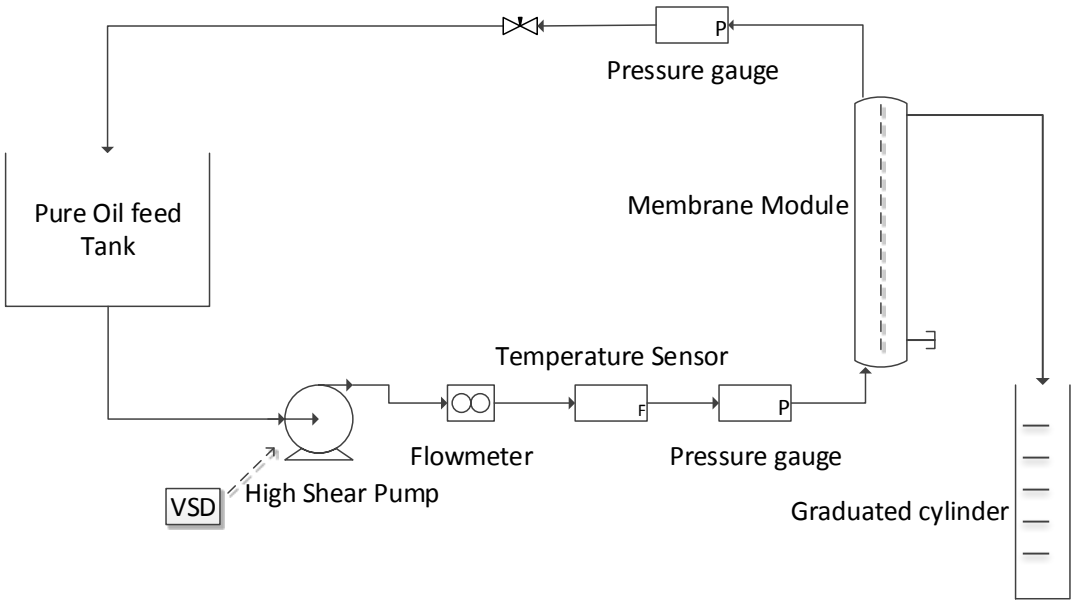

Figure 3-5: Schematic of membrane system for pure oil operation.

Experimental Procedure

Characterization of the 2.5x8 inch modules involved recirculating pure Isopar™ through the system. The transmembrane pressure and influent flow rate were adjusted; and permeated oil was collected and quantified either with a graduated cylinder and stop watch or a weigh-scale and stop watch. For the larger membrane contactor, 4x28 inch

modules, the oil permeation rate was measured with a Micro Motion (Emerson, USA) flow meter. In both cases, transmembrane pressures were calculated as the average of the inlet and outlet pressure of the shell side. For low influent flow rate such as 3.8 L/min, pressure drop was typically 0.07 bar and could reach 0.7 bar for the large modules at 27 L/min. All experiments were performed in triplicates. Table 3-3 shows the conditions of all experiments conducted.

Table 3-3: Experimental conditions tested for membranes A, B, C, and D.

Membrane type	Isopar™ grade	Influent oil flow rate (L/min)	Transmembrane pressure (bar)
2.5-inch modules (A, B, and C)	L	3.8	1.4, 2.8, 4.1
	M	1.9	1.4, 2.8, 4.1
		3.8	0.7, 1.4, 2.1, 2.8, 3.4, 4.1
		5.7	1.4, 2.8, 4.1
	V	3.8	1.4, 2.8, 4.1
		11.3	1.4, 2.8, 4.1

Oil-Water Experiments

Experimental Apparatus

Two membrane systems were used for this study. One system was operated in a "one-pass through" mode, while the other system was operated in a closed loop for long term operation. Figure 3-6 shows the "one pass through" schematic, where oil-water emulsions were sent through the membrane system in a single pass. The oil permeated on the tube side was measured, while the retentate was directly discarded.

Figure 3-7 shows the schematic for the system operated in a recycle mode. Two modules were used in series at all times to guarantee high oil removal on the shell side and recirculate water back to the feed tank for long-term operations. Only the performance in the first module was relevant to the experiments. The second module was used solely as a guard to remove any oil before recirculating the water back to the tank.

For both systems, oil was injected into the main water line using a peristaltic pump (Thermo Fischer Scientific, USA) used for oil concentration control. The high shear pump was used to mix and circulate the emulsion through the system. The modules were mounted vertically. The emulsion would enter the bottom shell port and exit the top shell port, while permeated oil would flow out of the top tube side (the bottom port being capped). Influent flow rate and pressures were adjusted with a variable speed drive controlling the pump and a needle valve located on the outlet line. Influent flow rates were measured with Micro Motion (Emerson, USA) flow meters. Temperature was monitored with a Rosemount RTD sensor (Emerson, USA). Pressures on the shell side were collected with Rosemount pressure transmitters (Emerson, USA).

Three scales (Arlyn D-620T, USA) were used to measure oil mass injected in the system and recovered by each of the modules in series. All instruments were connected to a DeltaV (Emerson, USA) data acquisition system with real-time data collection for extended periods of time without interruption.

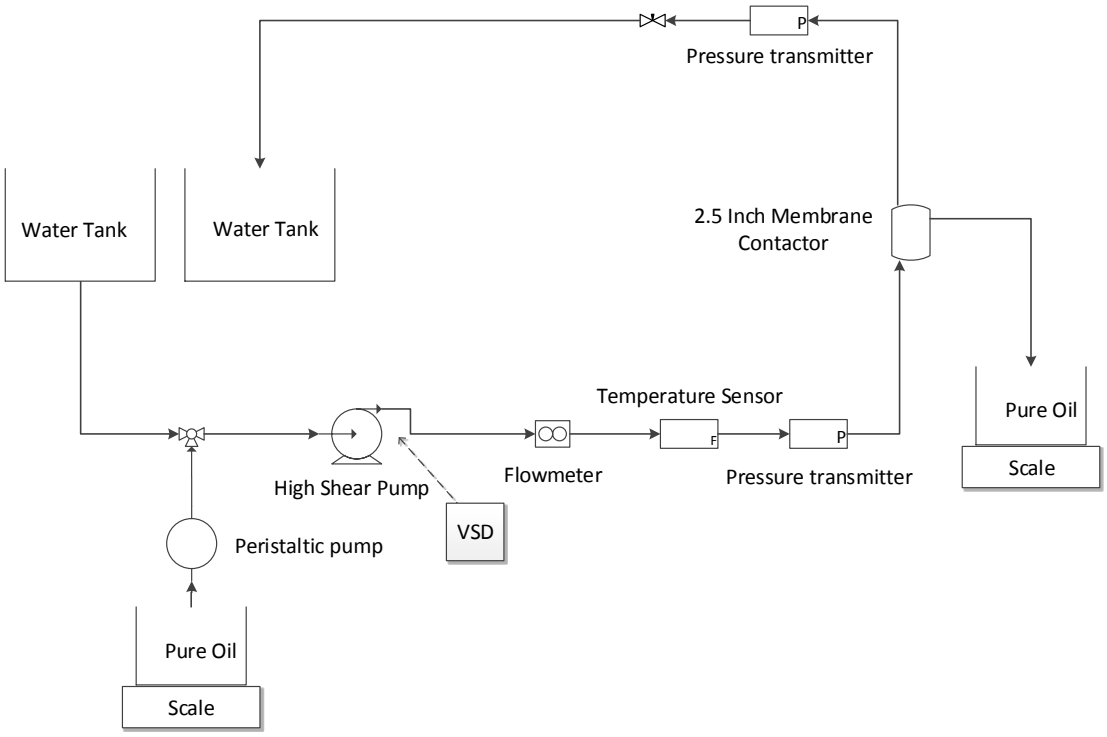

Figure 3-6: “One pass through” system schematic.

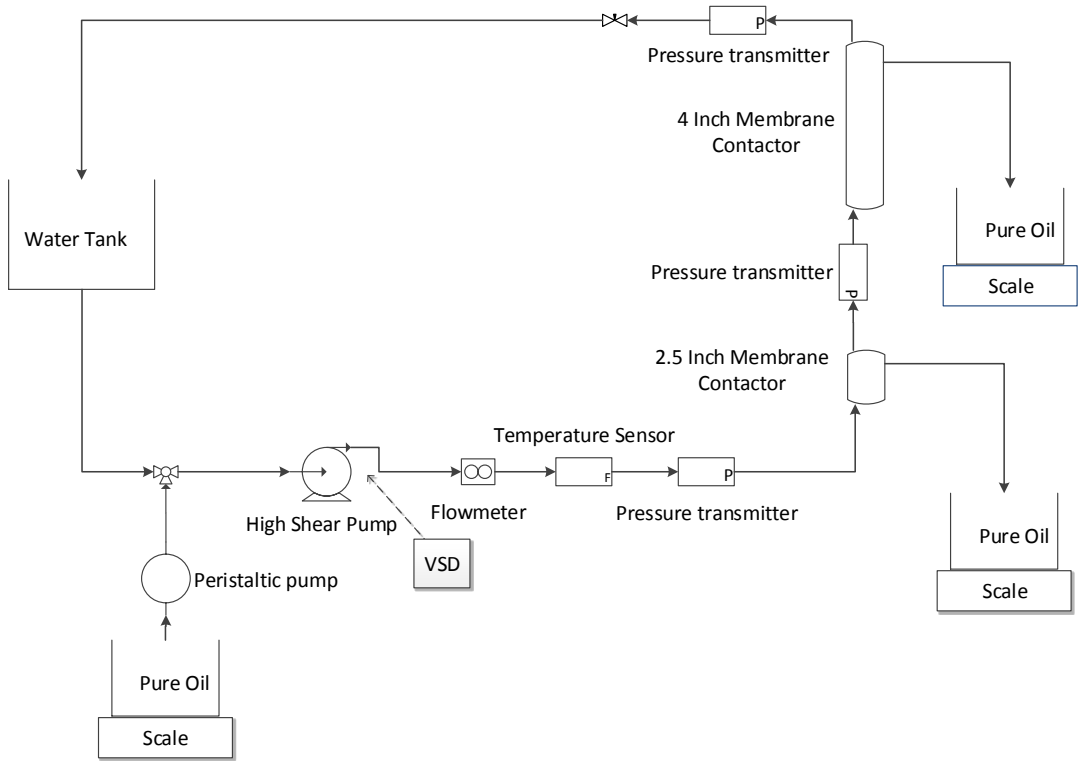

Figure 3-7: System schematic in recycling mode.

The apparatus was first used with pure water recirculating through the system to measure pressure drop on the shell-side of brand new modules with the pressure transmitters. The results are presented in Figure 3-8 and were used as a baseline to monitor any changes in pressure drop during oil-water experiments indicating possible fouling. The larger module had lower pressure drops than smaller module as expected by the larger cross sectional area.

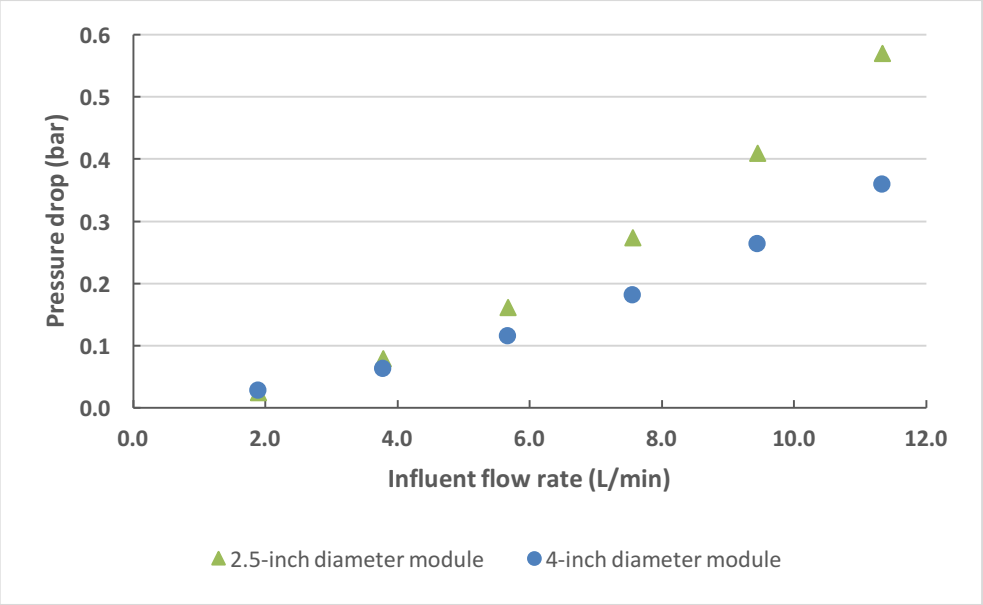

Figure 3-8: Measured water pressure drops for brand new modules

Experimental Procedure

Tests were performed by sending an oil-water emulsion to the shell side inlet of the module where oil permeated the membrane and was subsequently quantified with the scales. Oil concentration in the feed was controlled by the peristaltic pump and calculated on a volumetric basis. Transmembrane pressure was computed from the average of inlet and outlet pressures of the shell side (values were corrected for static pressure), while the tube side was left open to atmospheric pressure. Oil flux across the membrane was the

indicator used to characterize system performance. Oil recoveries were also calculated from the ratio of permeate oil volume to influent oil volume. The experimental plan is shown in Table 3-4. Each operating parameter among transmembrane pressure, viscosity, oil concentration, and influent flow were tested independently to study the effect on oil permeation and recovery.

Table 3-4: Oil/ water experimental plan

Operating conditions	Oil concentration study		Transmembrane pressure study	
Oil Concentration (%)	0.02, 0.05, 0.1, 0.25, 0.5, 1, 2, 5, 10, 20, 40, 60, 80, 90	2, 5, 10, 20, 40, 60, 80, 90	40	2
Membrane	A	A	A	A
TMP (bar)	1.4	2.8	1.4, 2.8, 4.1	0.7, 1.4, 2.8, 4.1
Influent flow rate (L/min)	3.8	3.8	3.8	3.8
Isopar™ Grade	M	M	M	M
Duration of experiments	20 min up to 12 days	20 min up to 2.5 hours	20 min	20 min up to 2.5 hours

Operating conditions	Influent flow rate study		Viscosity study			Fiber spacing study		High recovery
Oil Concentration (%)	2	40	20, 80	2	0.02	2	2	0.1
Membrane	A	A	A	B	A	A	B	C
TMP (bar)	1.4, 2.8	2.8	1.4	2.8	1.4	1.4, 2.8	1.4, 2.8	2.8
Influent flow rate (L/min)	1.9, 3.8, 5.7	1.9, 3.8, 5.7	3.8	3.8	3.8	3.8	3.8	3.8
Isopar™ Grade	M	M	L, M, V	L, M, V	L, M, V	M	M	M
Duration of experiments	20 min up to 1.5 hours	20 min	20 min	1.5 hours	7 to 8 days	1.5 hours	1.5 hours	5 days

The range of study for each parameter is shown in Table 3-5. Viscosity was chosen given the available Isopar™ grades. Maximum influent flow rates and transmembrane pressures were selected according to the manufacturer specifications.

Table 3-5: Summary of the range of operating parameters

TMP (bar)	Viscosity (cP)	Influent flow rate (L/h)	Oil concentration (%(v/v))
[0.7-4]	[1.5-12]	[113-340]	[0.02-100]

OIL-WATER MIXTURE CHARACTERIZATION

Oil and water were mixed with the high shear pump to obtain a non-chemically stabilized emulsion. An inline particle analyzer (JM Canty, Inc., USA) was used to observe and measure the droplet size distribution of the emulsion entering the membrane system. During measurements, more than 40,000 particles were accounted for to build a single particle size distribution. Most of the oil droplets were smaller than 10 μm and the mean droplet size was 4.7 μm as can be seen in Figure 3-9.

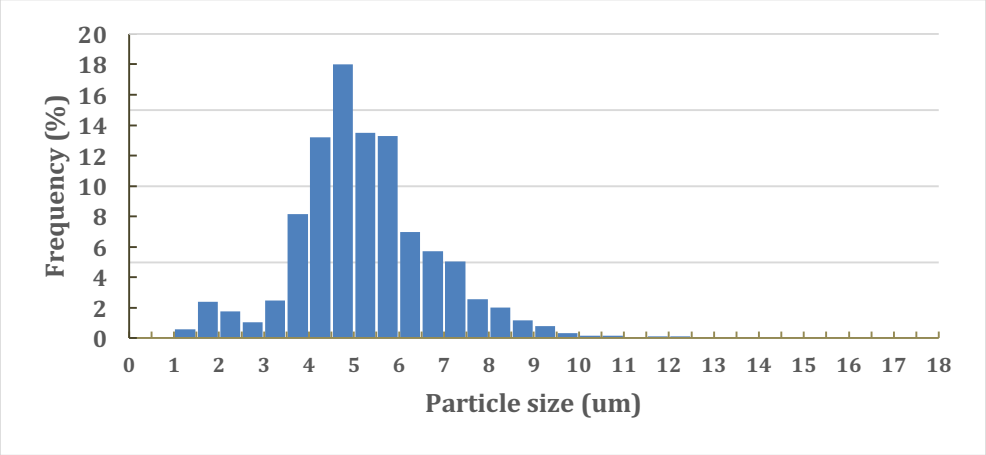

Figure 3-9: Typical droplet size distribution of Isopar™ -water non-stabilized emulsion entering the system. C_{oil} = 200 ppmv.

DATA ACQUISITION SYSTEM

The data acquisition system consisted of a computer connected to the instruments with different communication pathways. The four scales were linked to the computer

with a 4-way RS232-USB converter. The data sent continuously from the scales were then processed through an OPC program to identify and solely extract the mass digits. The pressure transmitters, the RTD sensor, and the flow meters were communicating with the DeltaV system through Wifi technology. An EXCEL spreadsheet was setup and the DeltaV add-in allowed real time data reading from DeltaV Control Studio outputs (Figure 3-10).

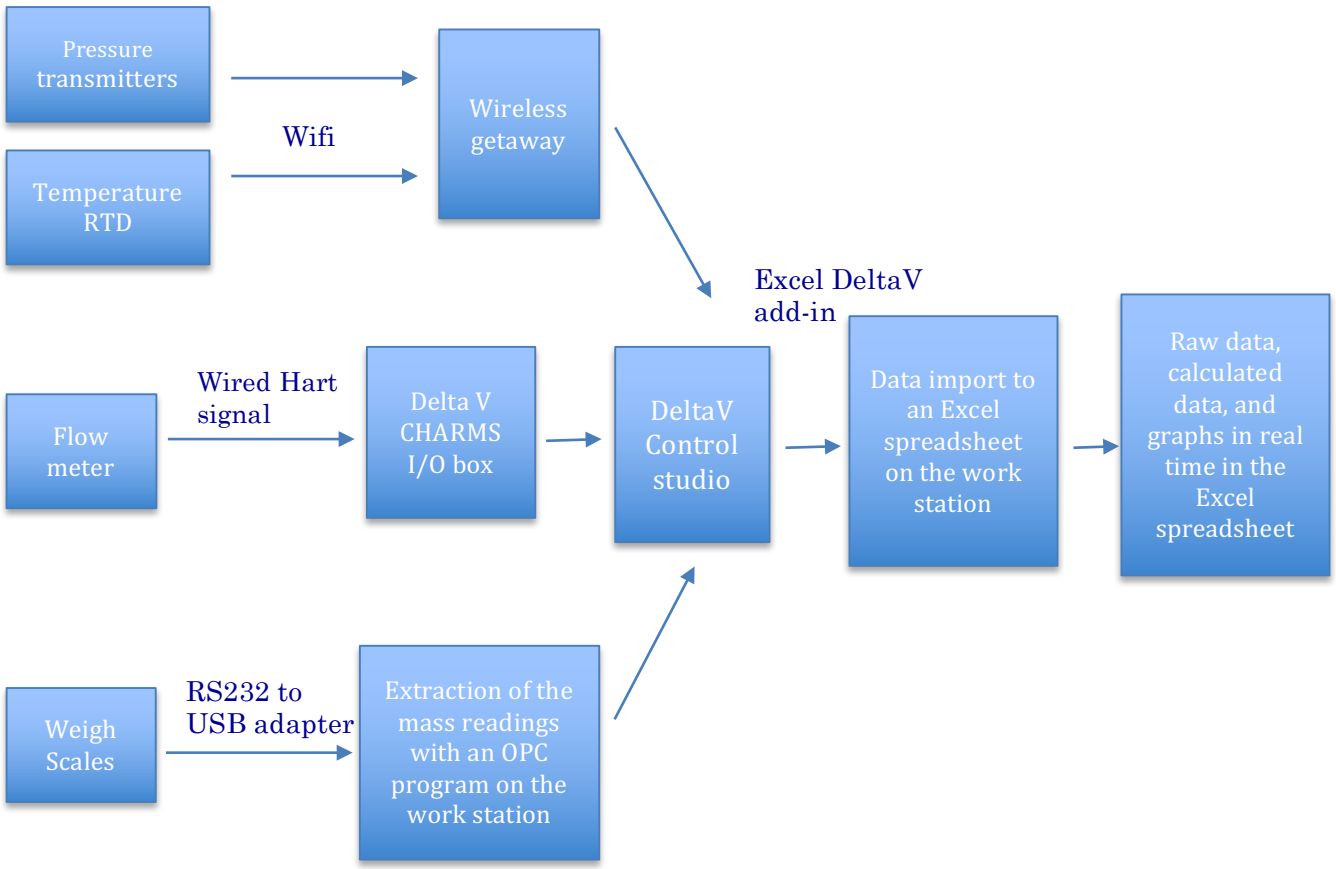

Figure 3-10: Data acquisition schematic

A VBA code was designed to periodically read and extract the live data from all the instruments and automatically populate "raw data" columns in an EXCEL spreadsheet. Those "raw data" columns in EXCEL were linked to columns containing formulas to calculate flux, recoveries and concentrations in real time. The data from these

columns were linked to a real time chart depicting oil flux, recovery, and pressure drop as a function of time for each membrane module as well as oil concentration in the feed. An example of the EXCEL spreadsheet is shown in Figure 3-11. All codes used for the data acquisition system can be found in Appendix C.

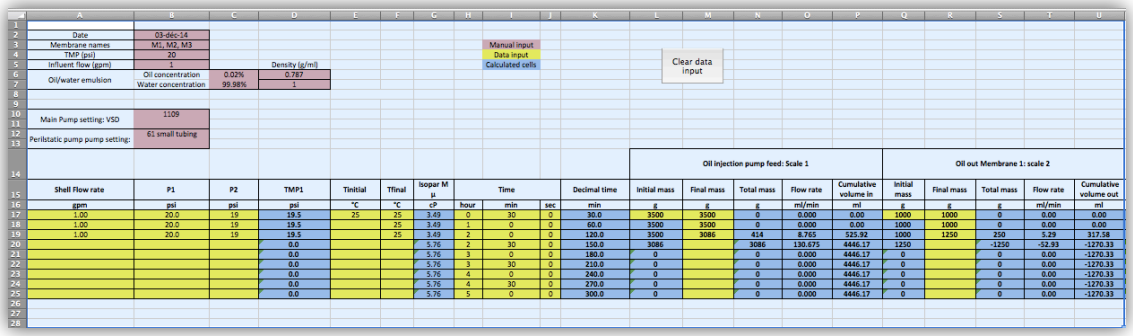

Date	03-déc-14							Manual input												
Membrane names	M1, M2, M3							Data input												
TMP (psi)	20							Calculated cells												
Influent flow (gpm)	1		Density (g/ml)																	
Oil/water emulsion	Oil concentration	0.02%	0.787																	
	Water concentration	99.98%	1																	
Main Pump setting: VSD	1109																			
Peristatic pump pump setting:	61 small tubing																			
											Oil injection pump feed: Scale 1					Oil out Membrane 1: scale 2				
Shell Flow rate	P1	P2	TMP1	Tinitial	Tfinal	Isopar M μ	Time			Decimal time	Initial mass	Final mass	Total mass	Flow rate	Cumulative volume in	Initial mass	Final mass	Total mass	Flow rate	Cumulative volume out
gpm	psi	psi	psi	°C	°C	cP	hour	min	sec	min	g	g	g	ml/min	ml	g	g	g	ml/min	ml
1.00	20.0	19	19.5	25	25	3.49	0	30	0	30.0	3500	3500	0	0.000	0.00	1000	1000	0	0.00	0.00
1.00	20.0	19	19.5		25	3.49	1	0	0	60.0	3500	3500	0	0.000	0.00	1000	1000	0	0.00	0.00
1.00	20.0	19	19.5		25	3.49	2	0	0	120.0	3500	3086	414	8.765	525.92	1000	1250	250	5.29	317.58
			0.0			5.76	2	30	0	150.0	3086		3086	130.675	4446.17	1250		-1250	-52.93	-1270.33
			0.0			5.76	3	0	0	180.0	0		0	0.000	4446.17	0		0	0.00	-1270.33
			0.0			5.76	3	30	0	210.0	0		0	0.000	4446.17	0		0	0.00	-1270.33
			0.0			5.76	4	0	0	240.0	0		0	0.000	4446.17	0		0	0.00	-1270.33
			0.0			5.76	4	30	0	270.0	0		0	0.000	4446.17	0		0	0.00	-1270.33
			0.0			5.76	5	0	0	300.0	0		0	0.000	4446.17	0		0	0.00	-1270.33

Figure 3-11: Excel spreadsheet for data acquisition. The yellow columns populated automatically over time. The blue columns are the calculated results linked to real time plotted charts.

MEMBRANE CHEMICAL CLEANING AND DISINFECTION

Two types of chemical cleaning were used after biological growth was identified in modules left over one month without activity. The first cleaning procedure was a multi-chemical based approach adapted from the recommended Liqui-Cel® application guidelines for “Severe Biological Soil Cleaning Protocol”. The exact cleaning procedure used is detailed in Table 3-6.

Table 3-6: Chemical cleaning used for biological fouling

Chemical Solution	**Time**
Recirculation of pure isopropyl alcohol until permeation on tube side	30 min
Drain contactor	
Recirculation of 5% w/w NaOH solution	2 h
Drain contactor	
Recirculation of 5% w/w citric acid	2 h
Drain contactor	
Rinse with water until pH in = pH out with pH paper	20 min
Drying with warm nitrogen flowing from the tube side to the shell side until warm flow felt on the only shell side port left open. Gas line pressure lower than 0.7 bar and temperature below 55°C	Overnight
Water test by recirculating water on shell side and pressurizing to 4.1 bar and making sure no water permeates to the tube side.	

The second cleaning procedure also used isopropyl alcohol but focused on sanitizing the membrane with chlorine. The procedure involved recirculation of a dilute chlorine solution in the system and through the inline membrane contactors. This disinfection procedure is detailed in Table 3-7.

Table 3-7: Disinfection procedure

Chemical solution	**Time**
Recirculation of pure isopropyl alcohol until permeation on tube side	30 min
Drain contactor	
Rinse contactor with water	20 min
Drain contactor	
Recirculation of a 100ppm chlorine solution (from bleach)	1 h
Rinse with water one pass through 2-3 times	40 min
Drying with warm nitrogen flowing from the tube side to the shell side until warm flow is felt on the only shell side port left open. Gas line pressure lower than 0.7 bar and temperature below 55°C	Overnight
Water test by recirculating water on shell side and pressurizing to 4.1 bar and making sure no water permeates to the tube side.	

Chapter 4: Pure Oil Characterization of a Hydrophobic Microporous Hollow Fiber Membrane Contactor.

ABSTRACT

Membrane technologies developed for the separation of oil-water emulsions have focused on hydrophilic membranes that can become fouled by viscous oil layers that form on the membrane wall surface. On the contrary, hydrophobic membrane technologies are promising in allowing long-term stable performance. The purpose of this paper is to introduce the re-purposing of a commercially available hydrophobic microporous hollow fiber membrane contactor for the recovery of insoluble oil from oil-water mixtures. This new technology overcomes the limitations associated with hydrophilic membrane systems, shows no sign of progressive performance decrease, and is efficient at separating oil and water for a broad range of oil feed concentrations. The current study focuses on characterizing the effect of governing parameters for the base case of pure oil feed on oil permeation across the microporous membrane wall. The experimental results demonstrate that increased transmembrane pressure and available surface area provided a linear improvement in oil permeation across the membrane wall while the viscosity had the inverse linear effect. The oil flux was determined to be independent of the feed rate. Experimental data were compared to typical models of flow through porous media, and the most accurate predictive model was identified for the present membrane contactor. The results presented in this paper set the foundation for the study of oil-water separation in hydrophobic hollow fiber membrane contactors and provide the upper limit of oil flux for oil-water mixtures.

INTRODUCTION

Insoluble oil and water mixtures are generated in the oil and gas, biofuel, and food industries as well as in natural environments contaminated by oil spills. Technologies are needed to separate the oil from the water, in a cost effective and reliable manner, and to obtain high-purity phases for downstream use or reuse. Separation of oil and water is particularly critical in many oil and gas industrial applications where wastewaters such as produced water are generated onshore and offshore and oil concentrations can range from 10 ppmv to 200,000 ppmv depending on the source (*24-27*). The treatment of produced water allows the water to be reused in the oil-extraction system, revalorized for other uses such as irrigation, or released into the environment (*5, 6, 92, 93*). Oil recovery contributes to the economic feasibility of many treatment processes and, in some instances such as biodiesel production (*94*), oil purification is the main objective of the process. Conventional technologies, such as three phase separators, hydrocyclones, flotation systems or mixed media filters, can be used for oil water separation but have lower efficacy for fine oil droplet emulsions and might not provide the needed degree of purity (*24, 44*). Membrane systems have become a popular alternative to traditional separation methods and much research has been undertaken to understand oil-water separation mechanisms (*46-48*). Membranes have the advantages of allowing high purification levels, are a rather inexpensive and flexible technology, and minimize the process footprint and weight for offshore applications (*43, 44*).

While hydrophilic membranes have been widely investigated for produced water treatment (*43, 46, 47, 55, 64*), a major drawback of the technology is the buildup of a viscous fouling layer at the membrane surface, which progressively decreases the efficiency and increases the energy-input of the overall process (*50, 54, 55, 67, 68*). Hydrophilic membranes are typically used to permeate water while oil is retained. Many researchers demonstrated that an increase in transmembrane pressure and influent flow rate increase water flux across hydrophilic membranes (*49-52*) but also potentially lead to

lower oil rejection (*50, 77*). Abadi et al. (*65*) showed that increasing temperature increased water flux by reducing the viscosity of the fouling layer on the membrane surface. Some hydrophobic materials have been investigated as well but were pretreated to allow water permeation and oil retention (*55, 63, 69*) similar to hydrophilic membrane processes.

Hydrophobic membranes have been traditionally used to break oil-water emulsions by coalescence (*59, 60, 84, 89*). Some studies have recently started investigating direct oil-water separations with hydrophobic membranes allowing oil permeation and water rejection (*8, 56*). In an earlier study, Tirmizi et al. (*59*) demonstrated that oil flux increased with increasing transmembrane pressure for hydrophobic membranes. The increase of cross flow velocity was shown to either decrease oil flux across the membrane or not affect the process depending on feed oil concentration. Previous works demonstrated the promising use of hydrophobic systems for reliable oil and water separations; however, the membranes were usually made from experimental materials, were of a small size, or the oil was adsorbed and not recoverable (*58*). Additional research is required to understand the fundamental mechanisms governing the separation of oil and water with larger scale hydrophobic membrane systems.

Early studies conducted with a commercially available hydrophobic membrane contactor that was licensed by the University of Texas to OpenAlgae LLC were conducted at the Separations Research Program (UT-Austin). The research investigated the use of this membrane contactor for the recovery of submicron algae oil from algal slurries. Manufactured by Liqui-Cel®, the contactor was originally developed for liquid-liquid extraction and is now widely used for degasification in the microelectronics industry (*15, 95*). The early oil-water studies consisted in feeding the membrane system with a solution of concentrated non-flocculated lysed algae. The contactor extracted the majority of the available nonpolar oil for most of the feedstocks. A US process patent

(*17*) issued in 2013 provides additional information along with two related patents (*18, 19*). Seibert (*20*) presented additional oil recovery performance data using the membrane contactor over multiple days. Tested with actual applications such as the recovery of nonpolar lipids from saltwater and freshwater micro-organisms, the technology showed promising results for the separation of oil and water. These initial studies showed that, contrary to hydrophilic membrane systems' typical fouling behavior, the hydrophobic microporous membrane contactor performance improved over time to reach high oil recovery (above 95%) with injected oil over a two-week test run. While the studies with actual and simulated feedstocks provided promising results, little was known about the fundamental mechanisms controlling the oil recovery. These initial data, while important, did not provide sufficient understanding to reliably design and engineer an optimized oil recovery system that could be applied to biological and petroleum based oils. As a result, fundamental and controlled studies were needed to evaluate the effects of transmembrane pressure, influent flow rate (residence time), oil concentration, and oil physical properties. The first step in investigating the separation of oil and water with the hydrophobic membrane contactor is to understand the effect of key parameters on the system under the maximized condition of pure oil feed.

A typical model to describe permeation of a single phase through membranes is the Hagen-Poiseuille equation (*96*). For hydrophobic membranes and in the absence of typical viscous membrane fouling, oil permeation mechanisms should follow the Hagen-Poiseuille law (Eq. 4-1) as detailed by Tirmizi et al. (*59*).

$$J = \frac{\varepsilon \cdot d_p^2 \cdot P_T}{32 \cdot L \cdot \mu} = k_{HP} \cdot \frac{P_T}{\mu} \qquad \text{(Eq. 4-1)}$$

Where:
J: flux
d_p: channel diameter (average pore size)
P_T: applied transmembrane pressure
μ: viscosity
ε: porosity
L: channel length (wall thickness)
$k_{HP} = \frac{\varepsilon \cdot d_p^2}{32 \cdot L}$

Other models have also been used to describe the flow of liquids through porous media such as the Ergun equation (*97*). Researchers have applied the Blake-Kozeny viscosity component of the Ergun equation in the case of hollow fibers (*98*) to correlate fiber bundle permeability to pressure drop and viscosity. The equation is typically used to model flow through sphere-packed columns but has been used successfully in other applications. The Blake-Kozeny equation applied to a hollow-fiber bundle results in Equation 4-2.

$$J = \frac{P_T \cdot d_p^2 \cdot \varepsilon^3}{A \cdot L \cdot \mu \cdot (1-\varepsilon)^2} = k_{BK} \cdot \frac{P_T}{\mu} \qquad \text{(Eq. 4-2)}$$

with A=150, d_p: Equivalent particle diameter and $k_{BK} = \frac{d_p^2 \cdot \varepsilon^3}{A \cdot L \cdot (1-\varepsilon)^2}$

In an early study, Macdonald and al. (*97*) pointed out the variability of A with change in particle shape, particle size, and porosity for flow through porous beds and suggested using A=180 instead of 150. With this correction, the Kozeny-Carman equation is obtained for the case of a packed bed of spherical solids, which has been applied to membrane flux predictions (*99*). In recent studies, Pacella et al. (*98*) and Madhani et al. (*100*) applied the Blake-Kozeny equation to hollow fiber bundles to refine the correlation of A with porosity and proposed linear correlations between A and ε. Such correlations allow to refine the application of the Blake-Kozeny equation to media with various porosities.

The purpose of the present work is to fundamentally characterize the hydrophobic hollow fiber membrane contactor for oil and water separation and evaluate the potential for oil permeation without hydrocarbon fouling of the membrane surface. Characterization of the system under pure oil conditions will serve as a baseline for determining the maximum oil permeation attainable with the membrane contactor under various operating conditions. Development of a model that describes membrane behavior

under various operating conditions and captures the impact of poorly quantified parameters such as porosity is also a significant goal of the research. To our knowledge only one other study investigated the use of hydrophobic hollow fiber membranes for the permeation of oil in oil-water separation (*59*), and additional work is required to understand the fundamental mechanisms of oil-water separation with such systems.

MATERIALS AND METHODS

Membranes

The membranes used in this study are manufactured by Liqui-Cel® (USA) and commercially available under the name Liqui-Cel® Extra Flow. The modules are composed of hydrophobic microporous hollow-fibers with a central baffle to eliminate shell side bypassing and evenly distribute fluid perpendicularly to the fibers. Modules with different intrinsic characteristics were investigated and are detailed in Table 4-1. Membranes A and B have the same module sizes, but the hollow fibers are spaced more widely for Module B to obtain a surface area half of Membrane A. Fiber types X50 and X40 differ in porosity and wall thickness. Membrane D has a different module size and hence presents longer fibers with larger surface area.

Table 4-1 : Membrane Geometry.

Module Name	Module size (diameter x length) (inch)	Fiber Type	Total Surface area (m^2)	Porosity (%)	Wall thickness (μm)	Pore size (μm)
A	2.5x8	X50	1.4	40	40	0.04
B	2.5x8	X50	0.7	40	40	0.04
C	2.5x8	X40	1.4	25	50	0.03
D	4x28	X50	20	40	40	0.04

All of these membranes have the same design, which is a polypropylene hollow-fiber flat sheet rolled into a cylindrical casing allowing pseudo cross-flow filtration.

While a distribution of pore sizes exists, the average measured pore size was 0.04 μm and 0.03 μm for the X50 and X40, respectively. The region outside of the fibers is referred to as the "shell side", while the volume inside is the "tube side" (Figure 4-1). Four ports allow the distribution of the fluid in and out of the module; two ports for each side.

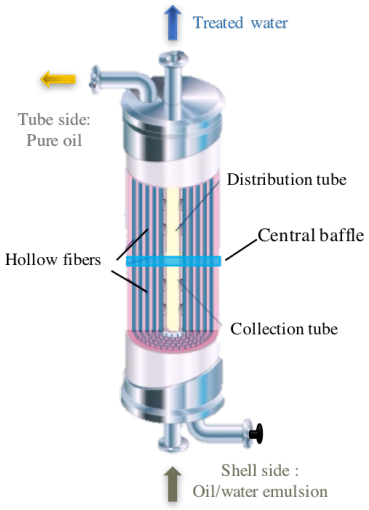

Figure 4-1: Extra flow Liqui-cel® membrane contactor in for oil-water separation configuration. Drawing adapted from Liqui-Cel®.

Reagents

Three Isopar™ oils manufactured from ExxonMobil (USA) were used to simulate hydrocarbons of produced water. The Isopar™ oils are controlled paraffinic mixtures and exist in different grades with varying viscosities as detailed in Table 4-2.

Table 4-2: Viscosities at 25°C of Isopar™ grades used for the study.

Isopar™ grade	Viscosity (cP)
Isopar™ L	1.5
Isopar™ M	3.5
Isopar™ V	10.7

The effect of temperature on viscosity was measured for all three grades of Isopar™ with a modular compact rheometer (Paar Physica MCR300, USA). The results

presented in Figure 4-2 were used to estimate oil viscosity during experiments with varying temperature conditions.

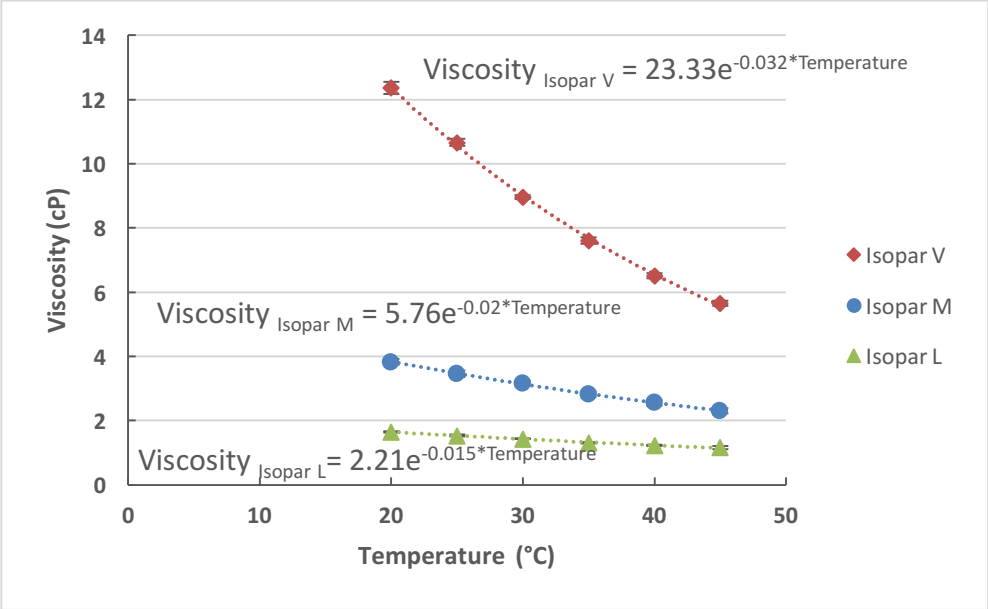

Figure 4-2 : Viscosity vs temperature for three Isopar™ grades. Legend: symbols = experimental data, dotted lines = best fit: exponential correlation. All experiments were conducted in triplicate; error bars are shown but are frequently smaller than the data symbols.

Experimental System

Figure 4-3 shows the schematic of the membrane system operated with pure oil. The feed was distributed through the system with a high shear pump (MTH pump, USA), and entered the membrane from the shell-side lower port. The retentate was sent back to the feed tank, while the permeate was collected in a graduated glass cylinder for quantification. The needle valve located downstream of the membrane module was used in coordination with the pump variable speed drive (Emerson, USA) to control transmembrane pressure and influent flow rate. The transmembrane pressure was calculated from the reading of two pressure gauges (Solfrunt, USA). No pressure gauge was used on the membrane tube side since it was left open to the atmosphere and oil

exited the system by gravity. The influent flow rate was measured with a MicroMotion flow meter (Emerson, USA). Temperatures were obtained using a Rosemount RTD sensor (Emerson, USA).

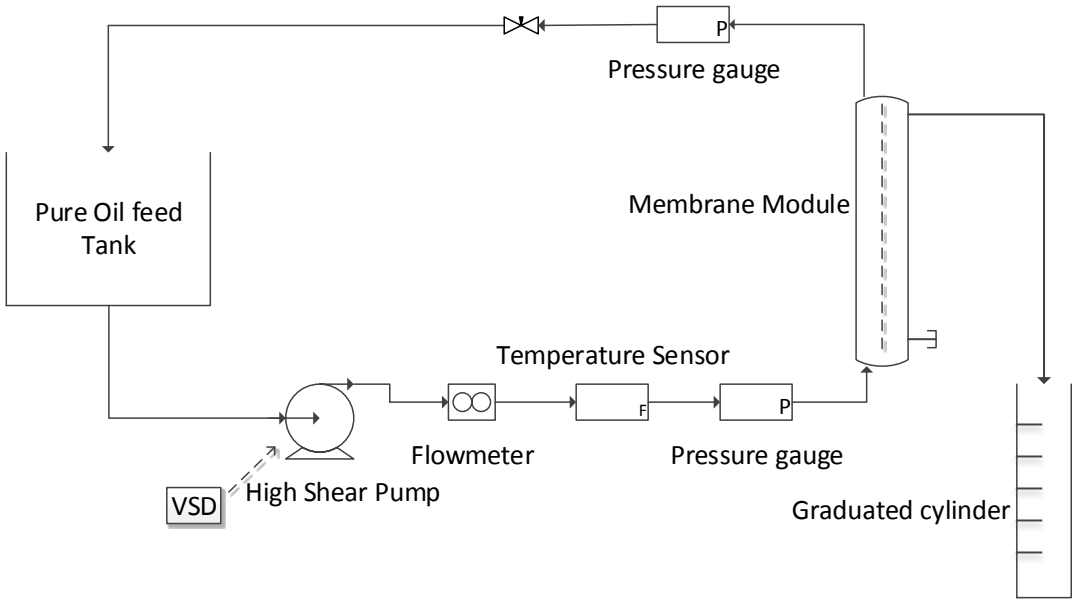

Figure 4-3: Schematic of membrane system used for pure oil experiment.

Experimental Procedure

Characterization of the 2.5x8 inch diameter modules involved recirculating pure Isopar™ through the system. The transmembrane pressure and influent flow rate were adjusted and maintained for the duration of the experiment and permeated oil was collected and quantified either with a graduated cylinder and stop watch or a weigh-scale and stop watch. At first, experiments conducted with the graduated cylinder were run until 12 liters had permeated across the membrane with time measurements recorded every liter. Once repeatability over time was demonstrated, experiments were conducted for 8 liters of oil permeated or 15 min. Mass was measured every 1.5 min using a scale.

For the larger membrane contactor, 4x28 inch modules, the oil permeation rate was measured with a Micro Motion flow meter (Emerson, USA) for a duration of 10 min with flow measurements recorded every minute. In both cases, transmembrane pressures were calculated as the average of the inlet and outlet pressure of the shell side. All experiments were performed in triplicate. Table 4-3 summarizes the conditions of all experiments conducted.

Table 4-3: Experimental conditions tested for membranes A, B, C, and D.

Membrane type	Isopar™ grade	Influent oil flow rate (L/min)	Transmembrane pressure (bar)
2.5-inch modules (A, B, and C)	L	3.8	1.4, 2.8, 4.1
	M	1.9	1.4, 2.8, 4.1
		3.8	0.7, 1.4, 2.1, 2.8, 3.4, 4.1
		5.7	1.4, 2.8, 4.1
	V	3.8	1.4, 2.8, 4.1
4-inch module (D)	M	11.3	1.4, 2.8, 4.1
		19.0	0.7, 1.4, 2.1, 2.8, 3.4, 4.1
		26.6	1.4, 2.8, 4.1

Pure oil operation of the polypropylene membrane contactor was found to present some risk. A clicking noise was detected and identified as static discharge in the system. Friction along the fibers with elevated influent flow rate and the lack of a conductive material resulted in the build up of an electrical charge in the module, which released periodically through a spark. Adequate grounding of the system and addition of a conductive element to the fluid is necessary for safe operation under pure oil conditions. To prevent the reoccurrence of static charging, minimal amounts of water were added to the feed. The only experiments with added water presented here were conducted with Membrane B.

RESULTS AND DISCUSSION

The results of this research fall within three different studies. First, the effect of operating parameters, such as temperature, viscosity, transmembrane pressure, and influent flow rate, were studied with the 2.5 inch diameter X50 small module Membrane A. Then, the performance observed between the various module contactors (Membrane A, B, C, and D) were compared to investigate the effect of intrinsic membrane characteristics such as module size, surface area, and fiber type. Finally, the data were used to derive a model describing oil permeation in the membrane system.

Effect of Operating Parameters on Membrane Performance

Temperature and Viscosity

Oil viscosity change with temperature variations were measured and correlated for each Isopar™ grades as shown in Figure 4-2. These viscosity variations affect pure oil experiments on two levels. Using the three different grades of Isopar™ results in intrinsic different viscosities between experiments. However, within one experiment where a single Isopar™ grade is used, the viscosity was also observed to fluctuate due to temperature variations. Daily temperature changes and heat buildup due to pipe friction and pump recirculation explain variations in viscosity during a single experiment with a fixed set of conditions (fixed Isopar™ grade, transmembrane, flow rate). Figure 4-4 shows the effect of viscosity on oil permeation under different experimental conditions. The data demonstrate that even within triplicates, where the same Isopar™ grade was used, viscosity varied because of ambient temperature variation. The results suggest that oil flux is linearly related to the inverse of viscosity with coefficients of correlation higher than 0.99 for all three sets of conditions. Such a trend was expected since a fluid with higher viscosity creates a higher resistance to permeation from friction when contacting the pore walls as described by the Hagen-Poiseuille equation (*96*). The plot

additionally shows viscosity variations for a single Isopar™ grade due to temperature changes. To account for temperature changes between experiments, oil flux was subsequently corrected by multiplying viscosity and expressed in m^3-cP/m^2-s. Figure 4-4 also shows that higher transmembrane pressures improved oil permeation.

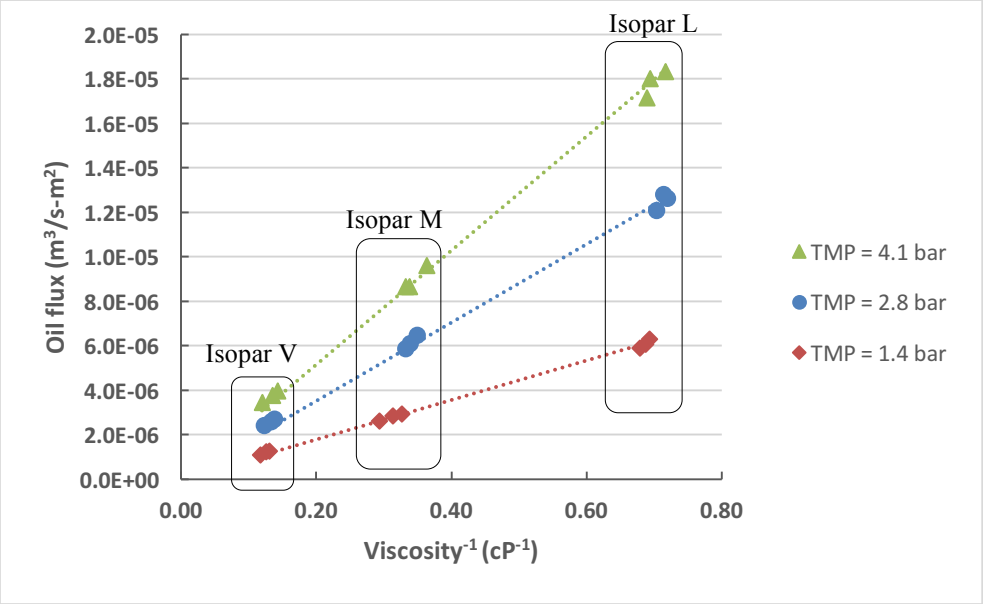

Figure 4-4: Effect of Viscosity on Oil Permeation. Legend: symbols = experimental data, dotted lines = linear best fit. Experimental Conditions: Isopar L, M, V; Influent flow rate = 3.8 L/min; Membrane A

Transmembrane Pressure

To further explore the impact of transmembrane pressure, oil flux was measured for various transmembrane pressures applied across the fibers of membrane A, while influent flow rate and Isopar™ grade were held constant. Each experiment was run in triplicate and showed good repeatability with a maximum coefficient of variation of 2.9%. The results shown in Figure 4-5 demonstrate a linear correlation between oil flux (corrected for viscosity) and transmembrane pressure with a correlation coefficient greater than 0.99. The permeation of oil is directly related to the force applied on the liquid contacting the membrane wall and pores. Tirmizi et al. (*59*) observed the same

linear correlation between transmembrane pressure and oil flux across hydrophobic membranes for a pure oil system as predicted by the Hagen-Poiseuille equation. However, it was also shown that the relationship between transmembrane pressure and flux changed as the mixture was converted from a continuous oil phase to a continuous water phase in the case of oil-water mixtures. Thus, the relationship shown in Figure 4-5 should only be applied to systems containing pure oil.

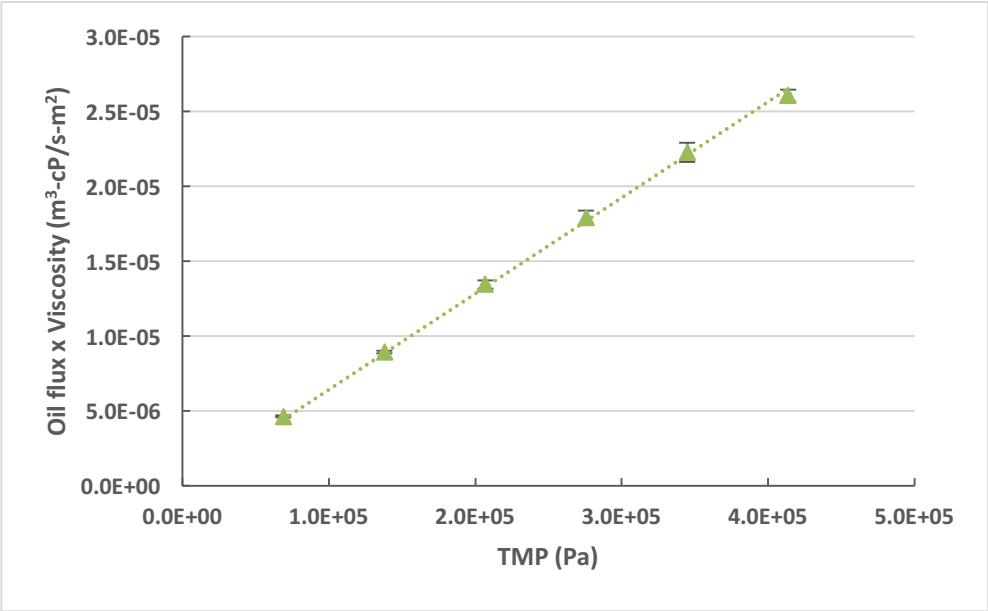

Figure 4-5: Effect of transmembrane pressure on oil flux corrected for viscosity. Legend: symbols = experimental data, dotted lines = linear best fit. Experimental conditions: Isopar™ M, Influent flow rate = 3.8 L/min; Membrane A. All experiments were conducted in triplicates; error bars are shown but are frequently smaller than the data symbols.

Influent Flow Rate

Experiments with three influent oil flow rates were conducted to determine the effect of detention time on oil permeation across the membrane. The results presented in Figure 4-6 show that regardless of the flow along the membrane walls, the oil permeated across the fibers was constant. Variations between all three sets of experiments did not exceed 2.6%. When running under pure oil conditions, the membrane is only in contact

with a single phase which allows complete wetting of the hollow-fibers. Theoretically, the total membrane surface area is effective for the pure oil tests. When working with oil-water mixtures, the influent flow rate is expected to impact the oil flux across the membrane as two phases will be in contact with the fiber surface. The effective surface area will be reduced and the chance of contacting oil drops to the membrane wall will strongly depend on the volume fraction of oil in the feed and residence time in the system. Thus, when water is added to the feed, it is expected that the influent flow rate will affect oil permeation by changing the detention time of the oil droplets in the system.

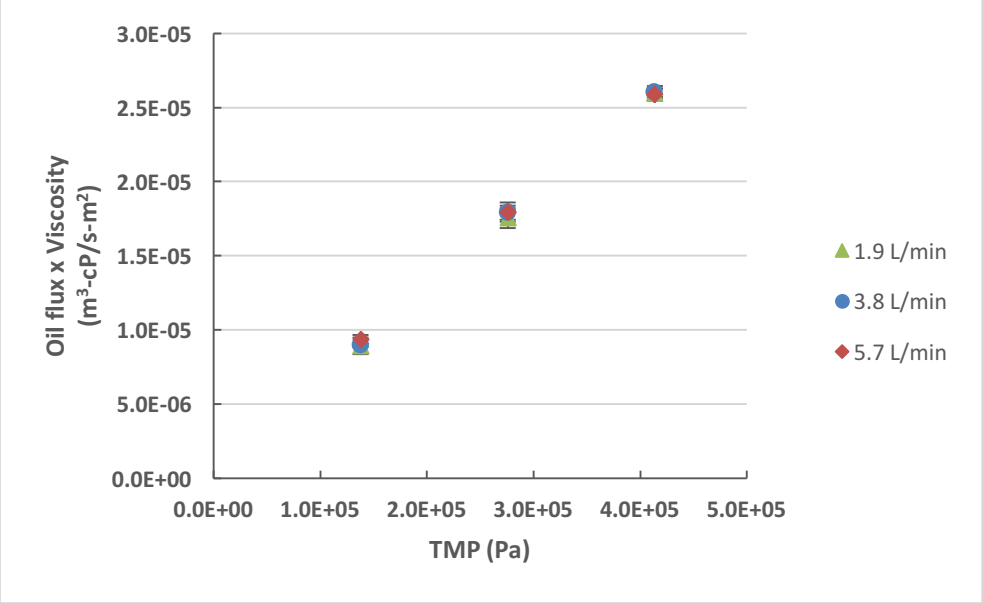

Figure 4-6: Effect of influent flow rate on oil flux corrected for viscosity. Experimental conditions: Isopar™ M, Membrane A. All experiments were conducted in triplicates; error bars are shown but are frequently smaller than the data symbols.

Effect of Membrane Characteristics on Performance

Surface Area

Membrane B utilizes the same design (casing and fiber length) but contains half the surface area of Membrane A. In Membrane B, the fibers are twice as far apart from each other as in Membrane A. Experiments were conducted on both membranes to

observe the effect of surface area on oil permeation. The results, presented in Figure 4-7, clearly show that the effects of transmembrane pressure and influent flow rate on Isopar M oil flux are consistent. Differences between the fluxes for the two membranes do not exceed 6.5% which falls within the standard deviations of the data sets (Figure 4-7).

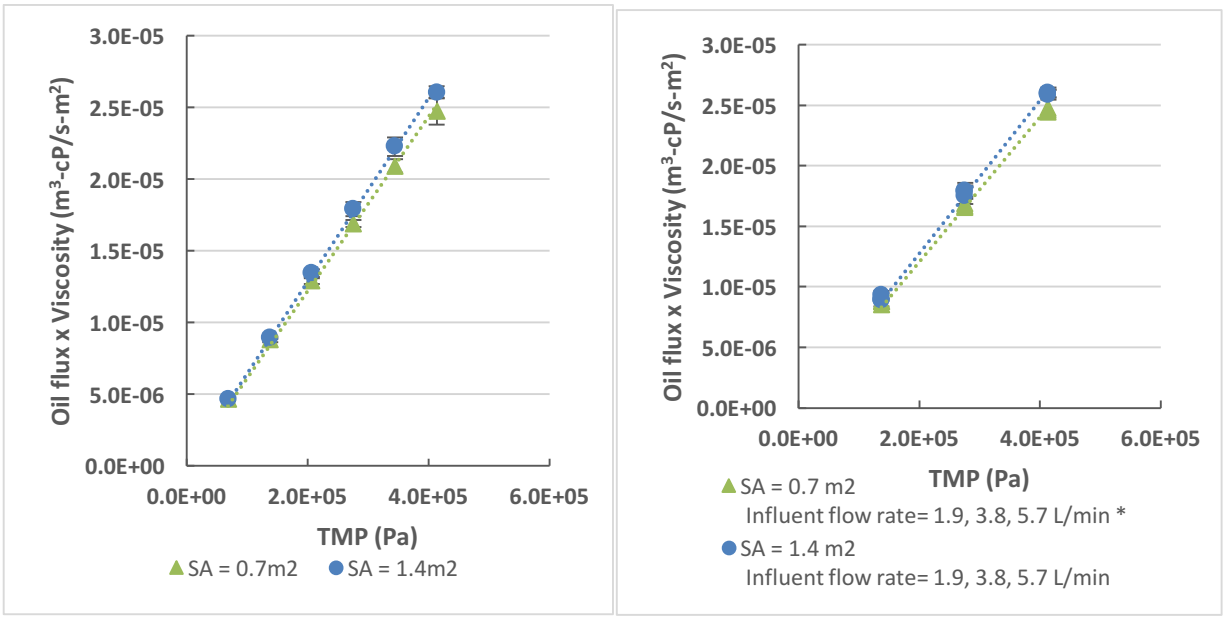

Figure 4-7: Comparison of module surface areas for oil flux vs transmembrane pressure. Legend: symbols = experimental data, dotted lines = linear best fit. Experimental conditions: Isopar™ M, Influent flow rate = 3.8 L/min unless stated otherwise, Membrane A and B. All experiments were conducted in triplicates; error bars are shown but are frequently smaller than the data symbols. Except for *, single replicate.

According to these observations, the Isopar M pure oil flux appears to be proportional to the membrane surface area. However, the relationship between oil flux and viscosity as a function of membrane surface area was more variable (Figure 4-8). The differences between the slopes of linear regression for surface areas of 0.7 m^2 and 1.4 m^2 were as high as 12.8%. Since results observed in Figure 4-4 suggest a strong linear correlation between oil flux and viscosity at a given surface area, and data in Figure 4-7 show linear dependence between oil flux and transmembrane pressure, such variability

may be attributed to experimental error. For the 0.7 m^2 module experiments, water at ppmv levels was added to the pure oil feed after identification of static charging possibly increasing the variability of the results and decreasing oil flux as observed in Figure 4-8. Therefore, as suggested by results, the effective surface area seems to equate to the available surface area in the case of pure oil feed for membranes of the same size. Such findings allow prediction of oil flux values when operating conditions, membrane size, and surface area are known.

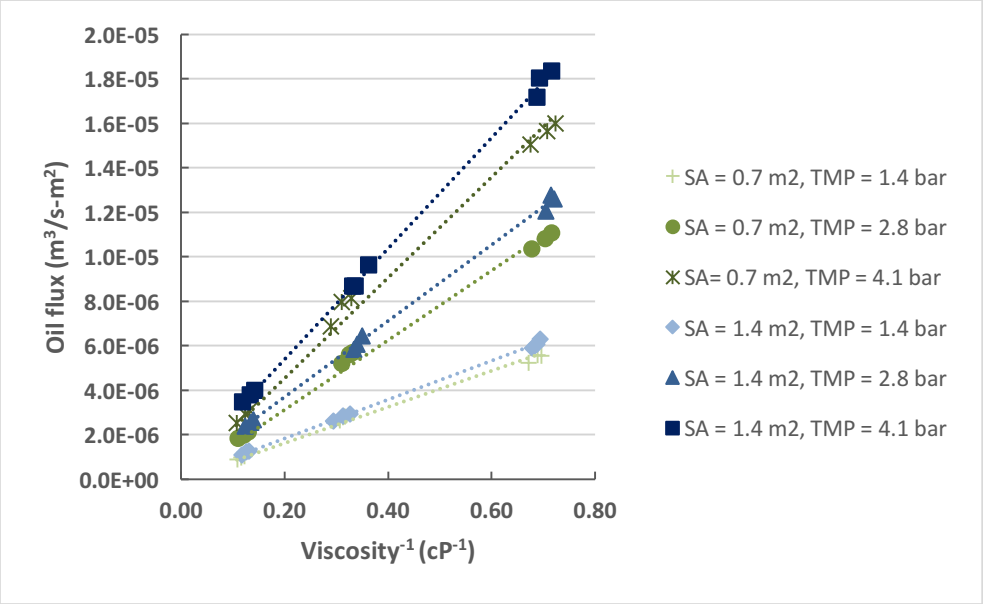

Figure 4-8: Comparison of module surface areas for oil flux vs viscosity. Legend: symbols = experimental data, dotted lines = linear best fit. Experimental conditions: Isopar™ L, M and V, Influent flow rate = 3.8 L/min, Membrane A and B

Module Size

The membrane modules used in this study are commercially available for a range of module sizes. Pure oil experiments were conducted on both 2.5 inch-diameter x 8 inch-length and 4 inch-diameter x 28 inch-length modules. The effects of transmembrane pressure and influent flow rate on oil flux were studied for both module sizes and the results are shown in Figure 4-9. The oil flux obtained for the larger module was

consistently lower than those for the smaller module regardless of the experimental conditions. The difference in slopes obtained from linear regressions of oil flux versus TMP for the two module sizes is 29.0%. That variability is higher than any observed error in our experiments suggesting that experimental error is not responsible for the differences observed. A possible explanation for such findings is module geometry. The larger module, not only has a higher surface area (20 m^2) but also contains longer fibers compared to the smaller module. The module was placed vertically during experimentation and the permeated oil overflowed through the top port of the tube side to avoid short-circuiting. Therefore, the pressure on the tube side at the bottom of the larger module is expected to be higher than for shorter fibers due to static pressure. Differences in internal pressure between the large and small module could not be measured since it occurs inside the module and cannot be detected at the tube side port. The approximate difference in fiber lengths between the small and the large module is 53 cm contributing to an estimated maximum static pressure of 4091 Pa at the bottom of the module. Therefore, the error due to static pressure could only contribute up to 6% in the flux. However, the pressure drop along the fibers in the larger module may also contribute to a lower internal pressure on the tube side, reducing the actual transmembrane pressure and leading to lower performance of the membrane. Additionally, in a study on flow patterns in hollow fiber membranes, Chang et al. (*101*) revealed the effect of air bubbles strongly attached to the fiber walls called dry points. The presence of those points may be reducing the effective surface area during pure oil permeation. In the case of the larger modules, the length of the fibers may also contribute to a more difficult release of the enclosed air bubbles, therefore, reducing the available surface area and flux across the membrane. Further research is warranted to evaluate this hypothesis.

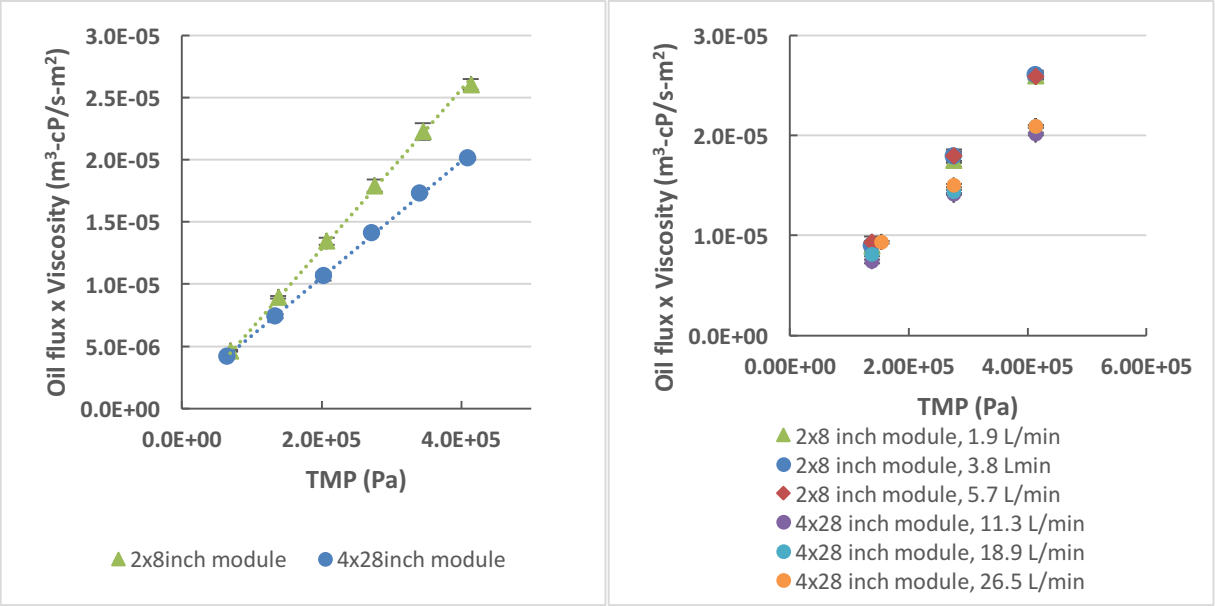

Figure 4-9: Comparison of module sizes for oil flux vs transmembrane pressure. Legend: symbols = experimental data, dotted lines = linear best fit. Experimental conditions: Isopar™ M, Influent flow rate = 3.8 L/min unless stated otherwise, Membrane A and D.

The results shown in the previous section suggest that when increasing the available surface area, the oil flux increases proportionally for a given membrane size. In addition, the latter findings suggest that fiber and, therefore, module lengths play an important role in the relationship of transmembrane pressure and oil flux.

Fiber Type

The membranes used are manufactured with two types of fibers identified as X40 and X50. The X50 fiber has a porosity of approximatively 40% and a wall thickness of 80 µm, while the X40 has a lower porosity of approximatively 25% and a thicker wall of 100 µm. Figure 4-10 shows the comparative results between X50 and X40 fibers for various transmembrane pressures and influent flows. As expected from observation of the Hagen Poseuille and Ergun predictions, the oil flux measured was lower for the X40 than the X50 membranes for a same set of operating conditions. The difference between the

X40 and X50 fiber performance can be compared to predictive models accounting for differences in porosity and wall thickness.

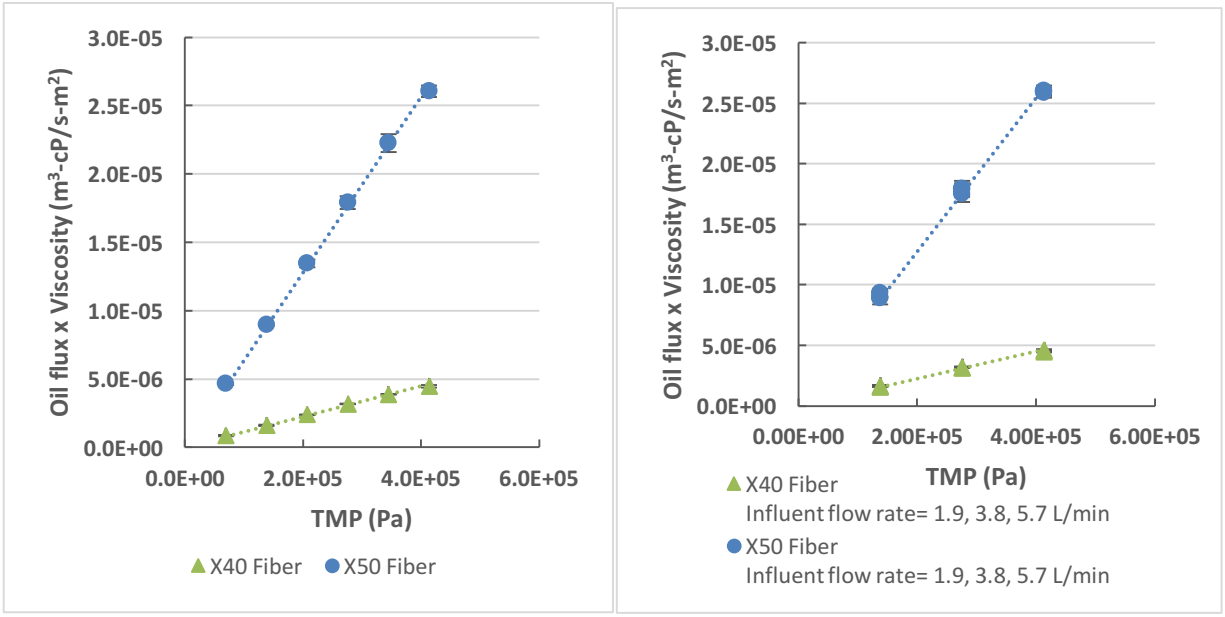

Figure 4-10: Comparison of fiber type for oil flux vs transmembrane. A) Influent flow rate = 3.8 L/min. B) Influent flow rate = 1.9, 3.8, and 5.7 L/min. Experimental conditions: Isopar™ M, Membrane A and C.

Model

The results presented in Figure 4-4 to Figure 4-10 demonstrate the linear correlation between transmembrane pressure, inverse viscosity, and oil flux as represented in Equation 4-3. Influent flow rate was also confirmed to have no significant impact on the process for pure oil conditions. Those observations are in agreement with the Hagen-Poiseuille and Kozeny-Carman models.

Model describing oil permeation for X50 2.5 inch modules:

$$Oil\ Flux = k \cdot \frac{P_T}{\mu} \qquad \text{(Eq. 4-3)}$$

Using the data obtained with Membranes A and C, the experimental permeability constants k can be computed and results are shown in Table 4-4.

Table 4-4: Permeability constants for X50 and X40 fibers

Fiber Type	X50	X40
Porosity	0.4	0.25
Wall thickness (µm)	40	50
Average pore size (µm)	0.04	0.03
Experimental permeability constant k (m)	6.5E-14	1.1E-14

The Hagen-Poiseuille and Kozeny-Carman permeability constants for each fiber type were computed. The equivalent particle diameter used for the Kozeny-Carman equation was determined with the assumption that the porous membrane surface is equivalent to packed spheres with interstices being the pores. Derived from the definition of porosity, the equivalent mean particle diameter is shown in Equation 4-4.

$$d_p = d_{pore} \cdot \left(\frac{1-\varepsilon}{\varepsilon}\right)^{\frac{1}{3}} \quad \text{(Eq. 4-4)}$$

Pacella et al. (*98*) and Madhani et al. (*100*) studied the flow of liquids between hollow fiber bundles and proposed adjusting the constant A with varying bundle porosity for a porosity range of 0.4 to 0.8. The equations proposed by the two studies are A_1 = 542*ε-128 and A_2 = 497*ε-103 respectively. Table 4-5 presents the permeability constants for each of these models with adjusted A values for both X50 and X40 fibers. The Hagen Poiseuille model largely overestimates the experimentally determined constants. The model is usually accurate for describing flux through membranes with parallel pores. However, membrane pores often present more complex pore geometry.

Table 4-5: Permeability constants for X50 and X40 fibers determined with the various models

		Hagen-Poiseuille Model	Blake-Kozeny Model			
			A=150	A=180	Correlation A_1	Correlation A_2
X50	k_{model} (m)	5.0E-13	6.2E-14	5.2E-14	1.0E-13	9.7E-14
	$k_{experimental}/k_{model}$	0.13	1.05	1.26	0.62	0.67
X40	k_{model} (m)	1.4E-13	6.9E-15	5.8E-15	1.4E-13	4.9E-14
	$k_{experimental}/k_{model}$	0.08	1.65	1.98	0.08	0.23

Therefore, models describing flow through porous media can lead to better membrane flux predictions (*99*). The Blake-Kozeny permeability constants are closer but none of the tested models predict the change of permeability from X50 to X40 fiber correctly. The Blake-Kozeny model with A=150 seems to be the best fit for the X50 fibers. The parity plot is presented in Figure 4-11 and shows good agreement between experimental and predicted values from the Ergun model for the X50 fiber with a coefficient of correlation greater than 0.99.

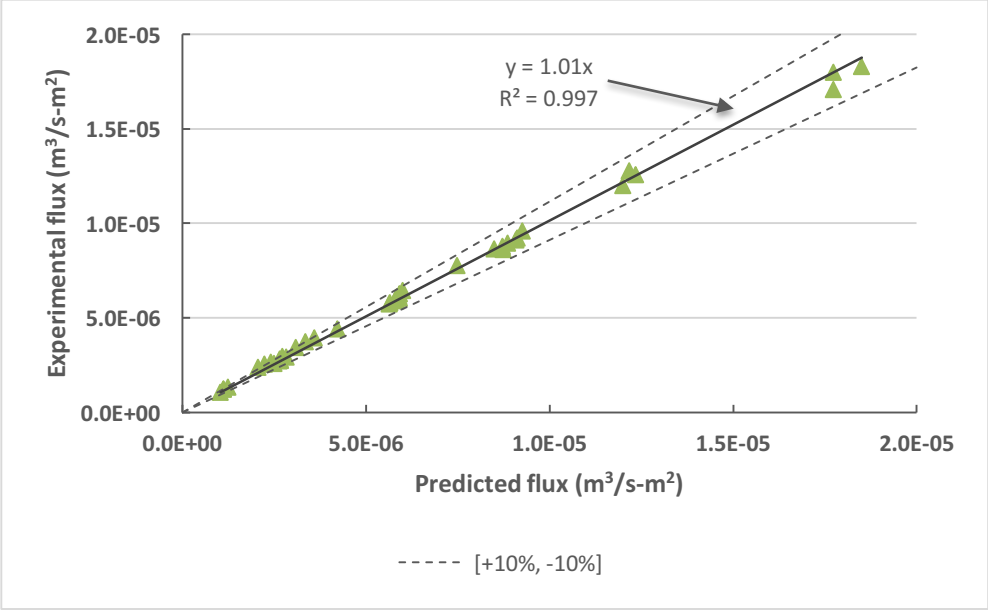

Figure 4-11: Parity plot for the X50 fiber membrane contactor data set.

The X40 fiber experimental results seem to not be well described by any of the presented models. The porosity of the X40 fibers is 0.25, which lies below the range usually studied (*98*). In an early study, Macdonald et al. (*97*) pointed out the importance of adjusting the constant A with various particle shape, equivalent particle size, and porosity. Therefore, additional experimental work would be needed to refine the correction of the A constant in the Blake-Kozeny equation to describe flux through membrane pores.

CONCLUSIONS

In the past, the use of hydrophobic hollow fiber membrane contactors for oil-water separation has not been extensively investigated. However, the technology shows significant potential for separation of oil and water. Under the baseline conditions of a pure oil feed it was possible to identify the impact of key operating parameters on oil flux. These impacts include:

- Higher viscosity was shown to linearly decrease the permeation of oil across the membrane contactor. Oil viscosity is related to temperature, which can, therefore, also change the system performance.
- An increase in transmembrane pressure was observed to linearly improve oil flux across the membrane.
- Influent feed flow rate was shown to have no effect on oil permeation. The membrane fibers were in contact with a single oil phase and, therefore, oil permeation was independent of retention time.
- A decrease in half the available membrane surface area proved to yield proportionally lower oil flux.

- Scale up between modules with different fiber length to surface area ratios was not solely based on scaling the surface areas. The smaller module performed more efficiently.
- X50 fibers were shown to allow higher oil flux over X40 fibers due to higher porosity and thinner walls. Therefore, the X50 fibers are recommended for future use in oil-water separation.
- Various predictive permeation models were compared to the measured experimental permeability. The most accurate model for the X50 fiber permeability was the Blake-Kozeny equation with the original Ergun constant of 150 as shown in Equation 4-5 below.

$$Oil\ Flux = \frac{P_T \cdot d_{pore}^2 \cdot\ \varepsilon^3 \cdot \left(\frac{1-\varepsilon}{\epsilon}\right)^{2/3}}{150 \cdot L \cdot \mu\ (1-\varepsilon)^2} \qquad \text{(Eq. 4-5)}$$

- The X40 fiber permeability could not be properly predicted by the models since the viscosity was out of the usual studied range. Additional research is needed to develop a correction for the A constant to fit lower porosity membranes. The identification of the model best describing permeability for the X50 fiber will allow predictions of the maximum oil flux and will be helpful in evaluating oil-water separation performance of the hollow fiber membrane contactor. Furthermore, the model can also be used as a performance guideline when utilizing the technology for oil purification purposes in the case of low water content in the feed.

EXAMPLE CALCULATION

Inputs:

Membrane material: Pore size $= 0.04 \cdot 10^{-6}\ m$

Porosity $= 0.4$

Wall thickness $= 40 \cdot 10^{-6}\ m$

Process:

Oil Viscosity $= 4$ cP $= 4 \cdot 10^{-3}\ Pa/s$

TMP $= 1.5$ bar $= 1.5 \cdot 10^{5}\ Pa$

Oil flux calculation:

$$Oil\ flux = \frac{TMP \cdot {d_{pore}}^2 \cdot (\frac{1-\varepsilon}{\varepsilon})^{\frac{2}{3}} \cdot \varepsilon^3}{150 \cdot L \cdot \mu \cdot (1-\varepsilon)^2}$$

$$= \frac{(1.5 \cdot 10^5) \cdot (0.04 \cdot 10^{-6})^2 \cdot (\frac{1-0.4}{0.4})^{\frac{2}{3}} \cdot 0.4^3}{150 \cdot (40 \cdot 10^{-6}) \cdot (4 \cdot 10^{-3}) \cdot (1-0.4)^2}$$

$$= \frac{(2.01 \cdot 10^{-11})}{(8.64 \cdot 10^{-6})}$$

$$= 2.32 \cdot 10^{-6}\ m/s$$

Chapter 5: New Application of a Microporous Hydrophobic Hollow Fiber Membrane Contactor for Oil-Water Separation.

ABSTRACT

Efficient oil-water separation is important in many industries. Treatment of produced water, for instance, requires technologies capable of withstanding variable feeds and removing micron size oil droplets while maintaining long term performance. In this study, the fundamental mechanisms and key process parameters controlling the separation of oil and water in a hydrophobic, hollow-fiber membrane contactor are evaluated. Two ranges of oil feed concentration were identified. For high oil feed concentrations above 40% (v/v), increases in transmembrane pressure, detention time, and temperature were shown to increase oil flux across the fiber walls, which is consistent with the results from pure oil experiments (Chapter 4). However, for dilute mixtures (less than 2% (v/v)), experimental results indicate that an increase in transmembrane pressure and temperature lowered oil flux. The design of each membrane module appeared to allow internal coalescence of oil droplets on the fiber surface followed by permeation of insoluble oil while maintaining water rejection. The results suggest that the stable formation of an oil film on the fiber walls is critical to the success of the process. In addition, several experiments carried out over two-week periods showed no signs of viscous fouling or flux reduction, suggesting that stable, long-term operation is possible.

INTRODUCTION

Oil-water separations are essential in processes associated with food, biochemical and chemical production as well as in the oil and gas industry. In particular, produced water treatment is driven by regulations controlling well disposal and environmental releases (*21, 22*) as well as by the financial interest in recovering oil contained in the wastewater. New technologies are needed to treat the oil and gas wastewater in an affordable and efficient way (*24*). Membrane technologies show great promise for oil removal in produced water as they are affordable, flexible, have a small footprint (*44*) and can recover small oil droplets not captured by conventional technologies (*63*). Many types of membrane systems have been investigated for oil-water separation including microfiltration (*46, 49-51*), ultrafiltration (*52-54*), nanofiltration (*45*), as well as a broad range of hydrophilic (*43, 46, 47, 55*) and hydrophobic (*8, 56-60*) materials.

Membranes can be used for oil-water separation through direct separation or coalescence followed by gravity settling. Direct separation of oil and water is achieved in a membrane system through sieving and membrane material selectivity (*46, 50, 63*). For hydrophilic membrane surfaces, water is permeated through the pores while oil is rejected by the membrane material. For hydrophobic materials, the oil permeates and water is rejected. Padaki et al. (*64*) identified several process parameters that control oil and water separation in membranes including cross-flow velocity, transmembrane pressure, temperature and oil concentration in the feed (*61, 63, 64*). Mueller et al. (*61*) and later Chakrabarty et al. (*63*) demonstrated that with increasing transmembrane pressures, water flux through hydrophilic membranes increases. However, higher oil concentrations in the emulsion were shown to reduce water permeation across the membrane wall because of the progressive build-up of a viscous fouling layer at the hydrophilic membrane surface. This phenomenon has proven to limit the long-term removal efficiency and increase the energy requirements in hydrophilic systems. A higher cross-flow velocity was shown to enhance water flux by disturbing the viscous layer at the membrane surface. Many

research studies have focused on understanding the underlying mechanisms (*46, 50, 51, 102-104*) controlling viscous fouling and enhancing membrane surfaces to improve oil removal (*55, 57, 64*) in hydrophilic systems.

Similarly, Tirmizi et al. (*59*) demonstrated that oil flux increases through hydrophobic membranes with increasing TMP, as predicted by the Hagen-Poiseuille model. Lower oil concentrations were shown to decrease oil permeation because of a reduced probability for oil droplets to contact the membrane wall. Increasing cross flow velocity was found to increase oil flux across the membrane. A single phase of oil could be recovered along with high effluent water quality for a concentration of 1% (v/v) oil.

Nazzal and Wiesner (*76*) and Cumming et al. (*75*) demonstrated that, for hydrophilic membrane systems, when transmembrane pressure reaches a critical breakthrough value, permeation of both phases can occur for cross-flow or dead-end filtrations. As a result, applying a transmembrane pressure below the critical breakthrough value is necessary to obtain a pure permeate for both hydrophobic and hydrophilic materials used for conventional membrane filtration of oil and water. However, the effect of critical pressure breakthrough and dual phase permeation has also been used for enhanced oil-water separation through membrane coalescence (*60, 82-85, 88*). The membrane system is usually operated in dead-end or cross-flow filtration mode. The oil-water mixture is forced through the pores and oil droplets coalesce by contacting the pore wall leading to higher oil droplet sizes. As a result, subsequent gravity separation is enhanced. Hlavacek (*88*) demonstrated the increase in droplet size after permeation through a polypropylene membrane. A higher transmembrane pressure (TMP) increased permeation rates and improved coalescence and time of settling, while an increase in temperature allowed higher permeation and better separation efficiency. Microchannel studies were conducted to simulate and observe coalescence mechanisms at pore scale and identify important parameters (*86, 105*). Kawakatsu et al. (*86*) used a see-through microchannel to observe coalescing and phase inversion mechanisms of triolein droplets

in water while permeating a hydrophobic PTFE pore. The formation of larger oil droplets was observed, which aided the subsequent oil-water gravity separation. De-emulsification efficiency improved with oil concentration and flow rate in the micro-channel corresponding to operating a membrane with higher transmembrane pressure. Chen et al. (*105*) also demonstrated that longer channels led to longer contact times and higher coalescence efficiency. Furthermore, several researchers including Kawakatsu (*86*), Hoffman (*60*), and Hong (*89*) emphasized the importance of operating with pore sizes small enough for the oil droplets to be able to contact the membrane surface but not so small as to re-disperse the emulsion.

Various membrane configurations have been tested for the separation of oil and water including flat sheet (*46, 50, 55*), tubular (*43, 52, 106*), spiral (*107*) and hollow fiber (*59, 88, 103*). However, most of the work conducted was with hydrophilic material for water permeation and oil rejection. To our knowledge, only one study investigated the permeation of oil through hydrophobic hollow fiber membrane contactors (*59*). Tirmizi et al. (*59*) showed promising results for oil-water separation with hydrophobic membranes; however the module sizes and the operating parameter ranges such as transmembrane pressure, oil concentration or influent flow rates were limited.

The purpose of the present study is to introduce the use of a commercially available, hydrophobic, hollow-fiber membrane contactor for the separation of oil and water. Early studies conducted with the membrane contactor that was licensed by the University of Texas to OpenAlgae LLC were conducted at the Separations Research Program (UT-Austin). The research investigated the use of the microporous membrane contactor for the recovery of submicron lipids from saltwater and freshwater microbial mixtures, including concentrated lysed microalgae slurries (*17-19*). The membrane contactor extracted the majority of the available nonpolar oil for most of the feedstocks. Backed by this success, additional mixtures were tested for up to two weeks (*20*) and demonstrated an increase of performance over time to reach high level recoveries above

95% without observation of the typical viscous fouling experienced by hydrophilic systems. While those early results were promising, little was known on optimization of the process performance and separation mechanisms. It is believed that the hollow fiber geometry of the membrane module allows internal coalescence of oil droplets between fibers combined with selective permeation of oil through the membrane. The present work aims at identifying the effect of key process parameters and understanding the underlying mechanisms of oil-water separation in the hollow fiber membrane contactor. In particular, a broad range of oil concentrations, transmembrane pressures, influent flow rates and viscosities are investigated for controlled oil-water mixtures.

MATERIALS AND METHODS

Membranes

The technology used in this study is a membrane contactor commercially available in various sizes, manufactured by Liqui-Cel® and referred to as Extra Flow Contactors. This contactor, originally developed for liquid-liquid extraction, is commonly used for de-gassing liquid applications such as oxygen removal from water in the microelectronic industry (*15*). The membranes have a hydrophobic microporous hollow-fiber design with a central baffle and shell-side distributor (Figure 5-1). The membrane contactors are available in various industrial module sizes including a 14-inch diameter version reported to process up to 2,090 L/min (*108*). The module design consists of a hollow-fiber sheet rolled into a cylindrical casing allowing a pseudo cross-flow filtration. Four ports allow circulation of fluids on the shell-side (outside of fibers) and the tube side (inside of fibers).

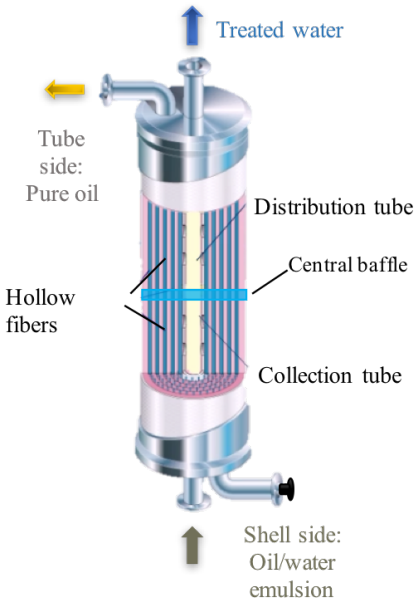

Figure 5-1: Extra flow Liqui-cel® membrane contactor in for oil-water separation configuration. Drawing adapted from Liqui-Cel®.

The characteristics of the three types of membrane contactors reported by Liqui-Cel® and used in this work are summarized in Table 5-1. Using a smaller surface area membrane contactor such as membrane module A allows identification of the limitations of the membrane contactor and the relative effect of operating parameters (i.e., it is not possible to compare performance over a range of parameter values if complete removal of the oil is observed over the entire range). Tests performed with membrane C allow for evaluation of the effect of surface area on system performance. Membrane B utilizes the same module size as Membrane A, but the hollow-fibers are spaced wider apart from each other to obtain half the surface area. The pore size distribution of the membranes was determined independently via scanning electron microscopy (Hitachi S5500 SEM/STEM, USA) with a gold and palladium coating of the membrane sample. Image analysis was conducted with the ImageJ image processing program developed by the National Institutes of Health (USA). As can be seen in Figure 5-2, a range of pore sizes was observed with a mean equal to 0.047 μm. Two fiber types are used in the manufacturing of these membrane contactors; the X50 fiber type was selected over the

X40 type to maximize oil permeation across a more porous and thinner membrane wall (Chapter 4).

Table 5-1 : Characteristics of membranes used in the study.

Module Name	Module size (Diameter x length) (inch)	Fiber Type	Surface area (m^2)	Porosity (%)	Wall thickness (μm)
A	2.5x8	X50	1.4	40	40
B	2.5x8	X50	0.7	40	40
C	4x28	X50	20	40	40

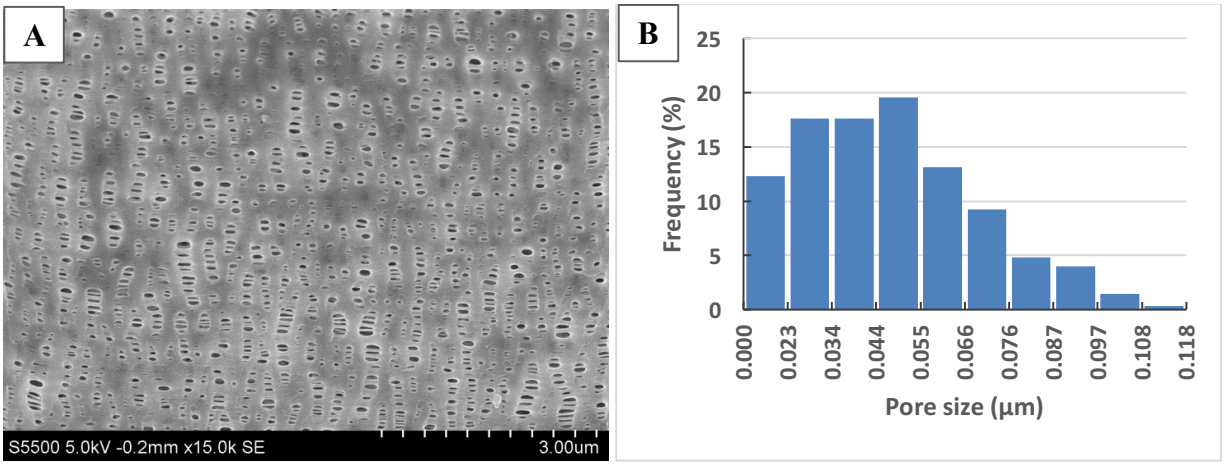

Figure 5-2: Pore size analysis of membrane pores. A) SEM picture; B) Pore size distribution obtained with ImageJ analysis.

Synthetic Oil and Non-stabilized Emulsion

Isopar™ , the synthetic oil used in this study, is a controlled mixture of paraffinic compounds manufactured by ExxonMobil. Various grades of Isopar™ oil have different viscosities as shown in Table 5-2.

Table 5-2: Viscosities at 25°C of Isopar™ grades used for the study.

Isopar™ grade	Viscosity (cP)
Isopar™ L	1.5
Isopar™ M	3.5
Isopar™ V	10.7

To generate the oil emulsion feed for the membrane contactors, oil and water were mixed with an in-line high shear pump (MTH pump, USA) to obtain micron size oil droplets in a water feed. An inline particle analyzer (JM Canty, Inc., USA) was used to observe and measure the droplet size distribution of the emulsion entering the membrane system. The majority of the oil drops were smaller than 10μm with an average drop size of 5.4 μm as shown in Figure 5-3. Due to the small droplet size, a 20 mL cloudy sample obtained from the pump discharge would typically require 12-24 hours to settle into two distinct phases.

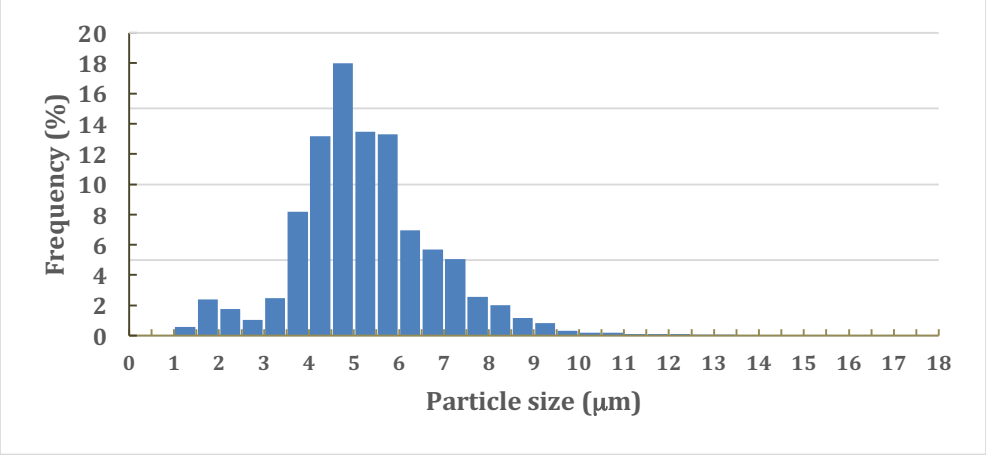

Figure 5-3: Droplet size distribution of Isopar™ -water non-stabilized emulsion entering the system.

Membrane Filtration System

Two membrane configurations were used for this study. In the first configuration, the module was operated in a “one-pass through” mode while in the second configuration

the system was operated in a closed loop mode to evaluate the performance over longer term operation. Figure 5-4 shows the "one pass through" configuration. The oil permeated on the tube side was measured, while the retentate was discarded. Figure 5-5 shows the system operated in recycling mode. Two modules were used in series at all times to guarantee high oil removal on the shell side and allow recirculation of oil-free water back to the feed tank for long-term operation. The removal of oil in the first module was used to assess the performance of the system at each operating condition, while the second module in the series was primarily used to remove the remaining oil from the water when the system was operating in recirculation mode. For practical reasons, experiments with oil concentrations higher than 10% (v/v) were operated in the "one-pass through" mode while the lower concentration experiments were conducted in recycle mode. In both the single pass and closed loop configurations, oil was injected into the main water line using a peristaltic pump (Thermo Fischer Scientific, USA) to control the influent oil concentration. The high shear pump (MTH pump, USA) mixed and circulated the emulsion in the system. Influent flow rate and pressures were adjusted with a variable speed drive (Emerson, USA) controlling the pump and a needle valve located on the outlet line. Influent flow rates were measured with Micro Motion flow meters. Temperature was monitored with a Rosemount RTD sensor (Emerson, USA). Pressures on the shell side were collected with Rosemount pressure transmitters (Emerson, USA).

Three weigh scales (Arlyn, USA) were used to measure oil mass injected in the system and recovered by each module in series. All instruments were connected to a DeltaV data acquisition system (Emerson, USA) allowing parameter control and real-time data collection for extended periods of time without interrupting operation.

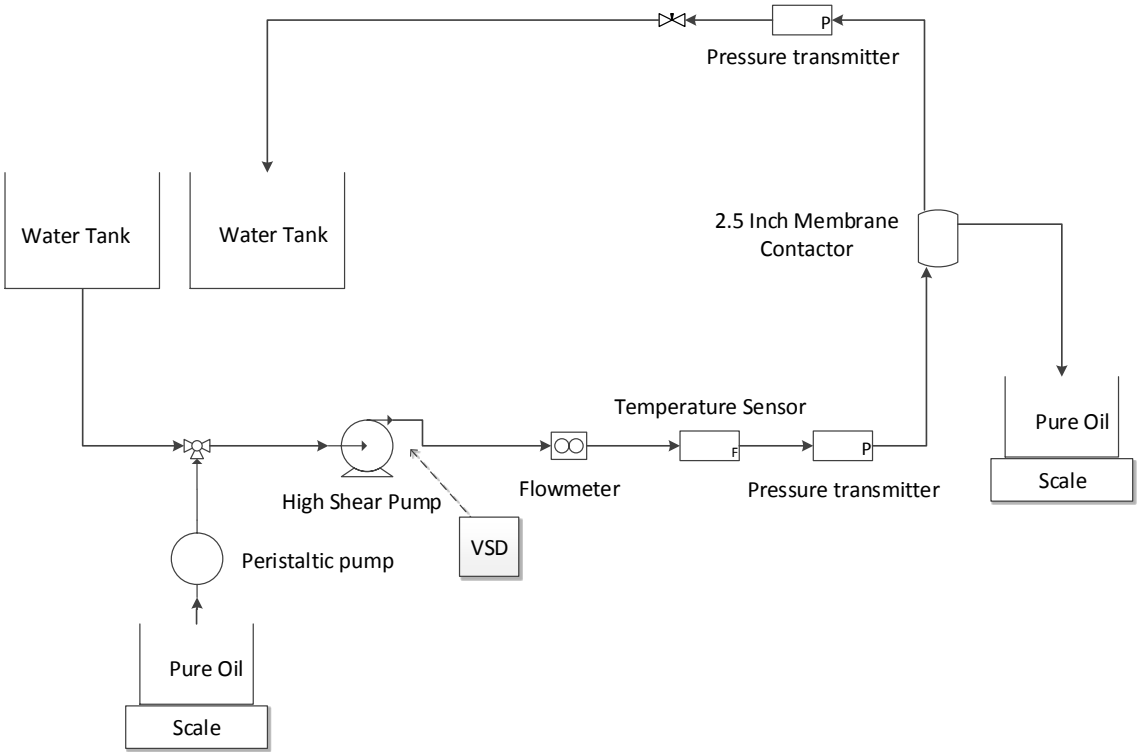

Figure 5-4: "One pass through" system schematic.

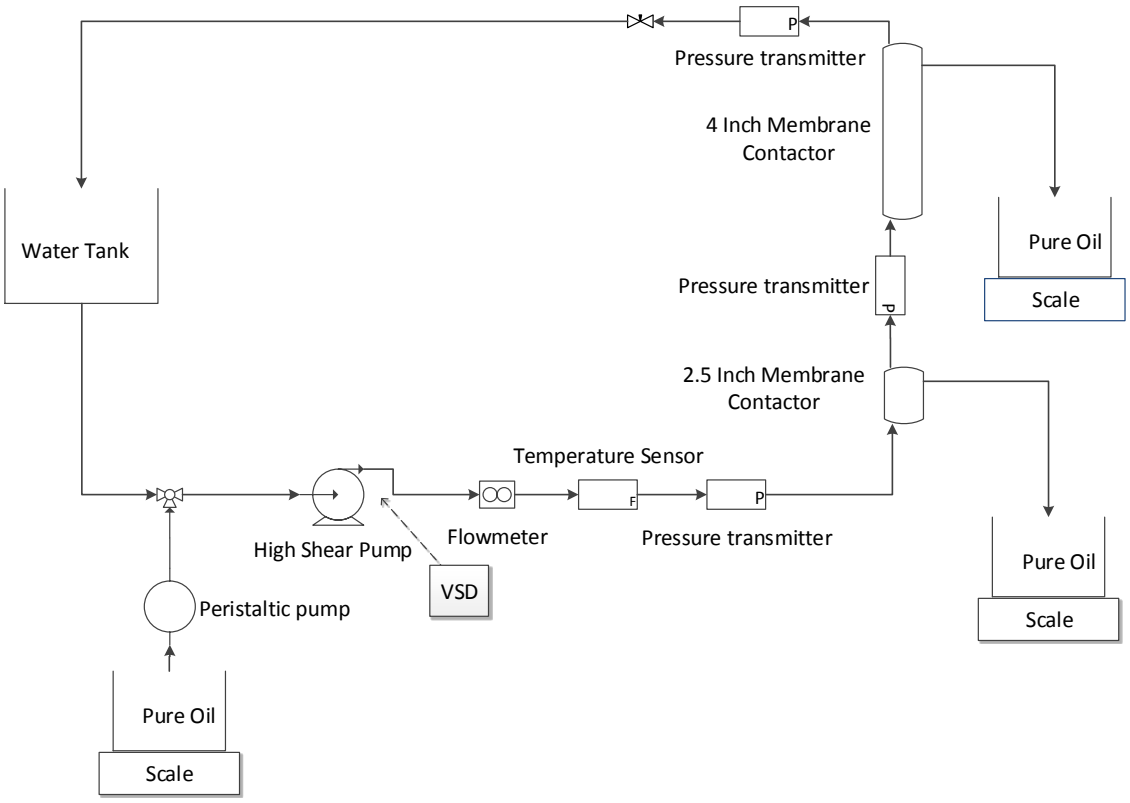

Figure 5-5: System schematic in recycling mode.

Oil-Water Experiments

Tests were performed by feeding an oil-water emulsion to the shell side inlet of the module where oil permeated the membrane and was quantified. Oil concentration in the feed was controlled by the peristaltic pump and calculated on a volumetric basis. Transmembrane pressure was computed from the average of inlet and outlet pressures of the shell side, while the tube side was left open to atmospheric pressure. Oil flux across the membrane was the indicator used to characterize system performance. Oil recoveries were also calculated from the ratio of injected to permeated oil volumes. The experimental plan is presented in Table 5-3. Experiments were design to test the effect of one operating parameter, while the others were maintained constant. The ranges of study of all parameters were chosen within the operational specifications of the membrane contactor.

Table 5-3: Experimental plan

Operating conditions	Oil concentration study		Transmembrane pressure study	
Oil Concentration (%)	0.02, 0.05, 0.1, 0.25, 0.5, 1, 2, 5, 10, 20, 40, 60, 80, 90	2, 5, 10, 20, 40, 60, 80, 90	40	2
Membrane	A	A	A	A
TMP (bar)	1.4	2.8	1.4, 2.8, 4.1	0.7, 1.4, 2.8, 4.1
Influent flow rate (L/min)	3.8	3.8	3.8	3.8
Isopar™ Grade	M	M	M	M
Duration of experiments	20 min up to 12 days	20 min up to 2.5 hours	20 min	20 min up to 2.5 hours

Table 5-3 (continued)

Operating conditions	Influent flow rate study		Viscosity study			Fiber spacing study		High recovery
Oil Concentration (%)	2	40	20, 80	2	0.02	2	2	0.1
Membrane	A	A	A	B	A	A	B	C
TMP (bar)	1.4, 2.8	2.8	1.4	2.8	1.4	1.4, 2.8	1.4, 2.8	1.4
Influent flow rate (L/min)	1.9, 3.8, 5.7	1.9, 3.8, 5.7	3.8	3.8	3.8	3.8	3.8	3.8
Isopar™ Grade	M	M	L, M, V	L, M, V	L, M, V	M	M	M
Duration of experiments	20 min up to 1.5 hours	20 min	20 min	1.5 hours	7 to 8 days	1.5 hours	1.5 hours	5 days

RESULTS AND DISCUSSION

Influent Oil Concentration

Experiments with oil feed concentrations ranging from 90% (v/v) to 200 ppmv were conducted to study the effect of increasing water content on oil permeation. Other parameters such as influent flow rate, transmembrane pressure and viscosity were maintained at constant values. As expected, the oil flux through the membrane decreased with decreasing influent oil concentration (Figure 5-6) as the probability of oil droplets contacting and permeating the membrane walls also decreased. The maximum oil flux attainable occurs when the influent is pure oil (oil concentration is 100% in Figure 5-6). Under such conditions, a single phase is in contact with the entire membrane wall surface and the effective coalescing surface area is believed to equate to the actual membrane

surface area. When adding water to the feed, the oil flux was consistently lower than for the pure oil conditions.

The pure oil experiment defines the maximum flux across the membrane for a given set of operating conditions. When water is added to the feed, the oil content flowing into the membrane can be higher than that flux under pure oil conditions. That is the case for experiments with oil concentration superior to 20% (v/v)) for the TMP = 1.4 bar curve presented in Figure 5-6. However, in those occurrences, the flux measured across the membrane was consistently lower than the flux observed with pure oil feed, which suggests that the effective surface area was smaller than the total surface area. The oil flux observed for experiments with lower oil content in the feed than the maximum pure oil flux was observed to decrease with decreasing oil concentration as well. These results suggest that the effective membrane surface area decreases with increasing water content. Therefore, for higher oil concentrations where the continuous phase is oil, the curves shown in Figure 5-6-A approach an asymptote to the pure oil flux value indicating that the effective surface area approaches the available surface area. At lower oil concentrations, below 2% (v/v), the oil flux is linearly related to oil concentration with a coefficient of determination higher than 0.999 (see Figure 5-6-B). Under such conditions, oil-water emulsions are highly dispersed and the probability for oil droplets to contact the fibers dictates oil permeation.

Figure 5-6 also shows that an increase in transmembrane pressure leads to an increase in oil flux for oil concentrations above 5% (v/v) as observed by Tirmizi et al (*59*). The results show that at a transmembrane pressure of 1.4 bar, the curve reaches a plateau above 20% (v/v) oil concentration, while the 2.8 bar curve consistently increases. When increasing transmembrane pressure is applied, water is forced onto the pores and may block the permeation of oil. Therefore, for lower pressure applied, the effective surface area may approach the total surface area faster than with higher transmembrane pressure as the effect of pore blocking by water is reduced.

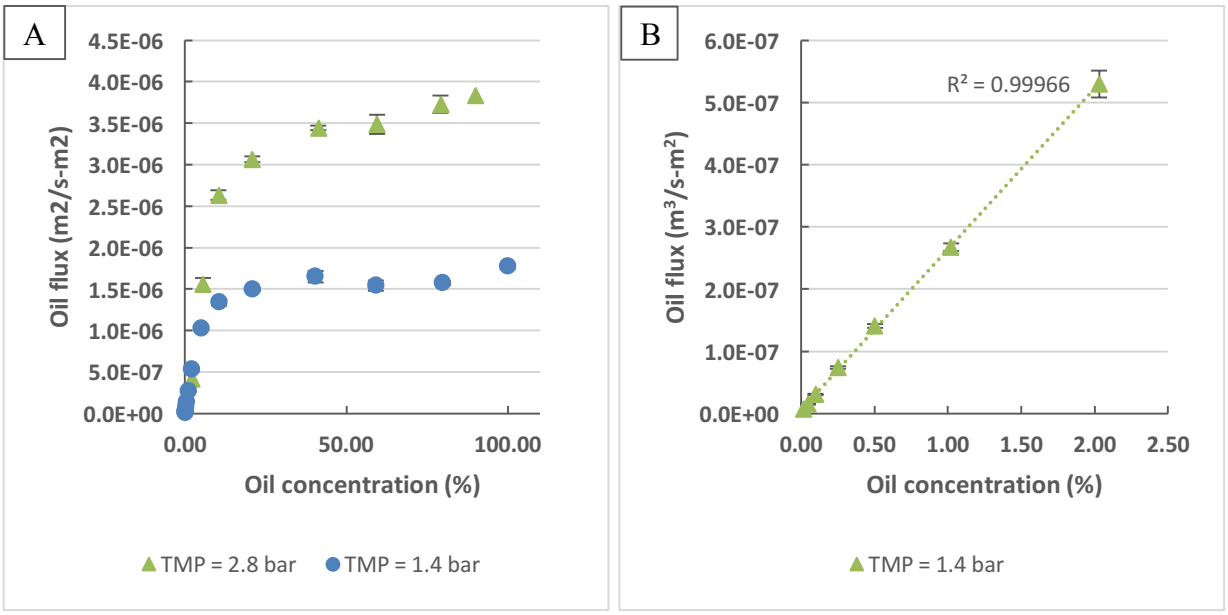

Figure 5-6: Effect of influent oil concentration on oil flux across the membrane. A) Oil flux as a function of oil concentration for transmembrane pressures = 1.4 bar and 2.8 bar; B) Results at lower oil concentrations, Transmembrane pressure = 1.4 bar; Experimental conditions: Isopar M; Influent flow rate = 3.8 L/min; Membrane A.

Long Term Performance

Typical hydrophilic membranes may experience fouling within minutes of exposure to oil-water mixtures (*50, 54*). For high oil concentrations such as 60% (v/v), the flux was constant for periods as long as 20 min (Figure 5-7-A) for the hydrophobic membrane contactors studied in this work. Experiments at lower oil concentrations were also conducted for extended periods of time and the oil recovery was observed to actually improve over time for a period of up to two weeks (Figure 5-7-B,C).

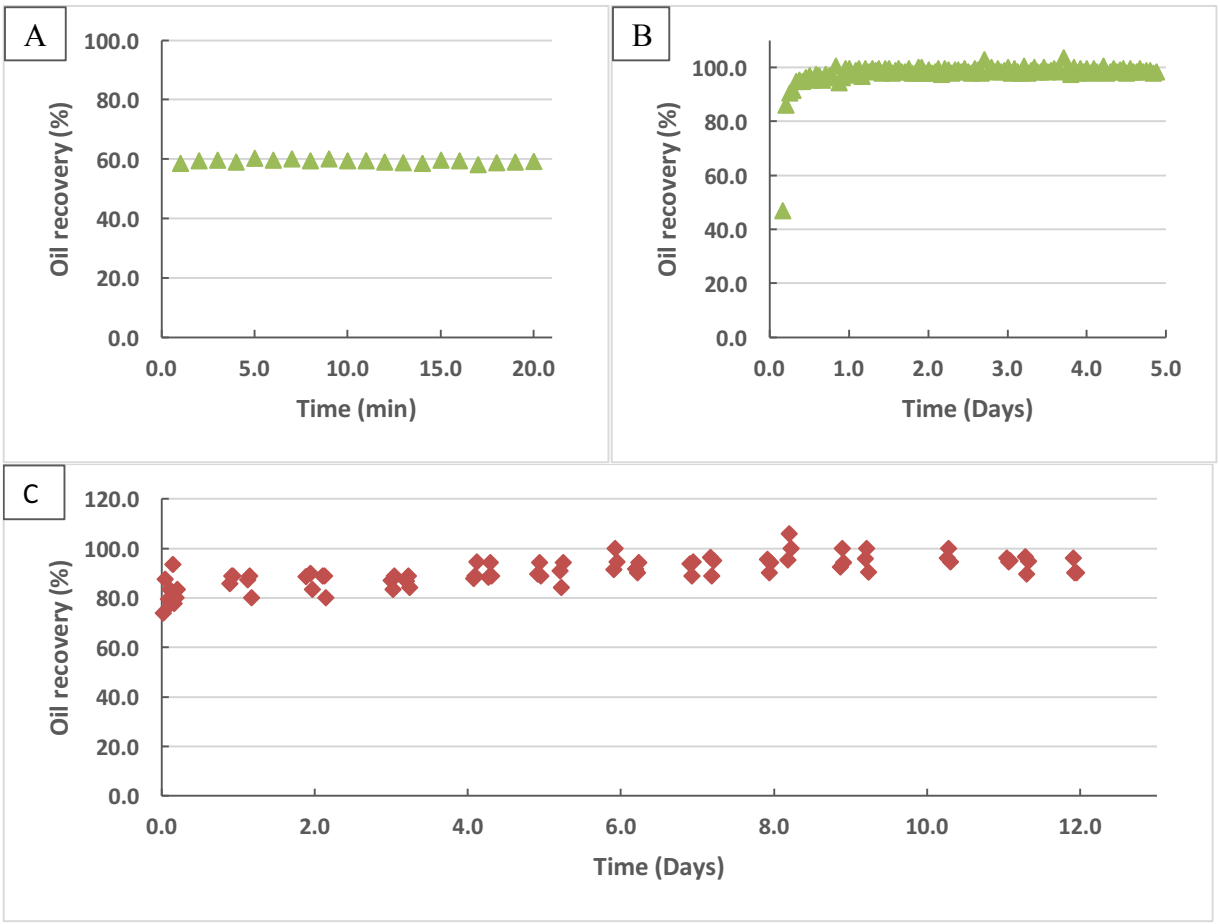

Figure 5-7: Oil recovery vs time. Experimental conditions: Isopar M; Influent flow rate = 3.8 L/min; Transmembrane pressure = 1.4 bar. A): C_{oil} = 1000 ppmv, Membrane A, SA = 1.4 m^2; B): C_{oil} = 1000 ppmv, Membrane C, SA = 20 m^2. C): C_{oil} = 200 ppmv; Membrane A, SA = 1.4 m^2.

Hydrophobic membranes have been used in the past for coalescence of oil-water emulsions where oil droplets coalesce by contacting the hydrophobic pore material (*86*, *87*). In these cases, a gravity settler is ultimately used to separate the two phases. The particular geometry and material of the modules used in the present study may allow coalescence to take place on the membrane fibers leading to the formation of an oil film coating the membrane wall. The transmembrane pressure applied across the membrane wall subsequently drives the selective oil transfer through the porous wall. The effective membrane surface area may be linked to the actual surface area of the oil film present on the fibers. Oil droplets may contact and coalesce with the oil layer rather than the non-

wetted membrane suggesting that cohesion forces are greater than the adhesion forces. For higher oil concentrations, the creation of the film may occur easily and rather instantaneously, but for more dilute mixtures, the growth and stability of the oil film on the fibers may be critical and dependent on oil concentration in the feed. This hypothesis is supported by the increase in oil recovery over time for dilute oil-water mixtures possibly due to the progressive oil film growth. Results shown in Figure 5-7 also demonstrate that oil recoveries up to approximatively 100% are attainable if enough membrane surface area is provided and for extended periods of time.

Transmembrane Pressure

After identifying two relevant concentration ranges that are governed by two distinct separation mechanisms, subsequent experiments were conducted at higher (C_{oil} = 40% (v/v)) and lower (C_{oil} = 2% (v/v)) concentrations to investigate the effect of transmembrane pressure on oil flux. At an oil concentration of 40% (v/v), the transmembrane pressure was found to be linearly related to oil flux (Figure 5-8-A). This result is consistent with previous experiments with pure oil feeds (Chapter 4 and Tirmizi et al. (*59*)) where increasing transmembrane pressure led to higher permeation rate.

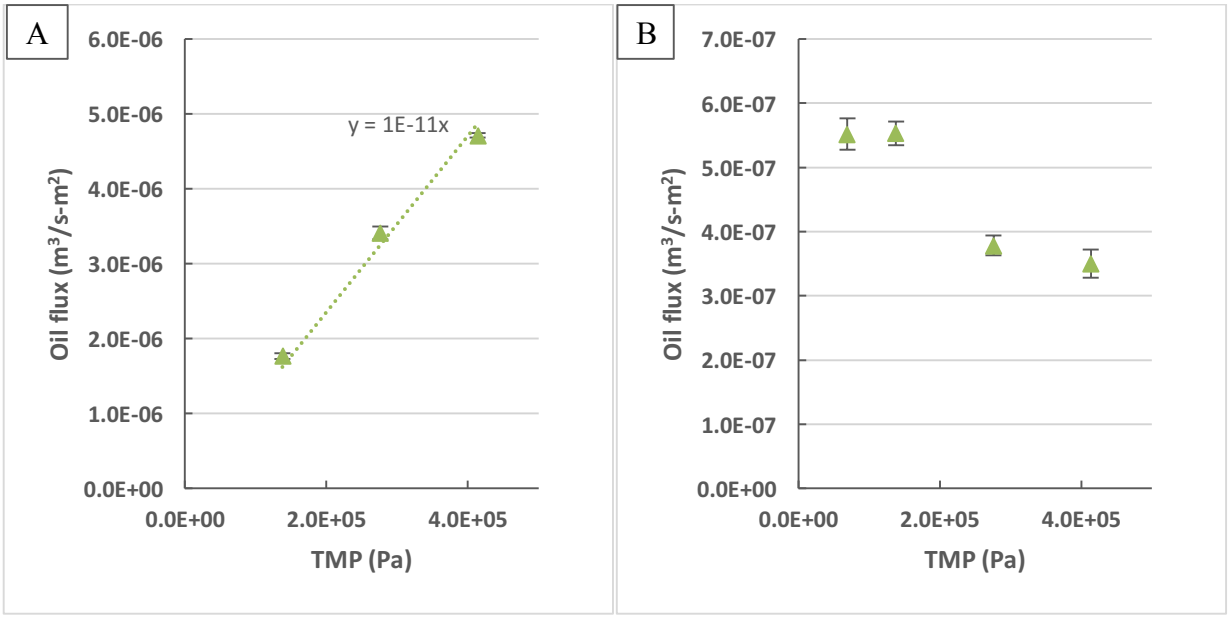

Figure 5-8: Effect of transmembrane pressure on oil flux. A) C_{oil} = 40% (v/v); B) C_{oil} = 2% (v/v); Experimental conditions: Isopar M; Influent flow rate = 3.8 L/min; Membrane A.

However, at a lower oil concentration of 2% (v/v), the effect of transmembrane pressure on oil flux reversed (Figure 5-8-B) and a lower transmembrane pressure yielded higher oil permeation. While this result may be counterintuitive, it is consistent with the oil permeation mechanisms proposed. Higher transmembrane pressure leads to higher compression force of the fluid onto the membrane wall. At higher transmembrane pressure, water is likely to be forced into the membrane pore entrance and prevent contact and permeation of oil through the fibers. As shown by Figure 5-2, the pore size distribution of the fibers is wide and larger pores are expected to be more easily blocked by water with increasing pressures, thereby reducing the effective surface area of the membrane. This phenomenon can be explained by lower water breakthrough pressures for larger pore size calculated from the Young Laplace equation (*75, 76*). In addition, the stability of the oil film on the fibers may be critical for oil permeation. At higher transmembrane pressure, oil may be forced through the pores at a rate preventing the oil

film from staying and growing on the fibers, permanently reducing the effective surface area. In contrast, operating with lower transmembrane pressure may lead to the formation and growth of a stable oil layer leading to consistently higher oil permeation through the pores as seen in Figure 5-8-B.

Influent Flow Rate

The effect of influent flow rate on oil permeation was studied and the results are shown in Figure 5-9.

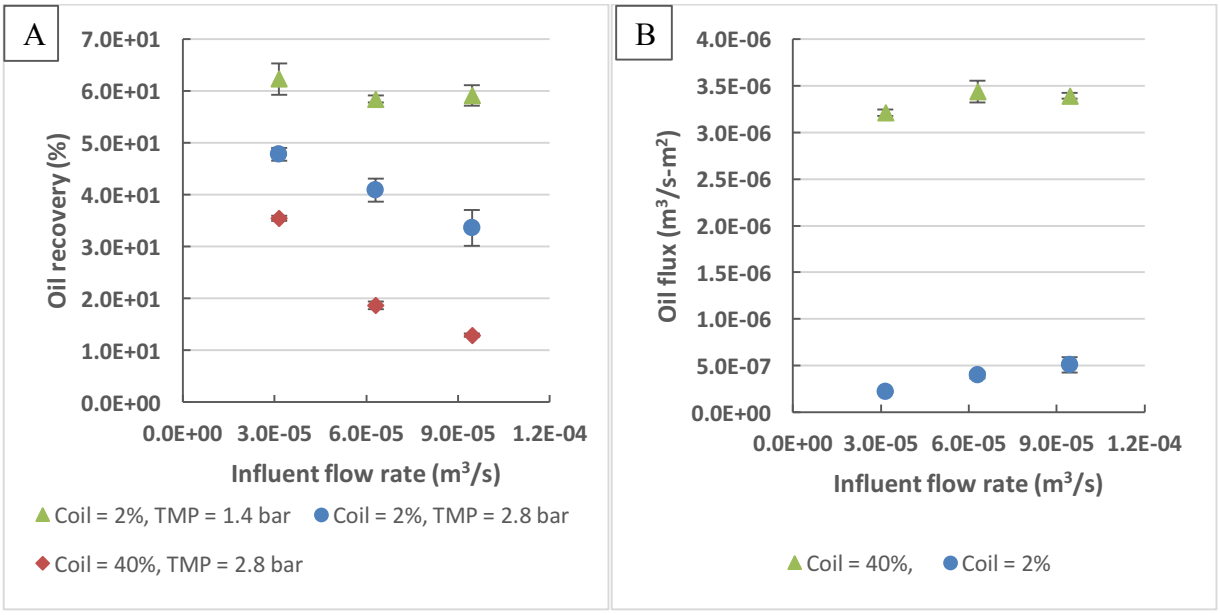

Figure 5-9: Effect on influent flow rate on system performance. A) Oil recoveries. Experimental conditions: Isopar M; C_{oil} = 2% and 40% (v/v); TMP = 1.4 bar and 2.8 bar; Membrane A. B) Oil flux. Experimental conditions: Isopar M; C_{oil} = 2% and 40% (v/v); TMP = 2.8 bar; Membrane A.

For C_{oil} = 40% (v/v), a 67% decrease in influent flow rate led to a 174% increase in oil recovery. For C_{oil} = 2% (v/v), a 67% decrease in influent flow rate led to a 37% and 5% increase in oil recovery for transmembrane pressures of 2.8 bar and 1.4 bar, respectively. Therefore, results suggest that influent flow rate is a more critical parameter for oil recovery at higher oil concentration and higher transmembrane pressures. For both

oil concentrations tested, lower influent flow rates improved oil recovery which can be explained by an increase in retention time for oil droplets in the membrane module. In the case of pure oil feed, the detention time did not impact the permeation of oil as the total surface area of the model was wetted with oil (Chapter 4). In the case of oil-water mixtures, longer retention times increases the chances for oil droplets to contact and coalesce on the membrane wall and be permeated across the fiber walls. At higher oil concentration, the fibers are assumed to be rapidly oil wet. Figure 5-9-B shows that with a 67% decrease in influent flow rate and; therefore, oil content, only a 5% decrease in oil flux was observed. At C_{oil} = 40%, the amount of oil sent in the system is higher than the flux measured under pure oil conditions and; therefore, an increase in oil content in the feed does not affect the permeation of oil. As a result, oil recovery decreases for increasing influent flow rate. At lower oil concentrations; however, oil deposition and formation of an oil film on the membrane wall seems to be the key component for oil permeation. At lower transmembrane pressure, the oil film is more stable leading to a higher effective membrane surface area. The affinity of oil to the membrane wall is stronger at lower transmembrane pressure, possibly reducing the effect of retention time for oil permeation.

Oil Viscosity

Oil viscosity is expected to influence oil flux across membranes and typically the higher the oil viscosity, the lower the oil flux observed as seen in previous studies (*64*). Tests with various Isopar™ grades were conducted with the membrane contactor to evaluate the effect of oil viscosity on the process. Under pure oil conditions, oil flux was shown to be inversely related to viscosity (Chapter 4); increased viscosity, led to reduced flux. At 80% (v/v) oil concentration, the flux seen in Figure 5-11-A decreased with higher viscosity but not linearly as observed in the pure oil experiments (Chapter 4). At 2% (v/v) oil concentration, results presented in Figure 5-11-B, confirm that increasing

viscosity leads to decreased oil flux. However, the magnitude of the viscosity effect decreased at higher transmembrane pressures. The effect of viscosity on flux inverts for more dilute oil-water mixtures (e.g., 200 ppmv water). As seen in Figure 5-11-C and 15, increasing viscosity increases oil flux possibly enhancing the stability of the oil film on the fibers. Two mechanisms may be competing for the permeation of oil in the present system. When enough oil is supplied at the pore entrance (for high oil concentrations), permeation is improved by transmembrane pressure and affected by viscosity. However, when the oil content is low, there is less oil available to cover the membrane surface and rapid permeation of oil may hinder long-term flux by reducing the long-term effective area. It may be possible to maintain a stable film at the surface of the fiber at higher viscosity and lower transmembrane pressure. The stability of the film may provide greater effective surface area and higher oil flux even though oil is transported at a lower rate across the fiber. Interestingly, at 2% (v/v) oil concentration and high viscosity, changes in transmembrane pressure did not affect oil flux significantly. This observation suggests that the predominant mechanism contributing to oil film stability was the viscosity and not the transmembrane pressure under these conditions.

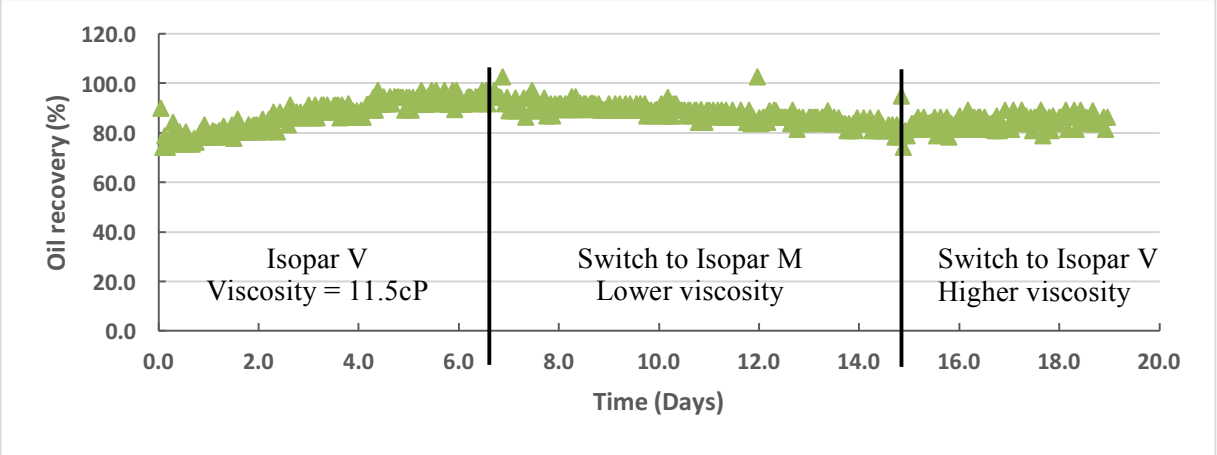

Figure 5-10: Effect of viscosity on oil recovery. Experimental conditions: Influent flow rate = 3.8 L/min; TMP = 1.4 bar; Membrane A, Isopar V used initially than switched to Isopar M and back to Isopar V.

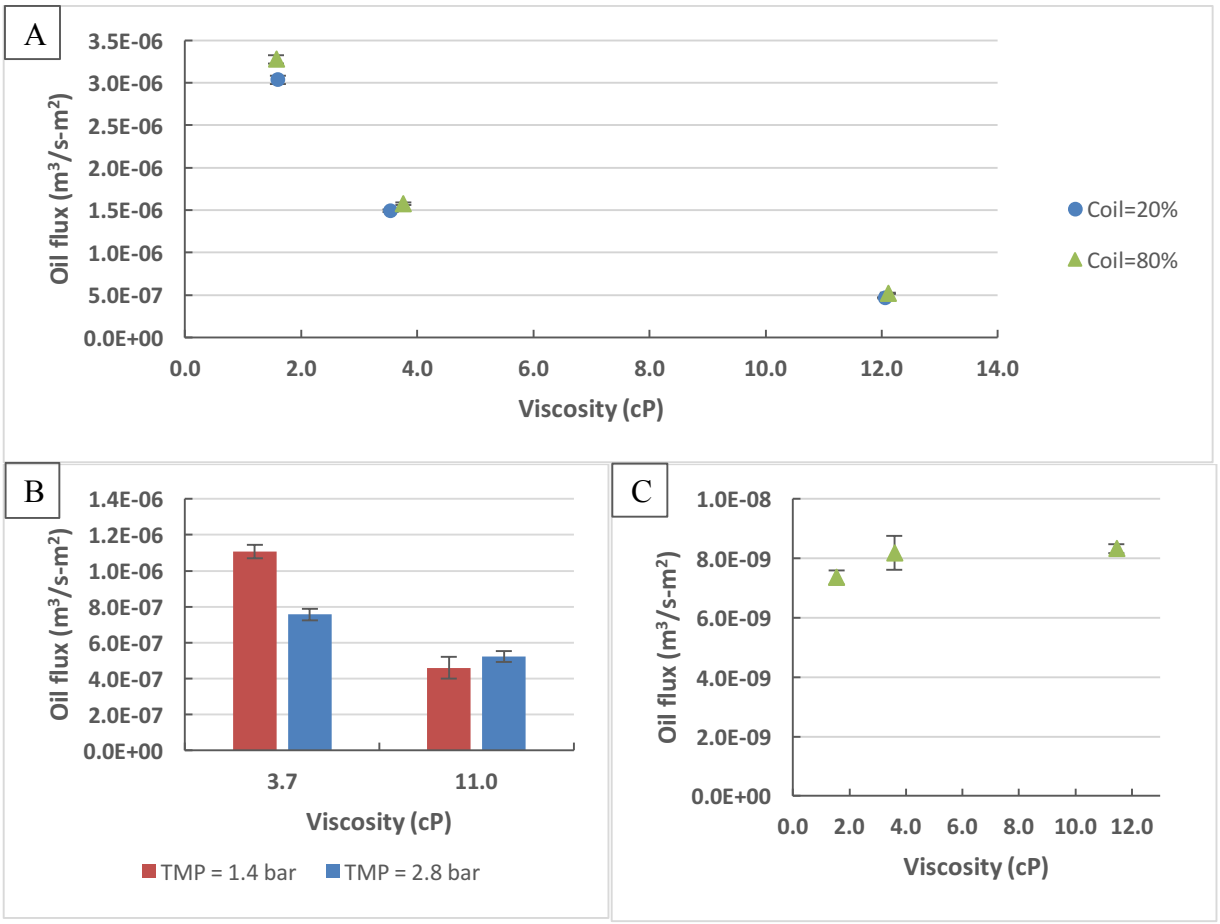

Figure 5-11: Effect of viscosity on oil flux. A) C_{oil} = 80% (v/v), TMP = 1.4 bar, Membrane A; B) C_{oil} = 2% (v/v), TMP = 1.4 bar and 2.8 bar, Membrane B; b) C_{oil} = 0.02% (v/v) = 200 ppmv, TMP = 1.4 bar, Membrane A; Experimental conditions: Influent flow rate = 3.8 L/min.

Fiber Spacing

The performance of two membrane contactors with different fiber spacing was compared and results are shown in Figure 5-12. Not surprisingly, oil recoveries were found to be higher with higher available surface area. However, the differences in oil flux, which is normalized by surface area in this figure, indicates that the smaller surface area membrane contactor was significantly more efficient in this case.

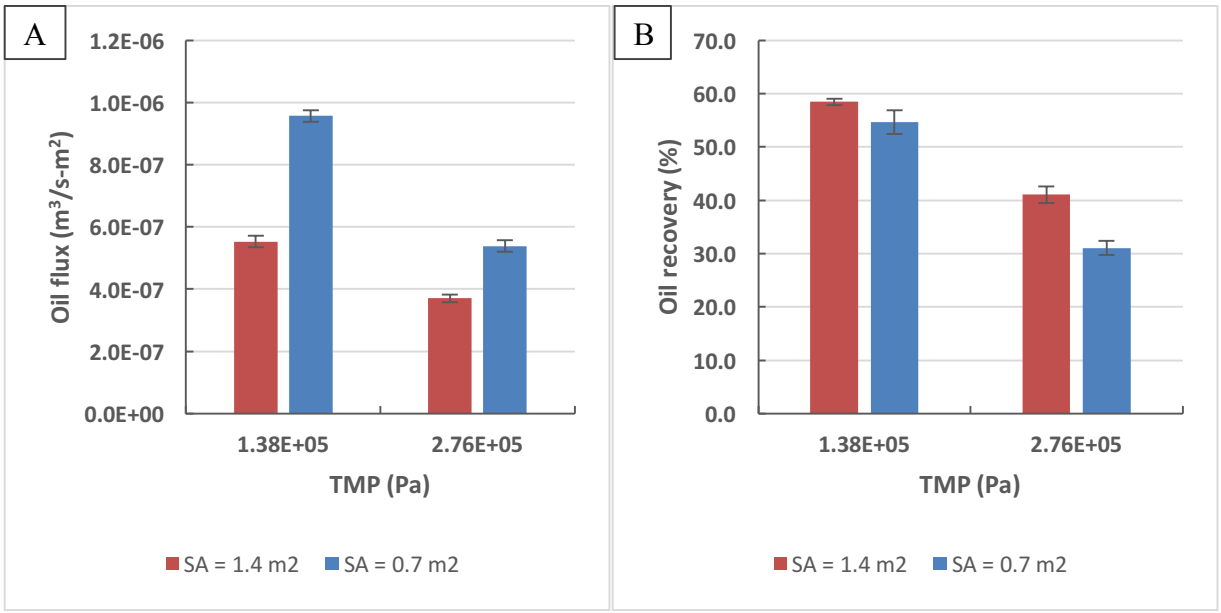

Figure 5-12: A) Effect of surface area on oil flux. B) Effect of surface area on recovery. Experimental conditions: Isopar M; C_{oil} = 2% (v/v); Influent flow rate = 3.8 L/min; Membrane A and B.

The two membrane contactors differ with respect to the spacing between the fibers, which ranges from approximatively 40 µm for the 1.4 m^2 module to approximatively 80 µm for the 0.7 m^2 module. The results suggest that wider spacing leads to higher oil flux. According to studies on coalescence in conventional membrane, coalescence occurs when oil droplets are small enough for the droplets to have a chance to contact the pore but not so small that the emulsion is re-dispersed (*60, 86, 89*). The space between fibers of the studied module could be thought of as a long pore where droplets coalesce between the fibers. The present results suggest that an increase of space between fibers from 40 to 80 µm is beneficial for the coalescence of the emulsion used in this work that had an average oil droplet size of 5.4 µm based on Figure 5-3. This result does not match the findings of research conducted with coalescence in membrane pores. Kawakatsu et al. (*86*) showed that if the pore is much larger than the oil droplet size, the drops can flow between the walls without coalescing. However, the difference with conventional coalescence in membranes and the present coalescence mechanism may be

the length of the coalescing channels. Membrane pores are only as long as the wall thickness, usually a few hundred micrometers. In the present case, the coalescing channels are the entire length of the module of approximatively 20 cm, increasing the chance for the oil droplets to contact the fibers wall. The increase of space between fibers may improve water flow distribution out of the coalescing area leading to better coalescence and stability of the film on the fiber. The 0.7 m^2 module yields 73% higher oil flux than the 1.4 m^2 module for low transmembrane pressure (1.4 bar). That increase is 45% higher at higher transmembrane pressure (2.8 bar). At higher pressure, the water may start blocking the larger pores; therefore, if water flows out more easily from the coalescing area, more efficient use of the effective surface area is made. At lower pressure, the water is even less compressed against the fiber wall leading to improved coalescence and permeation. A schematic detailing the proposed mechanism is shown in Figure 5-13. Such results seem to confirm that oil film stability on the fibers is critical for the establishment of the effective surface area of the membrane contactor.

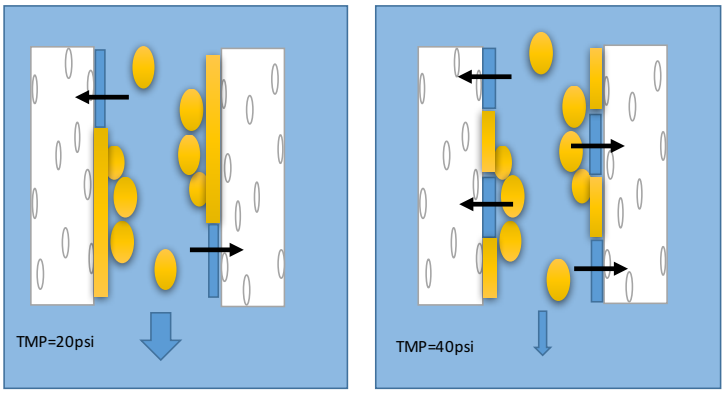

Figure 5-13: Schematic of oil droplet coalescence between fibers for two transmembrane pressures. The oil phase is in orange and the water in blue.

Comparison to an Equivalent Hydrophilic System

Comparing the performance of hydrophilic and hydrophobic membrane systems can be challenging since the permeated phases across the membranes are different. Experiments where oil recoveries approach 100% (such as results presented in Figure 5-7-C) with the membrane contactors can be compared to an equivalent hydrophilic system depicted in Figure 5-14. If 100% oil recovery is assumed with the hydrophobic membrane, an equivalent system would consist of a hydrophilic membrane permeating pure water. Therefore, for a 200 ppmv oil concentration experiment at transmembrane pressure of 1.4 bar and influent flow rate of 3.8 L/min with a membrane contactor of 1.4 m^2, an oil flux of $8.7*10^{-9}$ $m^3/s\text{-}m^2$ was measured. The equivalent water flux for a hydrophilic membrane would correspond to permeate the entirety of the water phase through 1.4 m^2 surface area, which equals a flux of $4.5*10^{-5}$ $m^3/s\text{-}m^2$. Moreover, the hydrophobic system studied here was shown to maintain such performance up to two weeks (Figure 5-7-C), which may not be the case of the equivalent hydrophilic system that may experience decrease of flux over-time due to viscous fouling. Recently, Zhu et al. (*109*) studied the use of a novel hollow-fiber membrane for oil-water separation with water permeation across a modified PVDF membrane surface. Higher water flux was measured than for typical PVDF membranes. The highest flux attained in this study under a transmembrane pressure of 3.4 bar and oil feed concentration of 500 ppmv was $1.9*10^{-5}$ $m^3/s\text{-}m^2$ prior to the observed decrease in performance due to fouling. Therefore, the results found in our study are comparable to the results observed for a hydrophilic system at start-up without the disadvantage of viscous fouling occurring over time, that would ultimately reduce the permeation flux.

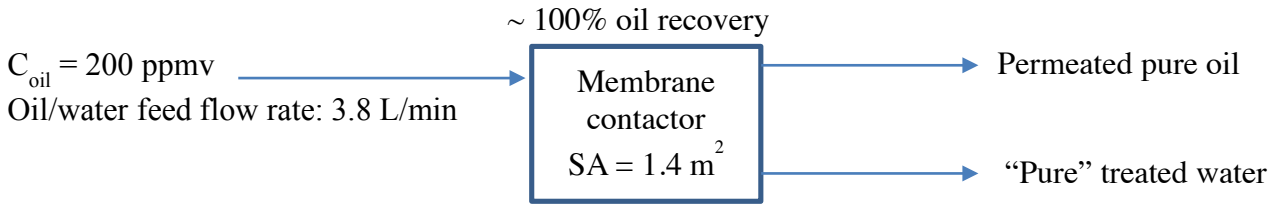

Figure 5-14: Schematic for equivalent hydrophilic system

Therefore, the present hydrophobic membrane contactor represents a viable competitor to hydrophilic systems as comparable oil removal capability is obtained but also maintained over time.

CONCLUSIONS

The research presented in this paper examined the use of a hydrophobic hollow fiber membrane contactor for the removal of insoluble oil from controlled oil-water mixtures. Various operating parameters, including transmembrane pressure, influent flow rate, viscosity, and oil concentration, were investigated to reveal the underlying mechanisms presiding over the successful separation of oil and water. Significant findings from the study include:

- Decreasing oil concentration was shown to decrease flux across membrane fibers, even in instances where the oil content was below the maximum amount of oil recovered under pure oil conditions. Experiments conducted over a range of conditions suggested that water addition decreased the effective surface area of the membrane contactor.
- Two concentration regions were identified that helped isolate the two fundamental processes dictating the separation of oil and water. At low oil concentration (below 2% (v/v)), the stability of an oil film on the membrane contactor appeared as the limiting mechanism, while at higher

oil concentrations, the system performance was in agreement with typical membrane separation behaviors.

- No viscous fouling or performance decrease was observed for up to two weeks of operation with the membrane contactors. High oil recoveries were attained when sufficient membrane area was used for a given oil feed concentration.

- Transmembrane pressure was shown to have different effects depending on the oil feed concentration range. For higher concentrations, increasing transmembrane pressure was confirmed to increase oil permeation. However, for oil concentrations below 2% (v/v), operating the system with lower transmembrane pressure was proven to be more beneficial by improving the oil film stability of the membrane wall.

- Increasing influent flow rate, which yields a lower detention time, was shown to decrease oil recoveries. This effect was less important for lower oil concentrations and transmembrane pressure, which further supports the hypothesis that the development and stability of oil films on the membrane fibers are critical in optimizing the performance of the contactor.

- Analogous to the transmembrane pressure, viscosity was shown to impact the system differently depending on the influent oil concentration range. The typical effect of decreasing permeation with increasing viscosity was observed for most of the oil concentration range. However, for very dilute mixtures (200 ppmv), higher oil viscosity seemed to contribute to oil film stability and oil permeation.

- Wider-spaced fibers were shown to improve oil flow per unit surface area by possibly improving water flow distribution out of the coalescing areas of the hollow fibers.

- The data presented in this paper seem to confirm the hypothesized mechanism that oil droplets coalescing on the fibers and progressively coating the membrane wall at low oil concentrations is key for successful operation. The stability of the oil film on the fibers is the critical mechanism at low oil concentration and leads to progressive improvement of performance over time.

- The hydrophobic membrane contactor can withstand and perform efficiently for a wide range of oil concentrations for which fouling in hydrophilic systems would be prohibitive, which makes this technology a prime candidate for many applications ranging from oil removal in very dilute oil-water mixtures to oil purification processes.

- These studies are based on systems possessing a high interfacial tension (~52 dynes/cm) and without solids; therefore, some caution should be applied. Future work should address the comparative effects of lower interfacial tensions and solids.

Chapter 6: Modeling of a Microporous Hollow Fiber Membrane Contactor for Oil-Water Separation

ABSTRACT

The separation of oil and water presents significant technical and economic challenges in many industries. In particular, technologies capable of separating insoluble oil and water are needed for oil and gas wastewater treatment, biofuel production, petrochemical processing, and in food manufacturing applications. Reliable and economical technologies with high oil removal capabilities over long term operation are required. Hydrophobic membrane systems are a promising technology for the recovery of pure oil as well as the production of high purity water streams from oil-water mixtures without the typical fouling problems observed with hydrophilic materials. In this study, the successful use of a hydrophobic microporous hollow fiber membrane contactor for the separation of insoluble oil from water is detailed. Oil flux performance is shown to be directly related to the effective surface area of the membrane contactor. A semi-empirical model is developed and relates the effective surface area to the operating parameters of the system such as transmembrane pressure, influent flow rate, oil viscosity, as well as to membrane characteristics. The model predicts the required surface area for a chosen oil recovery under a given set of operating conditions. For instance, an oil-water influent containing 0.1% (v/v) of oil with a viscosity of 4 cP and entering the system at a rate of 240 L/h would require 8m^2 of membrane surface area to reach 95% oil removal if operated under a transmembrane pressure of 1.5 bar. The model can be used to predict oil removal for a given surface area as well and, therefore, provides a valuable tool for design of a separation system with the membrane contactor.

INTRODUCTION

Many technologies have been developed to separate oil from water in oily wastewaters. Conventional treatment techniques such as hydrocyclones, gravity separators, gas flotation and centrifuges are good solutions for many applications in the oil and gas, food or metallurgical industries (*24*). However, high capital and operating costs along with poor removal efficiencies for micron size oil drops have limited the application of these technologies (*42-44, 88*). As a result, membrane systems have gained attention for their ability to efficiently capture smaller oil droplets (<10 μm) and achieve the high oil removals required for subsequent disposal or reuse of water streams (*21, 22, 44, 63*). Many types of membranes have been investigated including microfiltration (*46, 49-51*), ultrafiltration (*52-54*), nanofiltration (*45*), as well as different hydrophilic (*43, 46, 47, 55*) and hydrophobic (*8, 56-60*) materials. Hydrophilic membranes have proven useful for producing high quality water permeate. However, many studies have documented a progressive decrease in performance due to viscous fouling of the membrane surface (*46, 50, 51, 102-104*). Hydrophobic systems that permeate oil rather than water present great promise for preventing the typical fouling of the membrane surface by a viscous oil layer observed with hydrophilic systems. A few studies have focused on such technologies (*8, 56, 59*) but more work is needed to understand the mechanisms at play and characterize the performance in larger scale hydrophobic systems.

Of particular note are early studies conducted with a commercially available hydrophobic membrane contactor that was licensed by the University of Texas to OpenAlgae LLC. Research conducted at the Separations Research Program (UT-Austin) investigating the use of this hydrophobic microporous membrane contactor for the recovery of submicron algae oil from algal slurries showed promising results in insoluble oil and water separation (*17-19*). The membrane contactor extracted the majority of the available nonpolar oil for most of the feedstocks. Originally developed for liquid-liquid

extraction, the membrane contactor has significant commercial applications associated with de-gassing of liquids such as the oxygen removal from water in the microelectronic industry (*15*). Seibert (*20*) presented additional oil recovery performance data using the membrane contactor carried out over multiple days. These initial studies showed that in contrast to the fouling behavior observed in hydrophilic membrane systems (*50, 54, 55, 67, 68*), the hydrophobic microporous membrane contactor performance improved over time to achieve high oil recovery (>95%) with injected oil over a two-week test run. While the studies with actual and simulated feedstocks provided promising results, little was known about the fundamental mechanisms controlling the oil recovery. These initial data, while important, did not provide sufficient understanding to reliably design and engineer an optimized oil recovery system that could be applied to biological and petroleum based oils. As a result, fundamental and controlled studies were performed using a module of limited surface area to evaluate the effects of transmembrane pressure, influent flowrate (residence time), oil concentration and oil physical properties (Chapter 4 and 5). The findings allow the development of a semi-empirical model to predict oil flux and recovery across the membrane contactor for long term steady state operation.

Modeling of membrane systems has focused on characterizing time dependent fouling behaviors in hydrophilic systems and defining breakthrough pressures (*50, 110, 111*). Huang et al. (*66*) developed a mechanistic model describing the limiting permeation of water in a highly hydrophilic UF membrane system. Fouling behavior was shown to follow Hermia's models and water flux was proven to become pressure independent over time. Viscosity, oil concentration and shear rate were confirmed as important parameters affecting water flux across the hydrophilic membranes. Other studies have compared experimental data collected from hydrophilic systems to the typical transport models used for microfiltration such as Brownian diffusion, shear-induced diffusion or inertial lift (*78*). Singh et al. (*47*) combined both Brownian and shear-induced diffusion in a model to obtain good agreement between predicted and measured steady state flux data in a

hydrophilic microfiltration system treating industrial oily wastewater. To develop models for hydrophilic microfiltration, an analogy is used between the solid particles in a liquid phase and the oil droplets in the water phase. Oil droplets are analogous to solid particles that progressively block the pores or form a layer at the membrane surface leading to a reduced steady state liquid flux across the membrane. However, in the case of hydrophobic systems and for concentrations where the continuous phase is water, the analogy does not hold since the "particles" (i.e., oil droplets) are actually permeated and not sieved as in conventional microfiltration. The experimental results presented earlier in Chapter 5 demonstrated that permeation behavior in hydrophobic microfiltration of oil-water mixtures differs from the typical trends observed in hydrophilic systems. In particular, transmembrane pressure and viscosity were shown to have opposite effects when the oil concentration was varied from high to low in the oil-water mixtures. While studies investigating the use of hydrophobic systems for the separation of oil and water have focused on identifying the key operating parameters involved in the filtration system (*56, 59*), no models to date have been presented.

The objective of this paper is to present a semi-mechanistic, semi-empirical performance model for the design and operation of a microporous hydrophobic membrane contactor for the recovery of insoluble oil from oil-water mixtures. Recent results suggest that the technology is applicable for applications ranging from oil purification to the treatment of very dilute oil-water mixtures such as would be typical of the final oil removal step in produced water treatment. The model can be used to determine membrane surface area and operating conditions needed to optimize process performance for a given oil-water stream.

MATERIALS AND METHODS

Experimental Data

Membrane Contactor

The membrane contactor used in previous studies with lipids from microalgae formed the basis for this work and, therefore, was selected for use in this study. The membrane contactor is commercially available (Extra Flow Contactor) and manufactured by Liqui-Cel® (a 3M Product). Various module sizes exist. The largest modules are reported to process up to 2,090 L/min of liquid in degassing applications. The membrane contactors are composed of hydrophobic microporous hollow-fibers packed in a cylindrical module (Table 6-1).

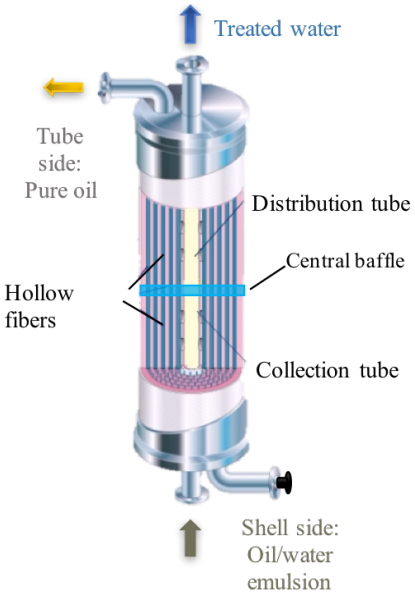

Figure 6-1: Extra Flow Liqui-Cel® membrane contactor in for oil-water separation configuration. Drawing adapted from Liqui-Cel®.

The geometric characteristics of the membrane contactors selected for this study are presented in Table 6-1. While modules containing two different available hollow-fiber characteristics (X50 and X40) were initially evaluated, the contactors containing X50 fibers were selected because these modules were found to produce higher oil permeation rates while preventing breakthrough of water (Chapter 4). The 2.5-inch

diameter module is the smallest commercially available module and is especially useful for observing changes in performance as a function of operating conditions because it was possible to achieve less than 100% removal for experimentally reasonable operating conditions. The module's sensitivity allowed for an improved understanding of the oil-water separation and identifying optimum operating conditions.

Table 6-1: Membrane characteristics for the 2.5 inch diameter X50 Liqui-Cel® Extra Flow Contactor selected for the study.

Module size (Diameter x length) (inch)	Surface area (m^2)	Pore Size (μm)	Porosity (%)	Wall thickness (μm)
2.5x8	1.4	0.04	40	40

Synthetic Oil

Various Isopar™ grades were used as the synthetic oil for this study. Isopar™ oils are controlled mixtures of paraffinic compounds and manufactured by ExxonMobil (purchased from Nexeo Solutions, USA). Each Isopar™ grade has a different viscosity as shown in Table 6-2.

Table 6-2: Viscosities at 25°C of Isopar™ grades used in the study.

Isopar™ grade	Viscosity (cP)
Isopar™ L	1.5
Isopar™ M	3.5
Isopar™ V	10.7

Pure Oil Experiments

Experiments were conducted with pure oil feeds under various experimental conditions detailed in Table 6-3 to determine the membrane contactor's baseline performance (Chapter 4). The effect of transmembrane pressure, oil viscosity, and

membrane characteristics on oil flux was observed and successfully compared to the Ergun equation.

Table 6-3: Experimental conditions for pure oil feed experiments with the membrane contactor.

Isopar™ grade	Influent oil flow rate (L/h)	Transmembrane pressure (bar)
L	227	1.4, 2.8, 4.1
M	113	1.4, 2.8, 4.1
	227	0.7, 1.4, 2.1, 2.8, 3.4, 4.1
	340	1.4, 2.8, 4.1
V	227	1.4, 2.8, 4.1

Oil-Water Experiments

Experiments were conducted during which the separation of oil-water mixtures were monitored and assessed under various operating conditions presented in Table 6-4.

Table 6-4: Experimental conditions for oil-water experiments with the membrane contactor.

Operating conditions	Oil Concentration (%)	TMP (bar)	Influent flow rate (L/h)	Isopar ™ Grade	Duration of experiments
Oil concentration study	0.02, 0.05, 0.1, 0.25, 0.5, 1, 2, 5, 10, 20, 40, 60, 80, 90	1.4	227	M	20 min up to 12 days
	2, 5, 10, 20, 40, 60, 80, 90	2.8	227	M	20 min up to 2.5 hours
TMP study	40	1.4, 2.8, 4.1	227	M	20 min
	2	0.7, 1.4, 2.8, 4.1	227	M	20 min up to 2.5 hours
Influent flow rate study	2	1.4, 2.8	113, 227, 340	M	20 min up to 1.5 hours
	40	2.8	113, 227, 340	M	20 min
Viscosity study	20, 80	1.4	227	L, M, V	20 min
	0.02	1.4	227	L, M, V	7 to 8 days

The oil and water emulsions were created with an in-line high shear regenerative turbine pump (MTH pump, USA) to obtain micron size oil droplets in the water feed. Chemical emulsifiers were not used in this study. To monitor the droplet size distribution of the oil-water mixtures, an inline particle analyzer (JM Canty, Inc., USA) was used downstream of the high shear pump. The average droplet size was 5.4 μm and a distribution of pore sizes was observed where the vast majority of droplets was smaller than 10 μm. Due to the small droplet sizes, a 20 mL cloudy sample obtained from the pump discharge would typically require 12-24 hours to settle into two distinct phases.

Membrane Filtration system

Two experimental flow path configurations were used in this study: a "one-pass through" and a "recycling mode". The "one pass through" configuration consisted of feeding the oil-water emulsion to the membrane system in a single pass (Table 6-2). The product water was collected in a second tank. Oil permeation was measured on the tube side and the aqueous retentate was discarded. In the recycle mode configuration, a 2.5-inch diameter module was mounted in series with a 4-inch diameter "guard" module used to provide complete oil removal on the shell side and allow recirculation of oil-free water back to the feed tank. For both configurations, oil and water were emulsified and circulated in the system with the high shear regenerative turbine pump (MTH pump, USA). A peristaltic pump (Thermo Fischer Scientific, USA), connected to the suction of the high shear pump, provided control of the oil injection rate. The pump's variable speed drive and a needle valve located on the outlet line were used to control influent flow rates and pressures. Influent flow rates were measured with mass flow meters (MicroMotion, USA). Temperatures were monitored with Rosemount RTD sensors (Emerson, USA). Pressures on the shell side were measured with Rosemount pressure transmitters (Emerson, USA). Mass quantities of oil injected to the system and

permeating the membranes were monitored with three weigh scales (Arlyn, USA). A DeltaV data acquisition system (Emerson, USA) was used to continuously acquire instrument measurements.

Tests were performed by circulating an oil-water mixture though the membrane contactor from the bottom to the top shell-side ports. Influent oil concentration was computed as a volume fraction. Permeated oil was collected and quantified with the weigh scale from the top tube side port. Transmembrane pressure was calculated as the average pressure at the inlet and outlet ports, while the tube side was left open to atmospheric pressure. The performance of the system was evaluated based on oil flux and oil recovery.

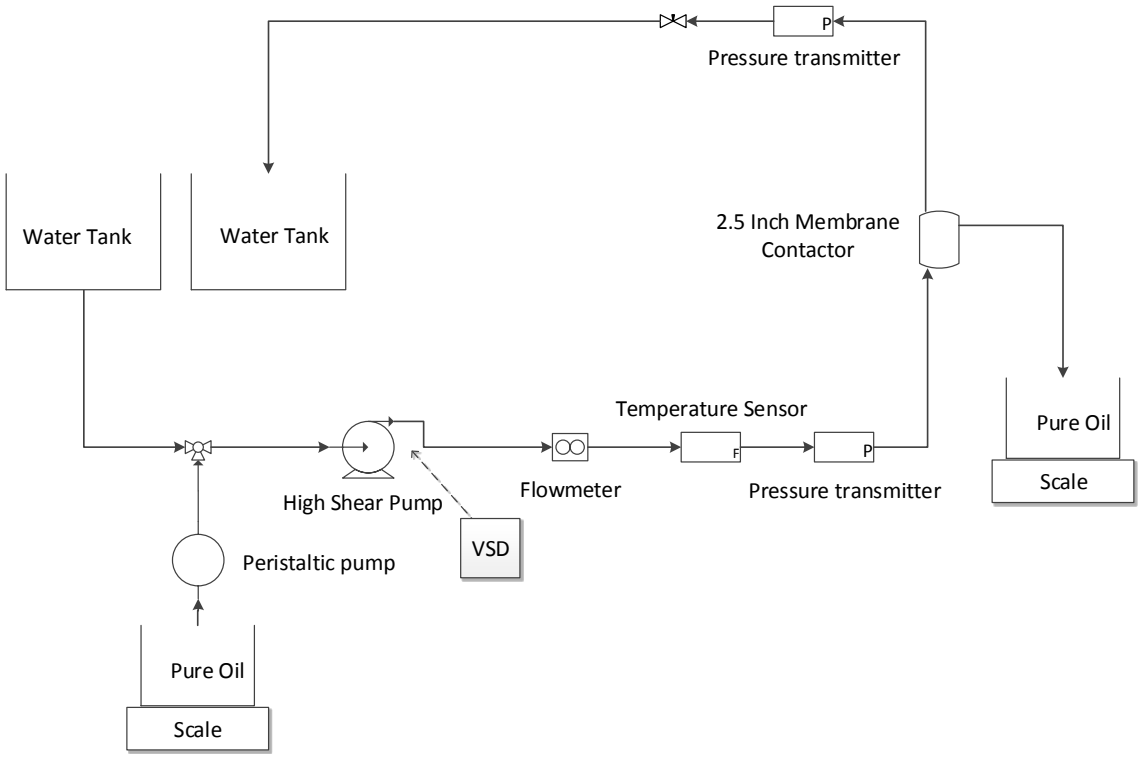

Figure 6-2: “One pass through” system schematic.

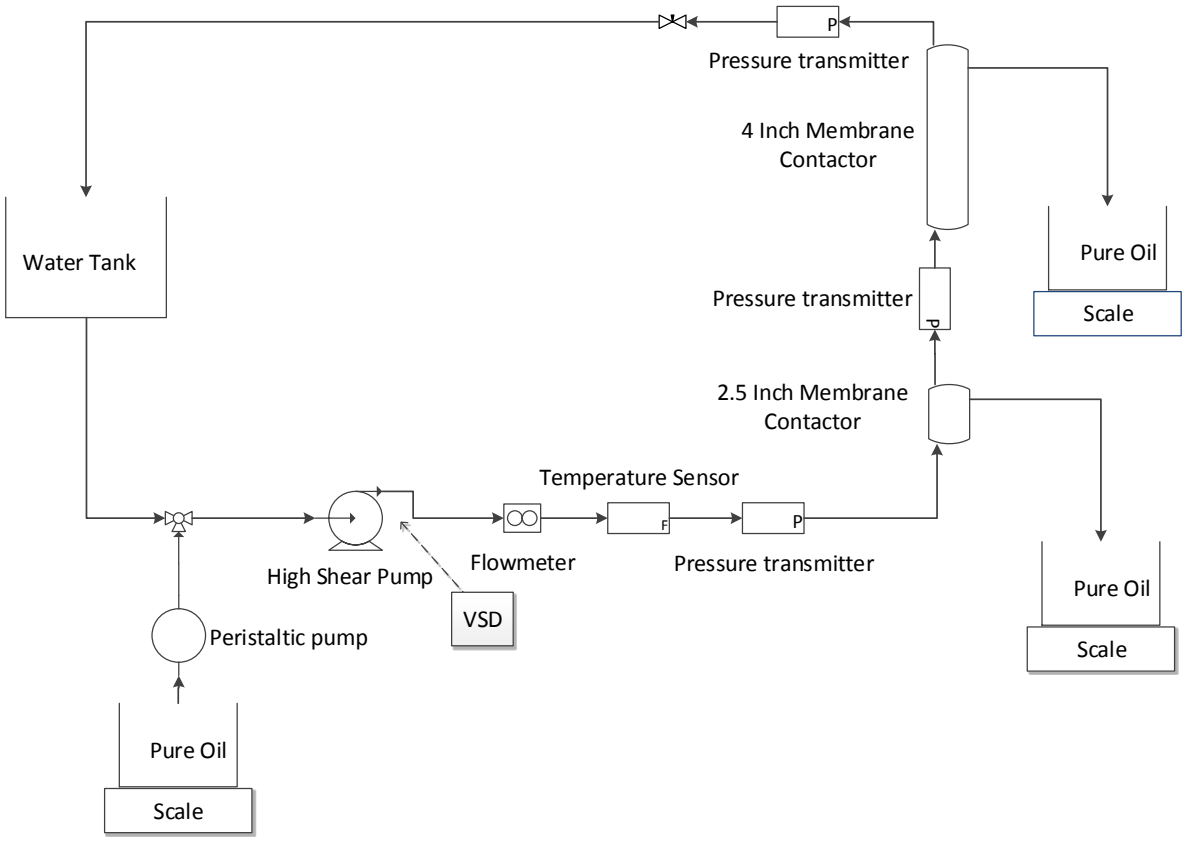

Figure 6-3: System schematic in recycling mode.

OIL FLUX AND SURFACE AREA MODEL DEVELOPMENT

Effective Surface Area

In this study, a new and novel model describing oil flux across a hydrophobic membrane is proposed. The model is fairly analogous to the approach used in packed column absorption (*112*). As shown in Equation 6-1, the oil transferred across the membrane walls is the product of an intrinsic oil flux (Oil $flux_{Pure}$) determined during the pure oil feed experiments and the effective surface area of the membrane. The effective membrane area for coalescence may be significantly less than the actual membrane area, especially at high water concentrations. The high concentrations of water may enter

pores or cause the membrane surface to become hydrophilic which results in effectively blocking transport of the oil.

$$Oil\ Transferred = Intrinsic\ Flux * a_e \quad \text{(Eq. 6-1)}$$

Equation 6-1 can be re-written to express oil flux across the membrane in terms of the intrinsic flux and the effective area ratio defined as the effective area over the total area of the membrane (a_e/a_p) (Equation 6-2).

$$Oil\ Flux_{O/W} = Oil\ Flux_{Pure\ oil} * \frac{a_e}{a_t} \quad \text{(Eq. 6-2)}$$

Where:

Oil $Flux_{O/W}$: Oil flux for oil-water mixtures in $m^3/s\text{-}m^2$
Oil $Flux_{Pure\ oil}$: Oil flux for pure oil feed conditions in $m^3/s\text{-}m^2$
a_e: Effective surface area in m^2
a_t: Total surface area in m^2
a_e/a_t: Effective area ratio

The membrane contactor performance depends on the intrinsic flux (Oil $flux_{Pure}$) and the effective area ratio, which depends on the entering oil rate. The first step in developing the model was to characterize the intrinsic flux using membrane characteristics and operating parameters. Pure oil feed experiments allowed quantification of the intrinsic flux of the system where the total membrane surface is assumed to be available and maximized oil permeation is observed. Then, assuming the effective area ratio equals the ratio of measured flux for oil-water experiments to pure oil feed flux, a model was developed to predict the effective area ratio as a function of the operating parameters. Finally, a complete equation for oil flux prediction as a function of transmembrane pressure, viscosity, oil concentration, influent flow rates and membrane characteristics can be obtained and used to predict surface area requirements as a function of operating conditions. An example calculation can be found at the end of this paper.

Pure Oil Conditions

The model describing the experimental data most accurately for pure oil feed filtration with the X50 membrane contactor is shown in Equation 6-3 (discussed previously in Chapter 4). The model is the Ergun equation originally developed for flow through packed columns and applied to flow through pores membranes.

$$Oil\ flux_{Pure} = \frac{TMP \cdot d_p^2 \cdot \varepsilon^3}{150 \cdot L \cdot \mu \cdot (1-\varepsilon)^2} = \frac{TMP \cdot {d_{pore}}^2 \cdot \left(\frac{1-\varepsilon}{\varepsilon}\right)^{\frac{2}{3}} \cdot \varepsilon^3}{150 \cdot L \cdot \mu \cdot (1-\varepsilon)^2} \qquad \text{(Eq. 6-3)}$$

Oil $Flux_{Pure\ oil}$: oil flux for pure oil feed experiments in $m^3/s\text{-}m^2$
d_p: Equivalent particle diameter (m): $d_p = d_{pore} \cdot (\frac{1-\varepsilon}{\varepsilon})^{\frac{1}{3}}$
TMP: Applied transmembrane pressure (Pa)
μ: Viscosity (Pa.s)
L: Membrane wall thickness (m)
ε: porosity

Oil-Water Mixtures

The effective surface area ratio was computed for the set of oil-water experiments described in Table 6-4 using Equation 6-2. The effects of transmembrane pressure, influent flow rate, viscosity, and oil concentration on effective area ratio were first analyzed. The trends observed for each parameter were then used to develop a model for the effective area ratio.

Effect of Oil Concentration

The experimental curve of effective area ratio plotted versus oil concentration seen in Figure 6-4 displays saturation behavior seen in other applications such as the Michaelis–Menten kinetics equation or the Langmuir adsorption isotherm. The membrane pores, which are directly related to oil permeation, can be considered as

available sites, while the driving force for accumulation onto the membrane wall is the oil concentration. At low oil concentrations, the effective area ratio is linearly related. Oil concentration linearly increases the probability for the oil droplets to contact the membrane wall. For higher oil concentrations, the curve reaches saturation where the effective surface area approaches the total surface area available for oil permeation. Therefore, a saturation model as presented in Equation 6-4 should provide a good fit to correlate effective area ratio to oil concentration (assuming that the ratio of flux to the pure oil feed flux is equal to the effective area ratio).

$$\frac{Oil\ Flux_{O/W}}{Oil\ Flux_{Pure\ oil}} = \frac{a_e}{a_t} = \frac{\mathrm{a}\cdot C_{oil}}{1+\mathrm{b}\cdot C_{oil}} \quad \text{with a and b constants.} \qquad \text{(Eq. 6-4)}$$

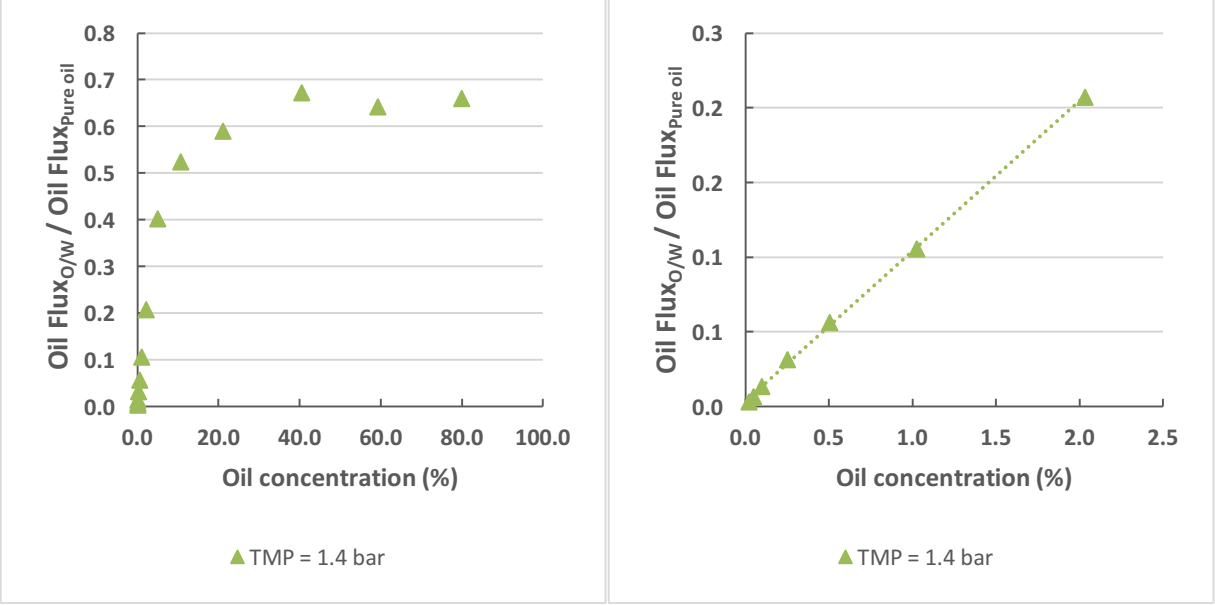

Figure 6-4: Experimental flux ratio vs oil concentration in the feed. Experimental conditions: TMP = 1.4 bar, Influent flow rate: 3.8 L/min, Isopar M. Good fit for a saturation model: $\frac{a_e}{a_t} = \frac{\mathrm{a}\cdot C_{oil}}{1+\mathrm{b}\cdot C_{oil}}$.

Effect of Other Operating Parameters

The effect of influent flow rate on oil recovery in the system for feed containing oil-water mixtures was attributed to changes in residence time of the oil droplets in the membrane module (Chapter 5). At higher feed oil content and higher influent flow rates, the effective surface area is shown to increase in Figure 6-5. This is analogous to the effective mass transfer area increasing with liquid rate in packed column absorption systems (*112*) .The effect of influent flow is less dramatic at higher oil concentrations that approach the ideal case of pure oil in the feed. Indeed, under pure oil conditions, the influent flow rate was determined to have no impact on the oil flux (Chapter 4).

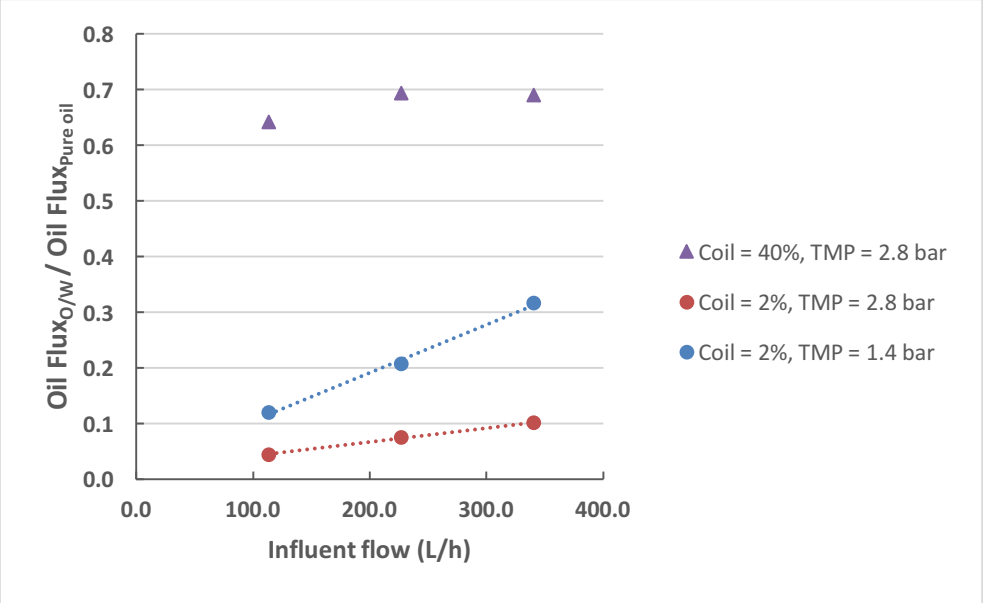

Figure 6-5: Effect of influent flow rate on flux ratio. Experimental conditions: Isopar M.

The effect of transmembrane pressure on oil permeation and recovery was investigated for oil concentrations ranging from 200 ppmv to 90% (v/v) in the feed (Chapter 5). For high oil concentrations, an increase in transmembrane pressure was found to increase the oil flux across the fiber wall (Chapter 5). This phenomena is well documented in membrane filtration systems (both for hydrophobic (*56, 59*) and hydrophilic (*50, 64*) membranes). For low oil concentrations (2% (v/v)), however, an

increase in transmembrane pressure was observed to decrease the oil flux across the fiber wall, which is likely a result of water entering and blocking the pore. Breakthrough of water will eventually occur if a higher transmembrane pressure were applied. This is consistent with the Young-Laplace relationship between pressure and the curvature of a water droplet at the entrance of a pore, which has a contact angle greater than 90 degrees. Larger pores have smaller breakthrough pressures than smaller pores according to the analysis of oil-water interfaces at the entrance of pores conducted by Nazzal et al. (*76*) While the critical pressure for the average pore size is well above relevant transmembrane pressure values for this system, there are pores within the distribution that are large enough to be at least partially filled (blocked) by water. Thus, the effective surface area could be affected by this phenomenon without water breakthrough. The effective membrane surface area calculated from Equation 6-1 above decreases with increasing transmembrane pressure with water in the feed (Figure 6-6). The decrease is more drastic for dilute oil-water mixtures for which more pores are exposed to water and subject to blocking. Therefore, there is a trade-off between forcing more oil through the pores with higher transmembrane pressure and reducing the useful surface area of the membrane. It should be noted that the effect of interfacial tension which would affect water breakthrough was not studied in this work.

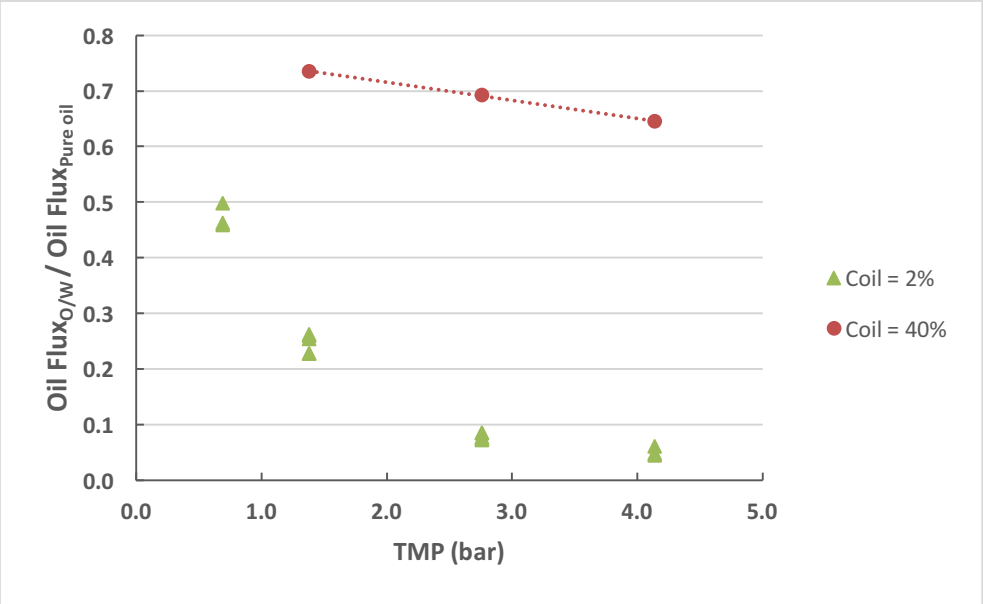

Figure 6-6: Effect of transmembrane pressure on flux ratio for two oil feed concentrations. Experimental conditions: Influent flow rate = 3.8 L/min, Isopar M.

Similarly, oil viscosity was shown to impact oil permeation in the membrane contactor depending on the feed oil concentration (Chapter 5). However, effective surface area seems to improve with increasing viscosity. Again, two mechanisms are balancing each other and affect the system differently depending on the oil concentration in the feed. Increasing viscosity appears to help grow and stabilize the oil film on the membrane surface and thereby increase the effective membrane surface area. However, for high oil concentrations, transport mechanisms are strongly affected by viscosity as demonstrated by the Ergun equation (Chapter 4). For very dilute mixtures, stability of the oil film seems to be the main contributor to higher oil flux.

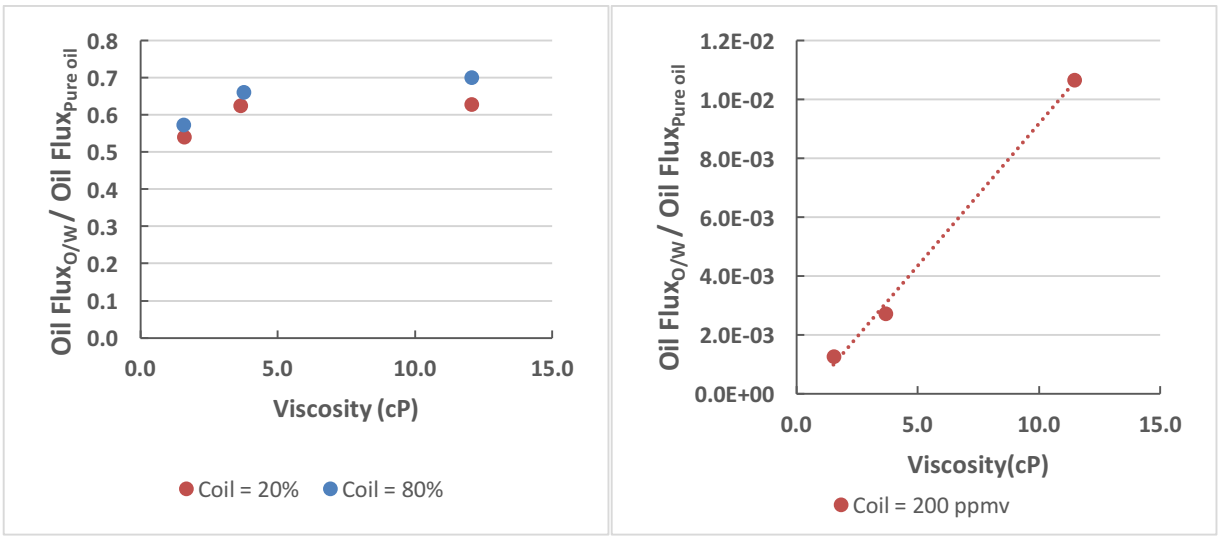

Figure 6-7: Effect of viscosity on flux ratio for various oil feed concentrations.
Experimental conditions: TMP = 1.4 bar, Influent flow rate = 3.8 L/min.

Effective Area Ratio Model

The data gathered and presented in the previous sections represented a total of 58 experiments obtained with the 2.5-inch diameter X50 membrane contactor. Table 6-5 summarizes the range of the parameters studied. MATLAB was used to fit the experimental data to the effective area ratio model presented in Equation 6-5. The nlinfit function was used to conduct a nonlinear regression for the over constrained system of 58 nonlinear equations. The results were obtained by iterative least squares estimation.

Table 6-5: Summary of the range of operating parameters used to develop the model

TMP (bar)	Viscosity (cP)	Influent flow rate (L/h)	Oil concentration (%(v/v))
[0.7-4]	[1.5-12]	[113-340]	[0.02-100]

$$\frac{a_e}{a_t} = \frac{9.27*10^{12} \cdot C_{oil} \cdot TMP^{-1.6} \cdot \mu^{1.0} \cdot Q^{0.3}}{1+2.65*10^{16} \cdot C_{oil} \cdot TMP^{-2.1} \cdot \mu^{1.1} \cdot Q^{0.4}} \qquad \text{(Eq. 6-5)}$$

With C_{oil}: oil volume fraction

TMP: Transmembrane pressure in Pa

μ: Viscosity in Pa.s

Q: Influent flow rate in m^3/s.

Transmembrane pressure, influent flow rate and viscosity were integrated into the model so that with changing oil concentration, the varying effect of each parameter was taken into consideration. The model was initially fit based on the lower oil feed concentration data (≤2%) to allow better accuracy in this concentration range. This approach resulted in a slightly underestimated fit at higher concentrations. The attempt to fit all data at once led to overestimated values for low oil concentrations, which is undesirable for engineering design purposes. A conservative fit in this range provides for a margin of safety for design purposes. For this reason, the first approach was selected to obtain a better fit at lower concentrations.

The residual plot seen in Figure 6-8 shows the desired random scatter of data points with a slight unbalance to the left due to a higher number of experiments conducted for low oil concentrations. In addition, the model was first fit with the lower oil concentration range leading to reduced residuals on the left hand side of the plot.

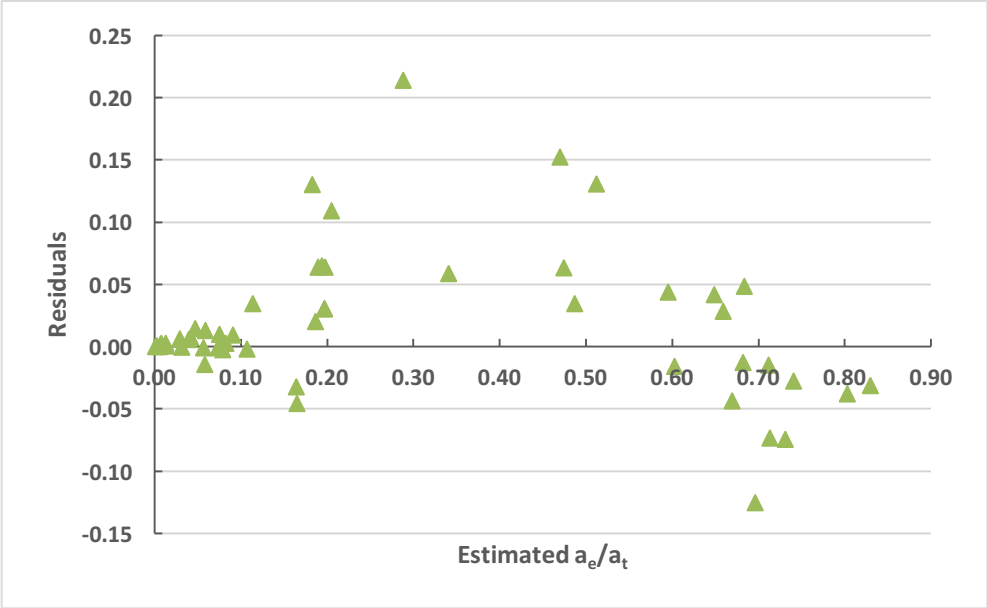

Figure 6-8: Residual plot for the complete oil-water experimental data set presented in Table 6-4.

The plot of experimental effective area ratio versus estimated values shown in Figure 6-9 shows a reliable linear correlation. Most of the simulated data points are within the 20% of the measured values. Therefore, the model can be used to obtain a good estimate of effective surface area across the membrane contactor for the set of experimental conditions examined in this study (Table 6-5).

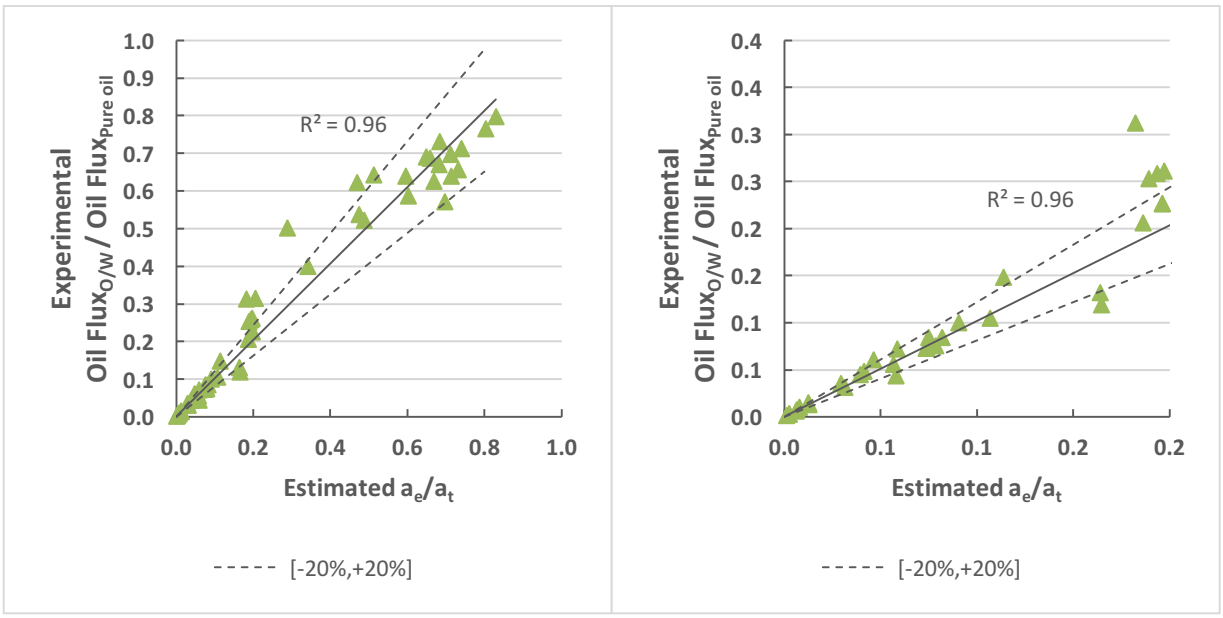

Figure 6-9: Experimental flux ratio vs a_e/a_t model estimated values. The model used is shown in Equation 6-5. The linear fit correlation factor of the solid line is 0.96.

Some of the uncertainty of the model arises from the higher variability of results obtained at lower oil concentrations. At low oil concentrations, the oil flux was observed to improve over time as steady state conditions were approached leading to possible higher error in selecting steady state oil flux (Chapter 5). Figure 6-10 shows a few examples of the model prediction compared to the experimentally measured data for various transmembrane pressures, viscosities, oil concentrations, and influent flow rates. The model fits are reasonable but in some cases the model underestimates the data. It should be noted the model is developed using chemical systems possessing a high interfacial tension (~52 dynes/cm) and should be used with some caution with systems with much lower interfacial tensions.

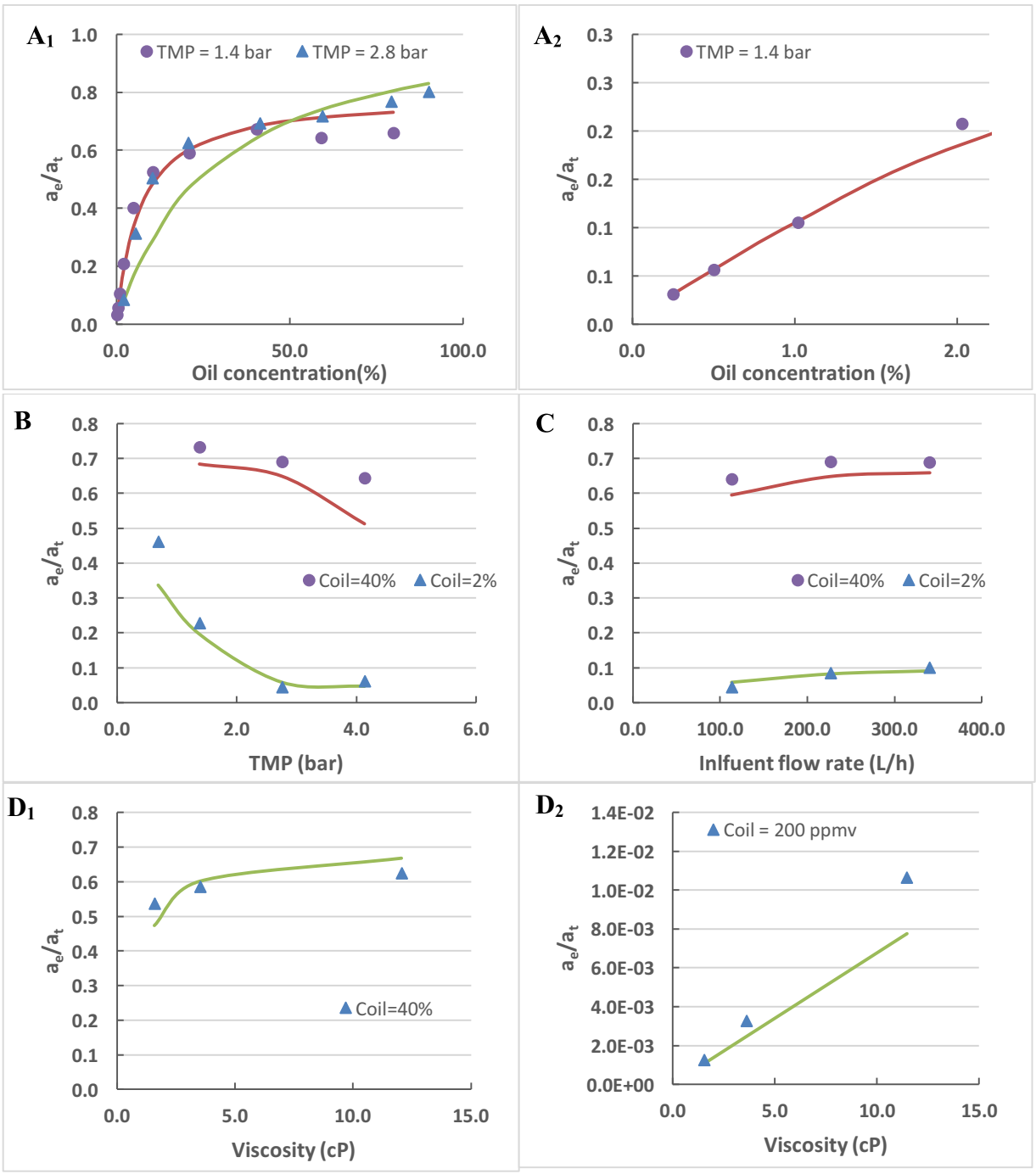

Figure 6-10: Examples of model fitting experimental data. Legend: symbols = experimental data, lines = model simulated values with Equation 6-5. Experimental conditions: $A_{1\text{-}2}$: Isopar M, Influent flow rate = 3.8 L/min; B: Isopar M, Influent flow rate = 3.8 L/min; C: TMP = 1.4 bar, Influent flow rate = 3.8 L/min; D: Isopar M, D_1: C_{oil} = 2%, TMP = 1.4 bar, D_2: C_{oil} = 40%, TMP = 2.8 bar.

The model can then be incorporated into Equation 6-2 and a model for oil flux prediction is obtained and shown in Equation 6-6 for modules with surface area less than or equal to 1.4 m^2.

$$Oil\ Flux_{O/W} = Oil\ Flux_{Pure} * \frac{a_e}{a_t} \quad \text{(Eq. 6-6)}$$

$$Oil\ Flux_{O/W} = \frac{TMP \cdot {d_{pore}}^2 \cdot (\frac{1-\varepsilon}{\varepsilon})^{\frac{2}{3}} \cdot \varepsilon^3}{150 \cdot L \cdot \mu \cdot (1-\varepsilon)^2} * \frac{9.27 * 10^{12} \cdot C_{oil} \cdot TMP^{-1.6} \cdot \mu^{1.0} \cdot Q^{0.3}}{1 + 2.65 * 10^{16} \cdot C_{oil} \cdot TMP^{-2.1} \cdot \mu^{1.1} \cdot Q^{0.4}}$$

Rearranging and separating the terms which remain constant from those which were varied:

$$Oil\ Flux_{O/W} = \frac{{d_{pore}}^2 \cdot (\frac{1-\varepsilon}{\varepsilon})^{\frac{2}{3}} \cdot \varepsilon^3}{150 \cdot L \cdot (1-\varepsilon)^2} * \frac{9.27 * 10^{12} \cdot C_{oil} \cdot TMP^{-0.6} \cdot Q^{0.3}}{1 + 2.65 * 10^{16} \cdot C_{oil} \cdot TMP^{-2.1} \cdot \mu^{1.1} \cdot Q^{0.4}}$$

Where:
Oil $Flux_{O/W}$: Oil flux across the membrane in $m^3/s\text{-}m^2$
d_{pore}: Membrane pore size (m)
TMP: Applied transmembrane pressure (Pa)
μ: Viscosity (Pa.s)
L: Membrane wall thickness (m)
ε: porosity

Comparison of experimental and simulated fluxes, shown in Figure 6-11, indicate that the coefficient of correlation of the linear fit is 0.96, indicating the model predicts the oil flux reasonably well for the 2.5-inch diameter X50 membrane contactor. Some variability is observed for higher oil concentration predictions in particular for transmembrane pressures higher than 1.4 bar and oil concentrations above 10% (v/v). The model can be used as a guideline for other hollow fiber membrane contactors but would require some preliminary assessment and model validation. In particular, the pure oil feed

flux component may differ from the Ergun equation when the porosity is below 40%. The permeability constant (here 150) has been shown to vary with porosity (Chapter 4).

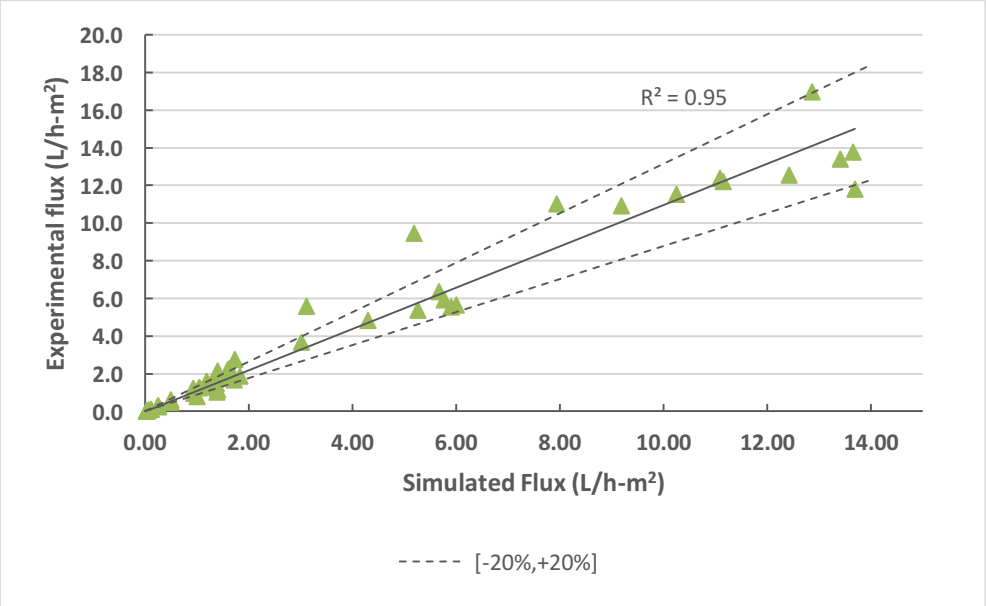

Figure 6-11: Experimental vs simulated flux for the X50 2.5-inch module contactor.

Design Example

The oil-water model shown in Equation 6-6 can be used for different purposes such as choosing the most efficient combination of operating parameters or determining the surface area needed to achieve the desired oil removal with the system. Figure 6-12 shows a few model simulations for every operating parameter affecting the process in the experimental ranges studied (Table 6-5). A number of conclusions can be drawn from Figure 6-12. A lower pressure will be more efficient for dilute mixtures (<2% (v/v) oil concentration), while higher transmembrane pressures will be preferable at high oil concentrations (40% (v/v) oil concentration) (Figure 6-12-$A_{1\text{-}3}$). Similarly, the model can be used to compare performance as a function of influent flow rates. In this case, operating at a higher transmembrane pressure will lead to higher oil flux and recovery

(Figure 6-12-$C_{1\text{-}2}$). Viscosity can also be used as an operating lever by changing temperature of a given influent stream for instance.

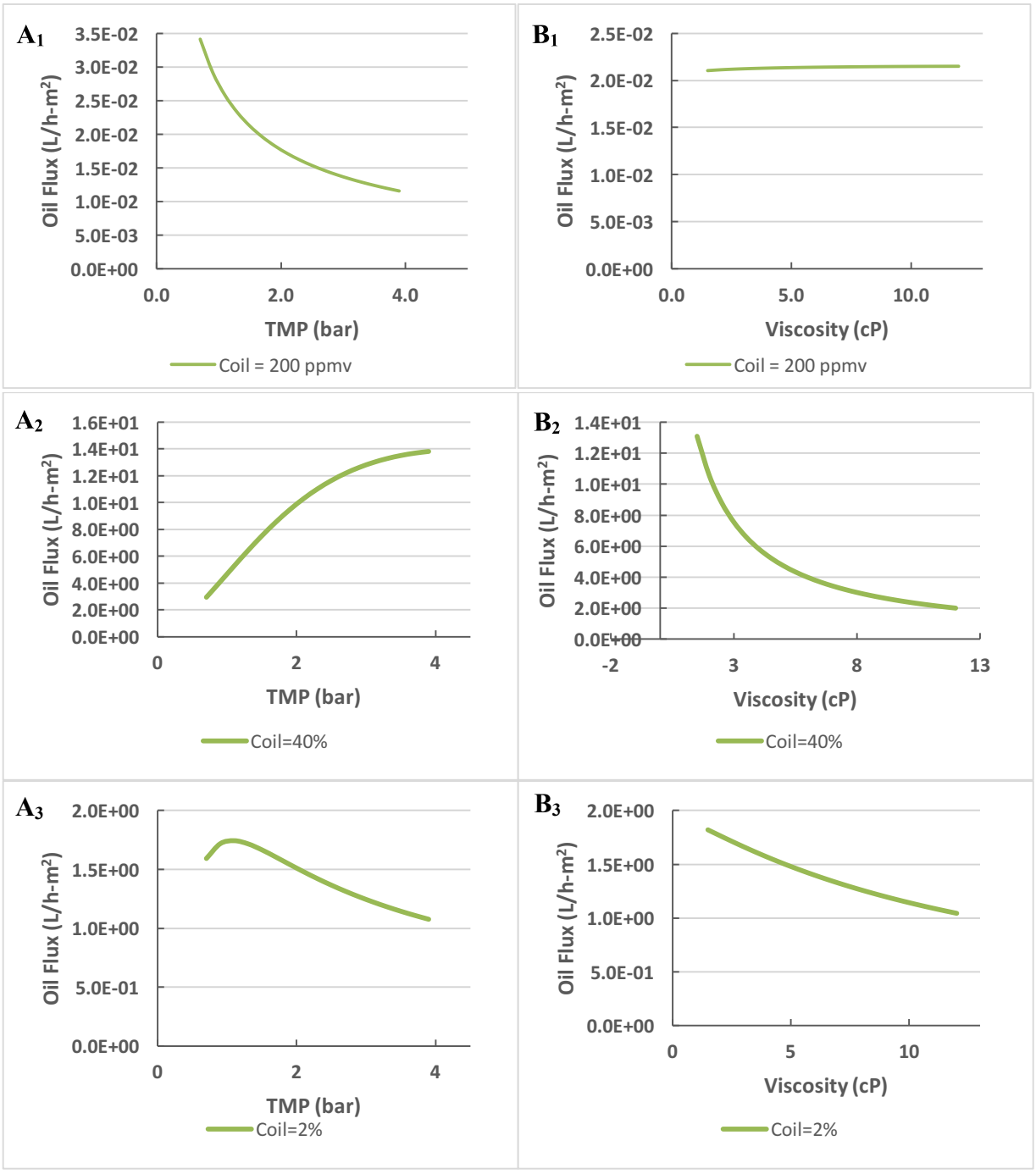

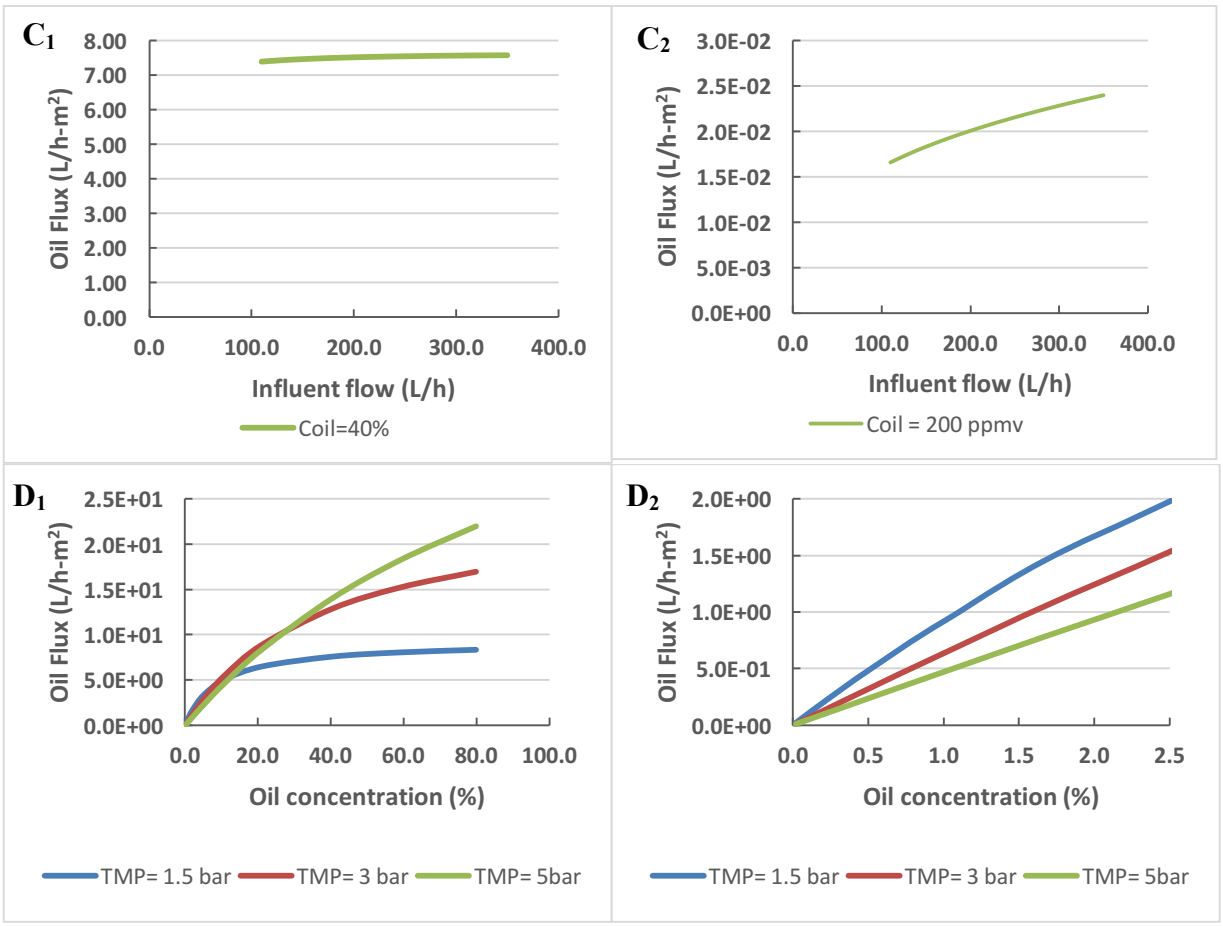

Figure 6-12: Model predictions for oil permeation. Experimental conditions: $A_{1\text{-}3}$: Viscosity = 3 cP, Influent flow rate = 240 L/h; $B_{1\text{-}3}$: TMP = 1.5 bar, Influent flow rate = 240 L/h; $C_{1\text{-}2}$: TMP = 1.5 bar, Viscosity = 3 cP; $D_{1\text{-}2}$: Viscosity = 3 cP, TMP = 1.5 bar, Influent flow rate = 240 L/h.

The model predicts the positive effect of increasing viscosity on oil permeation for dilute mixtures (< 200 ppmv oil concentration) and the negative effect of increasing viscosity for higher concentrations (Figure 6-12-$B_{1\text{-}3}$). Finally, Figure 6-12-$D_{1\text{-}2}$ shows the decrease of effective surface area with increasing water content in the feed. The model simulates all the trends observed in Chapter 4 accurately.

The effective surface area needed to reach a given oil recovery can then be determined with the selected operating conditions. The advantage of using the 2.5-inch diameter module for the experimental data is that surface area is small and performance

sensitivity can be accurately measured. The small module can be thought as a slice of the larger modules and, therefore, the model regarded as a differential equation.

$$Oil\ flux\ _{O/W} = Oil\ Flux_{Pure} * \frac{9.27 * 10^{12} \cdot C_{oil} \cdot TMP^{-1.6} \cdot \mu^{1.0} \cdot Q^{0.3}}{1 + 2.65 * 10^{16} \cdot C_{oil} \cdot TMP^{-2.1} \cdot \mu^{1.1} \cdot Q^{0.4}}$$

and $Oil\ flux\ _{O/W} = \frac{\mathrm{dq_{oil}}}{\mathrm{dA}} = Q \cdot \frac{\mathrm{dC_{oil}}}{\mathrm{dA}}$ with $\mathrm{q_{oil}} = \frac{\text{Volume of oil}}{\text{Time}}$

If $\alpha = 9.27 * 10^{12} \cdot TMP^{-1.6} \cdot \mu^{1.0} \cdot Q^{0.3}$

$\beta = 2.65 * 10^{16} \cdot TMP^{-2.1} \cdot \mu^{1.1} \cdot Q^{0.4}$

Then, $Oil\ flux\ _{O/W} = Oil\ Flux_{Pure} * \frac{\alpha \cdot C_{oil}}{1 + \beta \cdot C_{oil}}$

$$Q \cdot \frac{\mathrm{dC_{oil}}}{\mathrm{dA}} = Oil\ Flux_{Pure} * \frac{\alpha \cdot C_{oil}}{1 + \beta \cdot C_{oil}}$$

$$\frac{\mathrm{dC_{oil}}}{\mathrm{dA}} = \frac{Oil\ Flux_{Pure}}{Q} * \frac{\alpha \cdot C_{oil}}{1 + \beta \cdot C_{oil}}$$

$$\frac{Oil\ Flux_{Pure}}{Q} * \int_{A}^{0} \mathrm{dA} = \int_{C_i}^{C_f} \frac{1 + \beta \cdot C_{oil}}{\alpha \cdot C_{oil}} \mathrm{dC_{oil}}$$

$$\frac{Oil\ Flux_{Pure}}{Q} * \int_{A}^{0} \mathrm{dA} = \frac{1}{\alpha} \int_{C_i}^{C_f} \frac{\mathrm{dC_{oil}}}{C_{oil}} + \frac{\beta}{\alpha} \int_{C_i}^{C_f} \mathrm{dC_{oil}}$$

$$\frac{Oil\ Flux_{Pure}}{Q} * \mathrm{A} = \frac{1}{\alpha} \cdot \ln\left(\frac{C_i}{C_f}\right) + \frac{\beta}{\alpha} \cdot (C_i - C_f)$$

Determination of A:

$$\mathrm{A} = \frac{Q}{Oil\ Flux_{Pure}} * \left(\frac{1}{\alpha} \cdot \ln\left(\frac{C_i}{C_f}\right) + \frac{\beta}{\alpha} \cdot (C_i - C_f)\right)$$

Determination of C_f: (trial and error calculation)

$$C_f = C_i + \frac{1}{\beta} \cdot \ln\left(\frac{C_i}{C_f}\right) - \frac{\alpha}{\beta} * \frac{Oil\ Flux_{Pure}}{Q} \cdot \mathrm{A}$$

Upon integration between the influent and target effluent concentrations, an expression is obtained for predicting the required membrane surface area for a given effluent concentration and another expression is obtained to determine oil concentration in the water effluent for a given surface area. Example calculations are presented in the appendix. Projected values of surface area needed to obtain a chosen oil recovery can then be calculated. A few examples of the model application are shown in Table 6-6.

Table 6-6: Surface area predictions for 95% oil recovery.

Feed			Operating parameters		Model predictions
Oil concentration (%)	Viscosity (cP)	Oil content in feed (L/h)	Influent flow (L/h)	Transmembrane pressure (bar)	Surface area needed for 95% oil recovery (m^2)
0.1	4	0.24	240	1.5	7.6
0.1	4	0.24	240	3	11.5
0.1	4	0.48	480	1.5	12.4
30	6	72	240	1.5	27.3
30	6	72	240	3	18.5
30	6	144	480	3	33.6
0.01	1	0.08	800	1.5	17.6
0.01	10	0.08	800	1.5	17.6

An experiment was conducted with a 4-inch diameter module with an oil concentration of 1000 ppmv (Figure 6-13). An oil recovery superior to 99% was

observed, which is in agreement with the model predicting a minimum of 11 m^2 of required surface area to attain such recovery.

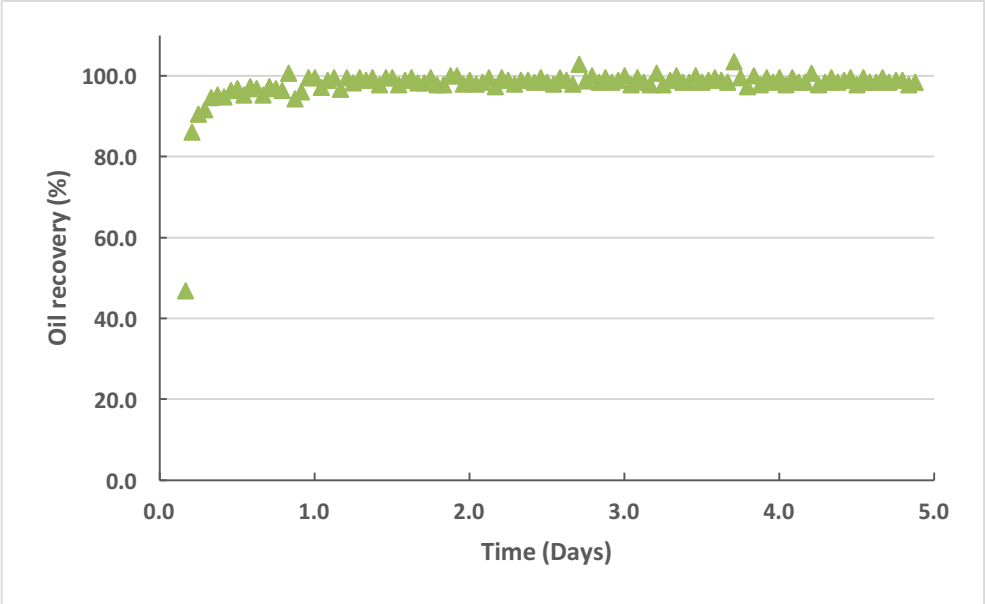

Figure 6-13: Oil recovery with a 4-inch module at C_{oil} = 1000 ppmv. Experimental conditions: Viscosity = 3.75 cP; Influent flow rate = 227 L/h; Transmembrane pressure = 1.4 bar, C_{oil} = 1000 ppmv, Membrane C, SA = 20 m^2.

A possible limitation associated with the proposed scale-up approach is the difference of shell-side pressure drop occurring in modules of different sizes. The model was developed with experimental data collected with the 2.5x8 inch module and flux predictions account for the pressure drop related to the small module size and working influent flow rates. If a larger module is selected for a higher surface area, the pressure drop profile may be different leading to less accuracy of the model prediction. Therefore, the model is useful in providing a first estimation of membrane performance.

CONCLUSIONS

Modeling of oil and water separation with membrane systems have mainly focused on hydrophilic materials. The present work allowed the development of the first model to date to predict oil permeation for the separation of oil-water mixtures with hydrophobic hollow fiber membrane contactors. The new modelling approach used the performance of the membrane contactor under pure oil feed conditions and the effective area ratio to predict oil flux with oil-water mixture operations. The model fits the experimental data well with a correlation coefficient of 0.95. The model reliably predicts oil permeation in the low oil concentration range and presents more uncertainty for high oil concentrations and high transmembrane pressures. Transmembrane pressure, viscosity, influent flow rate and oil concentrations are the input parameters that the operator can control to optimize the use of the membrane technology for oil-water separation. The model can be used to predict membrane surface area needed to obtain desired insoluble oil removal from an oil-water feed mixture. The effective area model developed in this work is based on studies using a high interfacial tension (~52 dynes/cm) and without solids, therefore, some caution should be applied. Future work should address the comparative effects of lower interfacial tensions and solids.

NOMENCLATURE

C_{oil}: Oil concentration, V/V ratio is used in the model

TMP: Transmembrane pressure (Pa)

Q: Influent flow rate (m^3/s)

μ: Viscosity (Pa.s)

Flux: Oil flux ($m^3/s\text{-}m^2$)

C_i: Feed oil concentration (volumetric ratio)

C_f: Effluent oil concentration (volumetric ratio)

q_0: Oil flow rate in feed (m^3/s)

A: Design surface area (m^2)

Oil $Flux_{O/W}$: Oil flux across the membrane in $m^3/s\text{-}m^2$

Oil $Flux_{Pure\ oil}$: Oil flux across the membrane obtained with pure oil feed in $m^3/s\text{-}m^2$

d_{pore}: Equivalent particle diameter (m): $d_p = d_{pore} \cdot (\frac{1-\varepsilon}{\varepsilon})^{\frac{1}{3}}$

d_{pore}: Membrane pore size (m)

L: Membrane wall thickness (m)

ε: porosity

APPENDIX

Example Calculations

A. Determination of surface area required for 95% oil removal

Inputs:

Membrane material: Pore size $= 0.04 \cdot 10^{-6}\ m$

Porosity $= 0.4$

Wall thickness $= 40 \cdot 10^{-6}\ m$

Process for 95% removal:

$C_i = (C_{oil})_{Feed} = 1000ppm = 1000 \cdot 10^{-6}$

$C_f = (C_{oil})_{Effluent} = 50ppm = 50 \cdot 10^{-6}$

Feedrate $= 240\ l/hr = 6.67 \cdot 10^{-5}\ m^3/s$

Oil Viscosity $= 4$ cP $= 4 \cdot 10^{-3}\ Pa/s$

TMP $= 1.5$ bar $= 1.5 \cdot 10^5\ Pa$

1. Calculate Oil $Flux_{Pure}$

$$Oil\ flux_{Pure} = \frac{TMP \cdot {d_{pore}}^2 \cdot (\frac{1-\varepsilon}{\varepsilon})^{\frac{2}{3}} \cdot \varepsilon^3}{150 \cdot L \cdot \mu \cdot (1-\varepsilon)^2}$$

$$= \frac{(1.5 \cdot 10^5) \cdot (0.04 \cdot 10^{-6})^2 \cdot (\frac{1-0.4}{0.4})^{\frac{2}{3}} \cdot 0.4^3}{150 \cdot (40 \cdot 10^{-6}) \cdot (4 \cdot 10^{-3}) \cdot (1-0.4)^2}$$

$$= \frac{(2.01 \cdot 10^{-11})}{(8.64 \cdot 10^{-6})}$$

$$= 2.32 \cdot 10^{-6}\ m/s$$

2. Determination of α and β

$$\alpha = 9.27 \cdot 10^{12} \cdot TMP^{-1.6} \cdot \mu^{1.0} \cdot Q^{0.3}$$

$$= (9.27 \cdot 10^{12}) \cdot (1.5 \cdot 10^5)^{-1.6} \cdot (4 \cdot 10^{-3})^{1.0} \cdot (6.67 \cdot 10^{-5})^{0.3}$$

$$= 10.83$$

$$\beta = 2.65 \cdot 10^{16} \cdot TMP^{-2.1} \cdot \mu^{1.1} \cdot Q^{0.4}$$

$$= (2.65 \cdot 10^{16}) \cdot (1.5 \cdot 10^5)^{-2.1} \cdot (4 \cdot 10^{-3})^{1.1} \cdot (6.67 \cdot 10^{-5})^{0.4}$$

$$= 17.59$$

3. Determination of A

$$\text{A} = \frac{Q}{Oil\ Flux_{Pure}} * \left(\frac{1}{\alpha} \cdot \ln\left(\frac{C_i}{C_f}\right) + \frac{\beta}{\alpha} \cdot (C_i - C_f)\right)$$

$$= \frac{6.67 \cdot 10^{-5}}{2.32 \cdot 10^{-6}} * \left(\frac{1}{10.83} \cdot \ln\left(\frac{1000 \cdot 10^{-6}}{50 \cdot 10^{-6}}\right) + \frac{17.59}{10.83} \cdot (1000 \cdot 10^{-6} - 50 \cdot 10^{-6})\right)$$

$$= 28.75 * (0.277 + 0.0015)$$

$$= 8\ m^2$$

B. Calculation of effluent concentration for a surface area of 16 m^2 and TMP is reduced to 1 bar

Inputs:

Membrane material: Pore size $= 0.04 \cdot 10^{-6}\ m$

Porosity $= 0.4$

$$\text{Wall thickness} = 40 \cdot 10^{-6}\ m$$

$$\text{Membrane Area} = 16\ m^2$$

Process:

$$C_i = (C_{oil})_{Feed} = 1000\ ppm = 1000 \cdot 10^{-6}$$

$$\text{Feedrate} = 240\ L/h = 6.67 \cdot 10^{-5}\ m^3/s$$

$$\text{Oil Viscosity} = 4\ \text{cP} = 4 \cdot 10^{-3}\ Pa/s$$

$$\text{TMP} = 1\ \text{bar} = 1.0 \cdot 10^{5}\ Pa$$

1. Calculate Oil $\text{Flux}_{\text{Pure}}$

$$Oil\ flux_{Pure} = \frac{TMP \cdot {d_{pore}}^2 \cdot (\frac{1-\varepsilon}{\varepsilon})^{\frac{2}{3}} \cdot \varepsilon^3}{150 \cdot L \cdot \mu \cdot (1-\varepsilon)^2}$$

$$= \frac{(1.0 \cdot 10^5) \cdot (0.04 \cdot 10^{-6})^2 \cdot (\frac{1-0.4}{0.4})^{\frac{2}{3}} \cdot 0.4^3}{150 \cdot (40 \cdot 10^{-6}) \cdot (4 \cdot 10^{-3}) \cdot (1-0.4)^2}$$

$$= \frac{(1.342 \cdot 10^{-11})}{(8.64 \cdot 10^{-6})}$$

$$= 1.55 \cdot 10^{-6}\ m/s$$

2. Determination of α and β

$$\alpha = 9.27 \cdot 10^{12} \cdot TMP^{-1.6} \cdot \mu^{1.0} \cdot Q^{0.3}$$

$$= (9.27 \cdot 10^{12}) \cdot (1.0 \cdot 10^5)^{-1.6} \cdot (4 \cdot 10^{-3})^{1.0} \cdot (6.67 \cdot 10^{-5})^{0.3}$$

$$= 20.72$$

$$\beta = 2.65 \cdot 10^{16} \cdot TMP^{-2.1} \cdot \mu^{1.1} \cdot Q^{0.4}$$

$$= (2.65 \cdot 10^{16}) \cdot (1.0 \cdot 10^5)^{-2.1} \cdot (4 \cdot 10^{-3})^{1.1} \cdot (6.67 \cdot 10^{-5})^{0.4}$$

$$= 41.22$$

3. Determination of C_f by trial and error

$$C_f = C_i + \frac{1}{\beta} \cdot \ln\left(\frac{C_i}{C_f}\right) - \frac{\alpha}{\beta} * \frac{Oil\ Flux_{Pure}}{Q} \cdot \mathrm{A}$$
$$= 1000 \cdot 10^{-6} + \frac{1}{41.22} \cdot \ln\left(\frac{1000 \cdot 10^{-6}}{C_f}\right) - \frac{20.72}{41.22} * \frac{1.55 \cdot 10^{-6}}{6.67 \cdot 10^{-5}} \cdot 16$$
$$= 1000 \cdot 10^{-6} + 0.0243 \cdot \ln\left(\frac{1000 \cdot 10^{-6}}{C_f}\right) - 0.1869$$

Trial and error:

$$\text{First guess: } C_f \approx \frac{C_i}{\exp\left(\frac{0.1869}{0.0243}\right)}$$
$$\approx \frac{1000 \cdot 10^{-6}}{2189}$$
$$\approx 0.46 \cdot 10^{-6}$$

$C_f(x)$	$C_{f,calc}$
4.60E-07	8.20E-04
4.70E-07	3.05E-04
4.80E-07	-2.06E-04
4.75E-07	4.80E-05
4.77E-07	-5.30E-05

Therefore, $C_f \approx 0.477\ ppm$

$$\%\ Oil\ recovery \approx \frac{1000 - 0.477}{1000} * 100 = 99.95\%$$

Chapter 7: Practical Membrane Considerations

The research presented in the previous chapters focused on performance of the membranes in well-controlled experiments. However, membrane performance in field applications is often limited by membrane fouling caused either by inorganic precipitation or biological growth on the membranes. While no fouling, loss of performance or increase in pressure drop across the membranes were observed during the first six months of experiments with various membrane contactors (pure oil and oil-water experiments), an opportunity to evaluate biological fouling in the membrane presented itself after the modules were stored over a six-week period in which experiments had been halted[1]. This chapter addresses the discovery of this biofouling and provides an analysis of the impacts and potential remediation strategies for biological fouling in the membrane system.

MEMBRANE BIOLOGICAL FOULING

Over winter break 2014, modules were stored drained and all of the ports were capped. When process operation was resumed at the beginning of year 2015, a new 2.5-inch module was used but the 2014 4-inch "cleaning" module that was typically placed in series with a 2.5-inch module was reused. The system was initially started with an influent flow rate of 3.8 L/min and a transmembrane pressure of 1.4 bar, but the 2.5-inch module did not perform well compared to results obtained in previous experiment (see Figure 7-1).

[1] All results presented in previous sections were collected when no fouling was observed.

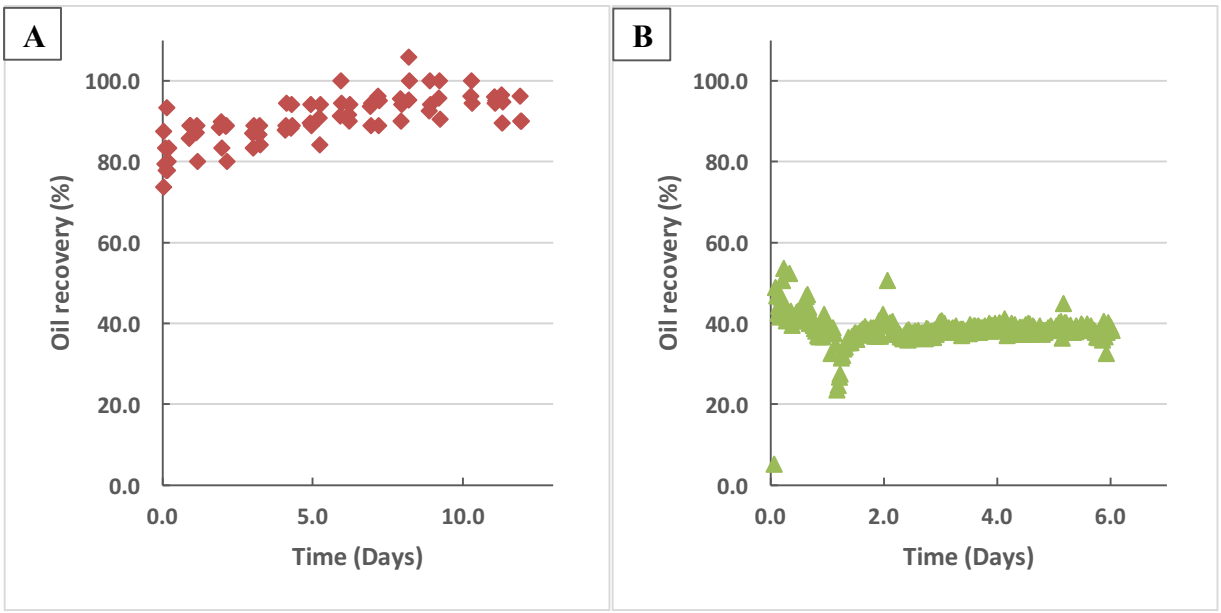

Figure 7-1: Oil recovery over time. A) Experiments conducted on a membrane after multiple experiments with high oil concentrations mixtures; B) Brand new module with 2014 4-inch cleaning module in series. Experimental conditions: Isopar M; Influent flow rate = 3.8 L/min; Transmembrane pressure = 1.4 bar, C_{oil} = 200 ppmv, Membrane A.

Over the next 10 weeks, a number of tests were conducted to determine the reason for the loss of performance and to evaluate strategies to regain performance. Figure 7-2 shows the recoveries observed for the 2.5-inch module during this period of time in which the membrane was operated with C_{oil} = 200 ppmv. Over the course of this period, operation was briefly interrupted and various treatments were applied to the membrane.

The first explanation considered for the loss of performance after starting the membrane was that the low oil concentration required time for build-up of an oil film on the fiber. This hypothesis would imply that performance would increase over time. However, the opposite result was observed; a decrease in oil recovery was observed from days 0 to 6.

The second hypothesis tested related to earlier observations of a cloudy layer in the water tank during initial start-up of a new module. Several brand new modules had been used during this research project and at start-up, oil that had permeated through the

module would always appear to have a higher tendency to foam, which would disappear as experiments proceeded and total oil recoveries approached 100%. If a sample was taken from the water tank, a slight white cloudy layer was observed on top of the water that did not resemble a typical oil layer. LC-MS tests were performed to identify the compound on multiple occasions. Only one sample suggested the presence of a compound with a structure similar to polyethylene glycol. However, the results could not be confirmed with subsequent sample analysis. In previous experiments, changing the water tank regularly eventually removed the cloudy layer suggesting that the membrane material initially leached a manufacturing compound in both the water and oil. This result suggests that membrane contactors may require a pretreatment consisting of water and oil flushing to eliminate the leaching chemical that did not seem to affect recoveries in previous experiments. However, such observations also suggested a possible explanation for the reduced recovery from the new 2.5-inch module with low oil concentration in the feed; the leached chemical that was recirculating from the water tank may have had a greater effect on performance under low oil conditions. Thus, the water in the recycling tank was changed which initially improved performance (see Figure 7-2) on day 6, but oil recoveries decreased again within hours.

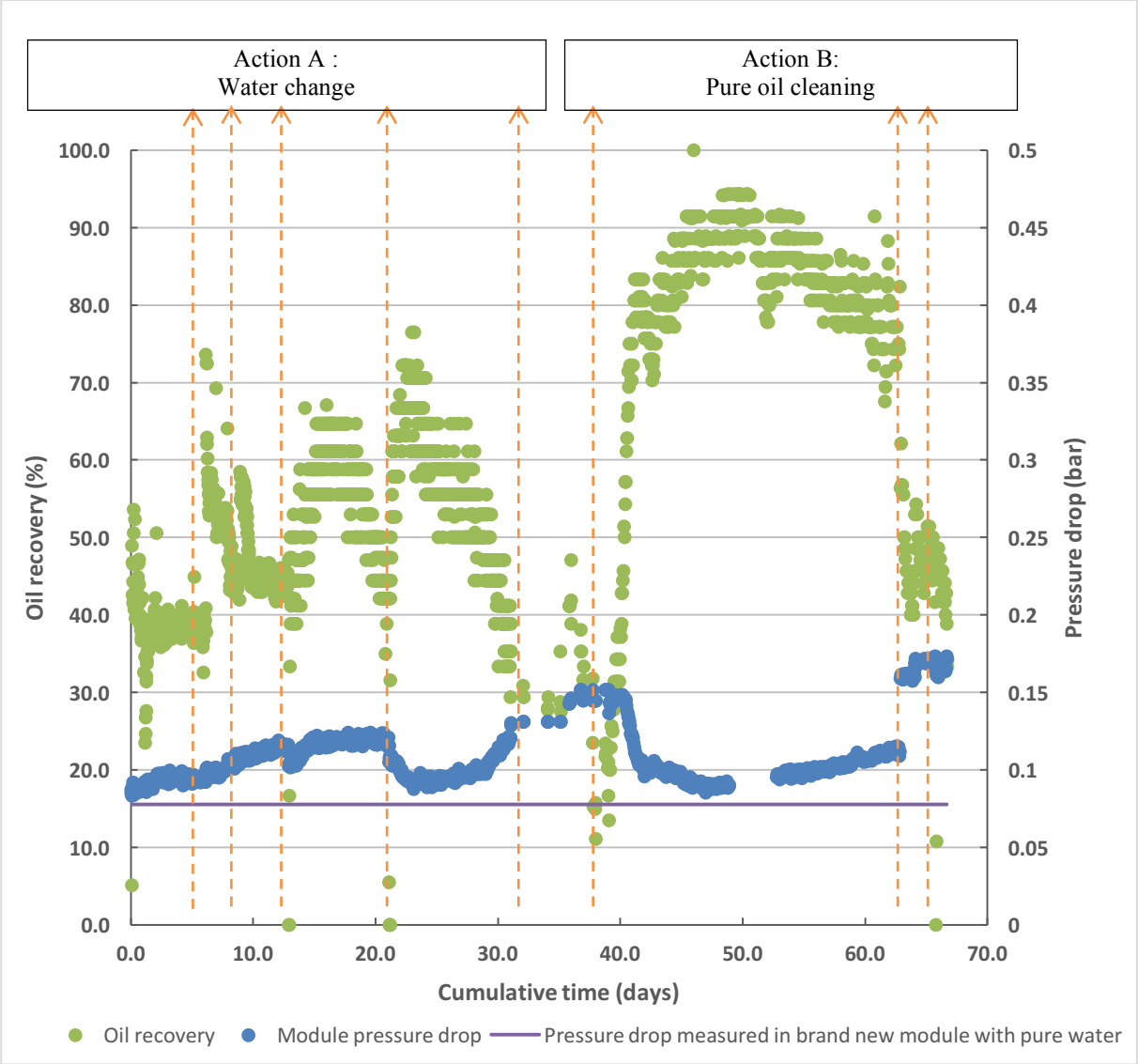

Figure 7-2: Oil recoveries and pressure drops for a 2.5-inch membrane contactor module for consecutive experiments where fouling was diagnosed. Experimental conditions: C_{oil} = 200 ppmv, Influent flow rate = 3.8 L/min, TMP = 1.4 bar, 2.5-inch module.

Despite repeated water changes, oil recoveries continued to decrease. A pure oil treatment was then conducted to attempt to jump start the buildup of the oil film on the fibers (Action B). The pure oil treatment consisted of shutting operation down, draining, recirculating 20 L of pure oil on the shell side until complete permeation was achieved.

The 200 ppmv oil-water experiment was subsequently resumed and oil recoveries improved for nearly 10 days (days 39 to 50) but then started to plummet again. Two subsequent pure oil treatments did not help restoring pure oil performance. During these experiments, an increase in pressure drop was always observed when oil recoveries decreased. Pressure drop was at its highest when neither the pure oil treatments nor the water changes could restore system performance. In comparison, typical pressure drops trends were steady when the system was operating normally as can be seen in Figure 7-3.

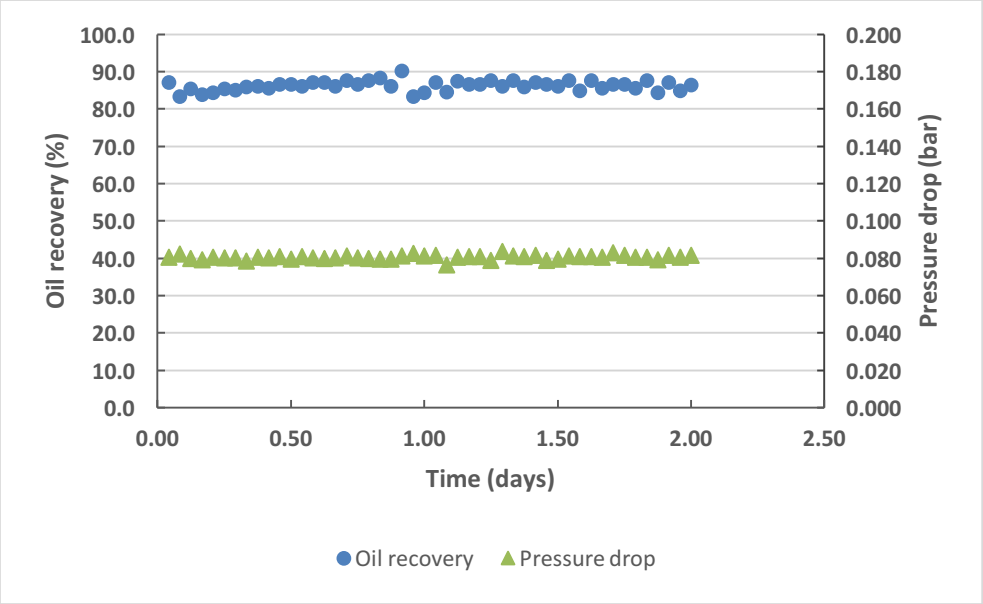

Figure 7-3: Typical oil-water experimental trends. Experimental conditions: C_{oil} = 1000 ppmv, Influent flow rate = 3.8 L/min, TMP = 1.4 bar, 2.5-inch module.

After each pure oil treatment and draining, water flowing back to the tank would always display a foamy layer between the oil and water phases that was visually different than the cloudiness observed at start-up. A picture of the foamy layer can be seen in Figure 7-4.

Polysaccharides (mg glucose/L)	Proteins (mg BSA/L)
152.0	195.0

Table 7-1: Polysaccharides and proteins levels in middle phase.

Figure 7-4: Unusual sample of drained liquids from membrane system after 40 days of operation. Top phase is Isopar™ M, bottom phase is water and unidentified compound in the middle phase.

The foamy layer clearly looked like a surfactant layer where droplets of both phases were mixed. In addition, the bottom phase, which is water was abnormally cloudy. The three phases were observed under an optical microscope and bacteria were visually detected at the interface of the oil and water phases. A sample of the middle phase was analyzed for protein and polysaccharides using the Pierce BCA kit (Thermo Fisher Scientific, Waltham, MA), a modified Lowry assay and the phenol/sulfuric acid method respectively (*113, 114*). The analysis was conducted by Sarah Keithley, a doctoral student familiar with the methods. Results showed the presence of polysaccharides and proteins in the sample. Since none of these compounds was added to the system intentionally, the source of the foamy layer was likely the by-products of biological activity.

MEMBRANE CLEANING

After confirmation of the biological fouling in the system, two rounds of chemical treatments were conducted on one of the modules to attempt to clean the membranes as described in the Materials and Methods section. The second module was saved without

cleaning for future analysis of the membrane. The first chemical treatment was conducted to loosen the biofilm from the membrane surface and was adapted from the Liqui-Cel® recommended cleaning procedure. Then, disinfection was performed using a chlorine solution treatment to attempt to inactivate the remaining microorganisms. Experiments were conducted again to determine if the chemical and disinfection procedures helped restore earlier performance. Figure 7-5 shows the results of the oil-water experiments conducted after the cleaning procedures and following two days of soaking the membranes in pure oil.

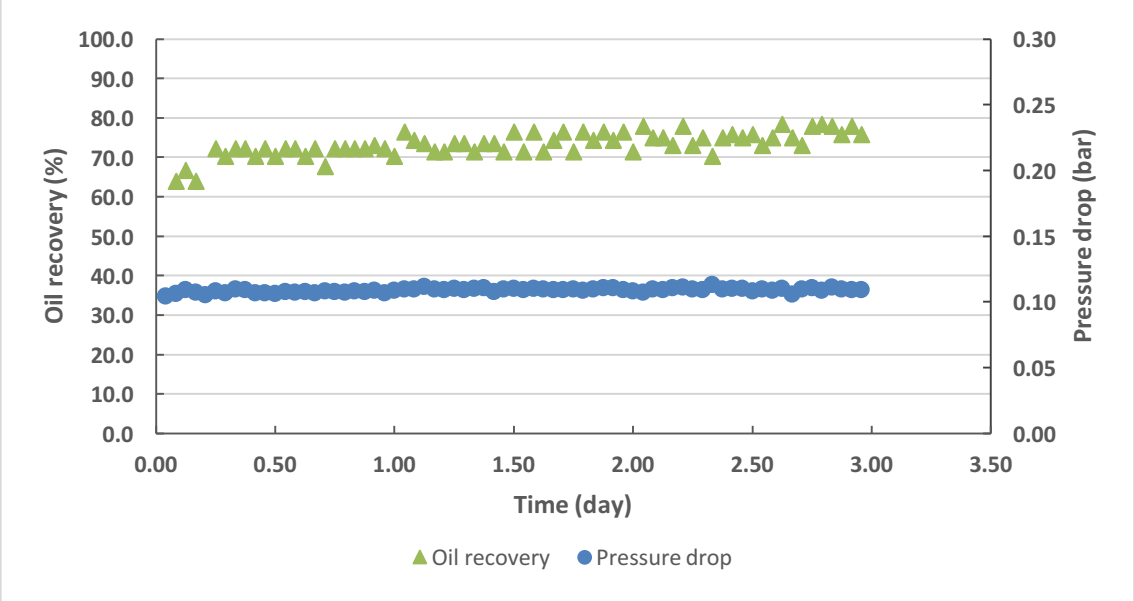

Figure 7-5: Oil-water experiments conducted on a 2.5-inch module after two chemical and one disinfection cleanings. Experimental conditions: C_{oil} = 200 ppmv, Influent flow rate = 3.8 L/min, TMP = 1.4 bar, 2.5-inch module.

The results, shown in Figure 7-5, suggest that the cleaning procedures helped restore some of the performance of the system for dilute oil-water experiments. The pressure drop was lower and steady but was still higher than observed for other brand new modules, suggesting that the cleaning procedure was not completely successful.

To further characterize the efficiency of the cleaning procedures, experiments with various oil concentrations were repeated with the cleaned module and compared to earlier results obtained with module without biological fouling. Results are presented in Figure 7-6. The results demonstrate that for high oil concentrations, the performance of the cleaned module plateaued at a maximum oil flux across the membrane fibers. For experiments with oil concentration higher than 1%, oil flux measured with the cleaned modules was consistently lower than in the original experiments. However, for more dilute mixtures, results were repeatable with previous experiments with no biological fouling. The results suggest that cleanings helped to partially recover the membrane surface area of the module, enough for the effective separation of dilute mixtures but not for higher concentration experiments.

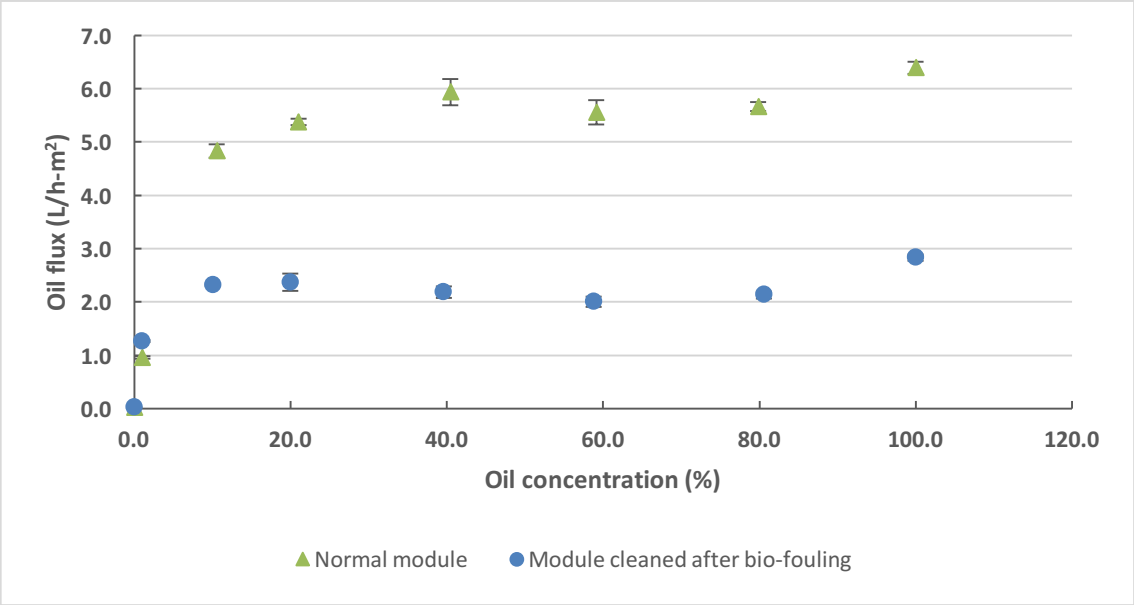

Figure 7-6: Comparison between the concentration curves of a normal module and a module chemically cleaned after biological fouling. Experimental conditions: 2.5-inch module, Influent flow rate = 3.8 L/min, TMP = 1.4 bar.

MEMBRANE AUTOPSIES

Analysis of the membranes (membrane autopsies) were conducted on three modules: the module having undergone the cleaning process, the module that was saved without any cleaning for comparison and a brand new module for reference.

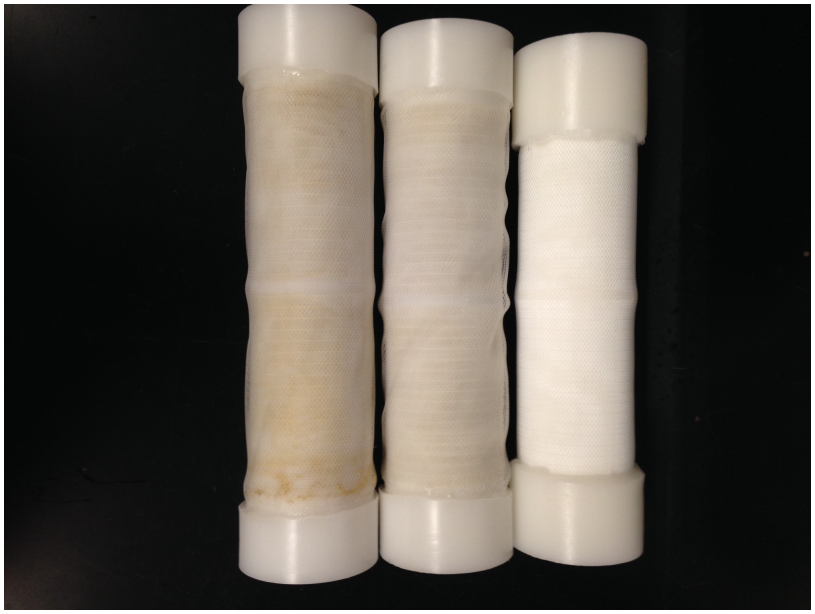

Figure 7-7: Membrane contactors autopsies. From left to right: Uncleaned contaminated module, Cleaned (Two chemical and one disinfection cleanings) module, brand new module.

Visual observation of the hollow-fiber bundles of both cleaned and contaminated (uncleaned) modules showed clear biological growth on the membrane material compared to the brand new module. The contaminated module seemed to have more biological deposits than the cleaned module and the cleaned module had some contamination compared to the brand new module. The hollow fiber bundle sizes were also observed to be different. The two used membrane modules had an overall length that was greater than the brand new module. Such observation can be explained by membrane swelling due to oil adsorption over time (*115*). The hollow fiber bundles were subsequently opened and observed with a scanning electron microscope. The top row of

Figure 7-8 shows the clean and unused membrane surface with open pores. On the second and third rows, biofilms can be observed on the fiber surfaces of both contaminated and chemically cleaned membranes. However, the biofilm on the chemically cleaned membrane contactor seems less dense than the biofilm on the uncleaned contaminated module. The cleaning procedure may have freed some surface area but was not fully successful in recovering all of the surface area.

As detailed previously, the early stage of oil-water filtration observed for the brand new module was unusual. Progressive improvement of oil recovery was expected as had been seen in Figure 7-1 instead of progressive decline of oil recovery for the 200 ppmv experiment. Therefore, signs of biological fouling may have occurred as early as after a few days of operation. The source of the microorganisms was likely from the 4-inch "cleaning" module that was restarted after sitting unused over the winter break. However, the cleanings were conducted more than a month later after operation recommenced. Earlier chemical cleaning may have limited the deposition and attachment of the biofilm in the module and may have proven more efficient.

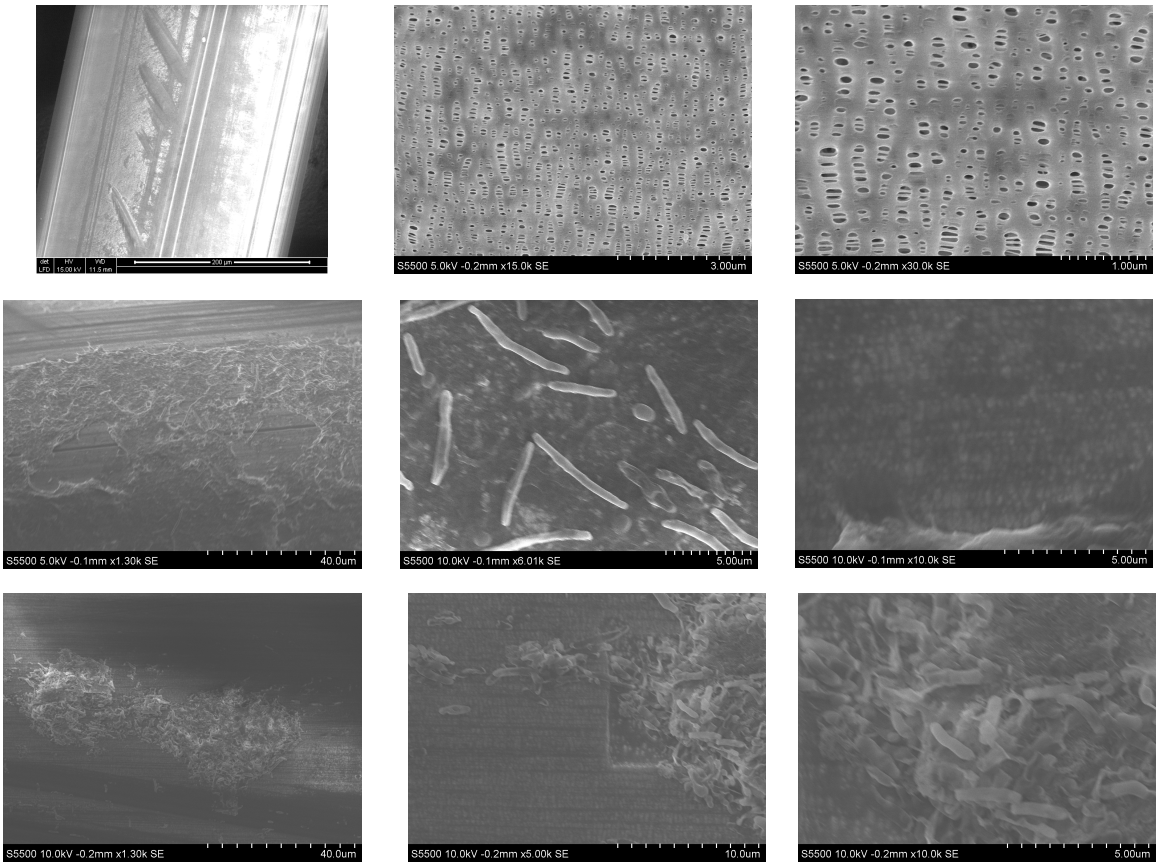

Figure 7-8: SEM images of hollow fiber membrane surface. From top to bottom rows: Brand new module, Cleaned (Two chemical and one disinfection cleanings) module, Uncleaned contaminated module.

TRANSMEMBRANE PRESSURE AND INFLUENT FLOW RATE EFFECTS

The particular effect of transmembrane pressure on oil permeation during separation of dilute oil-water mixtures with the membrane contactor was highlighted in Chapter 5. For experiments with a 2% oil concentration, an increase in transmembrane pressure was shown to decrease oil permeation and, therefore, recovery as water was blocking the larger pores on the fiber wall. Higher influent flow rate was also shown to decrease oil recoveries by reducing the detention time of oil droplets and their probability to be captured by the membrane surface. Further experiments were needed with dilute oil-water mixtures to confirm such findings. The new modules described in the present

chapter were intended to be used to confirm previously observed trends in the case of oil-water mixtures at 200 ppmv oil concentration. Therefore, before decreases in performance were formally identified as biological fouling, effects of transmembrane pressure and influent flow rate were studied with the modules after 20 days of operation. This work complements the data presented in Chapter 5 obtained with modules not contaminated by biological microorganisms. In the present case where modules were biologically contaminated, oil flux values cannot be compared to previous experiments but the data provides insight when comparing relative performance with the effect of a change in a single parameter such as transmembrane pressure and influent flow rate. The results are presented in Figure 7-9.

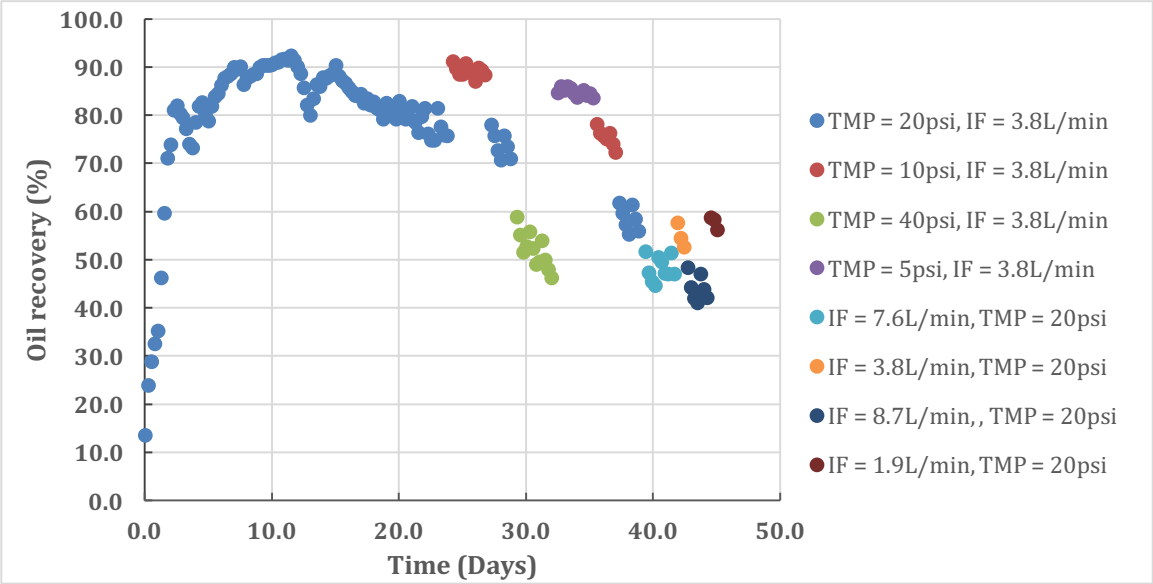

Figure 7-9: Oil recoveries for 2.5-inch module experiencing biological fouling for various transmembrane pressure and influent flow rates. Experimental conditions: Isopar M, 2.5-inch module, C_{oil} = 200 ppmv.

As suggested in Chapter 5, at 200 ppmv oil concentration, which corresponds to the dilute mixture range, both a decrease in transmembrane pressure and a decrease in influent flow rate led to an increase in instantaneous oil recoveries. Those results confirm

the trends observed previously even though in the present case the actual available surface of the membrane was reduced by biofilm growth on the membrane surface.

CONCLUSIONS

This chapter highlighted some of the challenges of membrane technologies for the separation of oil and water. First, when brand new membrane contactors were used, a white contaminant, likely leaching out of the membrane, was observed in the recycled water tank and oil permeating the fibers seemed foamier than usual. However, with regular water replacement and use of fresh oil, the white contaminant can be removed over time. When implementing the technology in the field, a first flush of the module with oil and water will allow removal of the contaminant.

Biological fouling was also observed to affect performance of the membrane over long period of operations. In this research, biological fouling was identified visually through formation of a surfactant-like compound that was present in liquids drained out of the modules and later confirmed to be protein and polysaccharides consistent with by-products of biological activity. Chemical and disinfection procedures helped restore some of the performance of the system by freeing some of the fouled membrane surface area. However, the initial membrane performance was not completely restored possibly because the cleaning and disinfection procedures occurred more than a month after the first signs of fouling. In field operations, regular disinfection procedures should be implemented to prevent the growth of biofilms on the membrane surface.

Finally, despite biological fouling in the membranes, the qualitative relationships between the transmembrane pressure and oil recovery, and influent flow rate and oil recovery were consistent with findings shown in Chapter 5. Lower transmembrane pressure and influent flow rates were shown to improve oil recovery in the module for an oil concentration of 200 ppmv in the membrane feed.

Chapter 8: Membrane Start-up and Operating Configuration

During the course of this experimental work, some experiments reached steady state almost immediately while others had varying transient start-up periods. Therefore, start-up procedures appear to be an important factor in the successful membrane contactor operation. This chapter details the findings and provides some recommendations for start-up optimization and membrane operating configuration.

MEMBRANE START-UP AND CONDITIONING

When running pure oil experiments or high oil concentration experiments (>5%), the measured oil flux did not show a time dependency and steady state values were attained almost immediately. However, as discussed in earlier chapters, for dilute mixtures, system performance varied and improved over time due to the progressive growth of an oil film on the fiber wall which increased the effective membrane surface area over time. Whenever a brand new module was used and depending on the oil concentration in the feed, the transition to steady state ranged from a few hours to a few days (Figure 8-1). When running very dilute experiments such as oil concentrations of 200 ppmv, the module did not perform well at start-up, but if these experiments were started after running higher oil concentration experiments, allowing the fibers to be wetted with oil, very high recoveries were attained rapidly (Figure 8-1-D). The growth of the oil layer on the fiber wall is hindered by two potential obstacles that require time for development of an oil layer. First, in typical hollow fiber membrane filters, "dry" points have been observed where air bubbles are trapped in the fibers and onto the walls preventing the use of the total surface area (*116*). Therefore, over the course of the filtration process, air bubbles may be slowly pushed out allowing the oil film to grow. Second, even though the membrane material is initially hydrophobic, if exposed to a hydrophilic mixture over time, the affinity of the surface for oil may change (*59*).

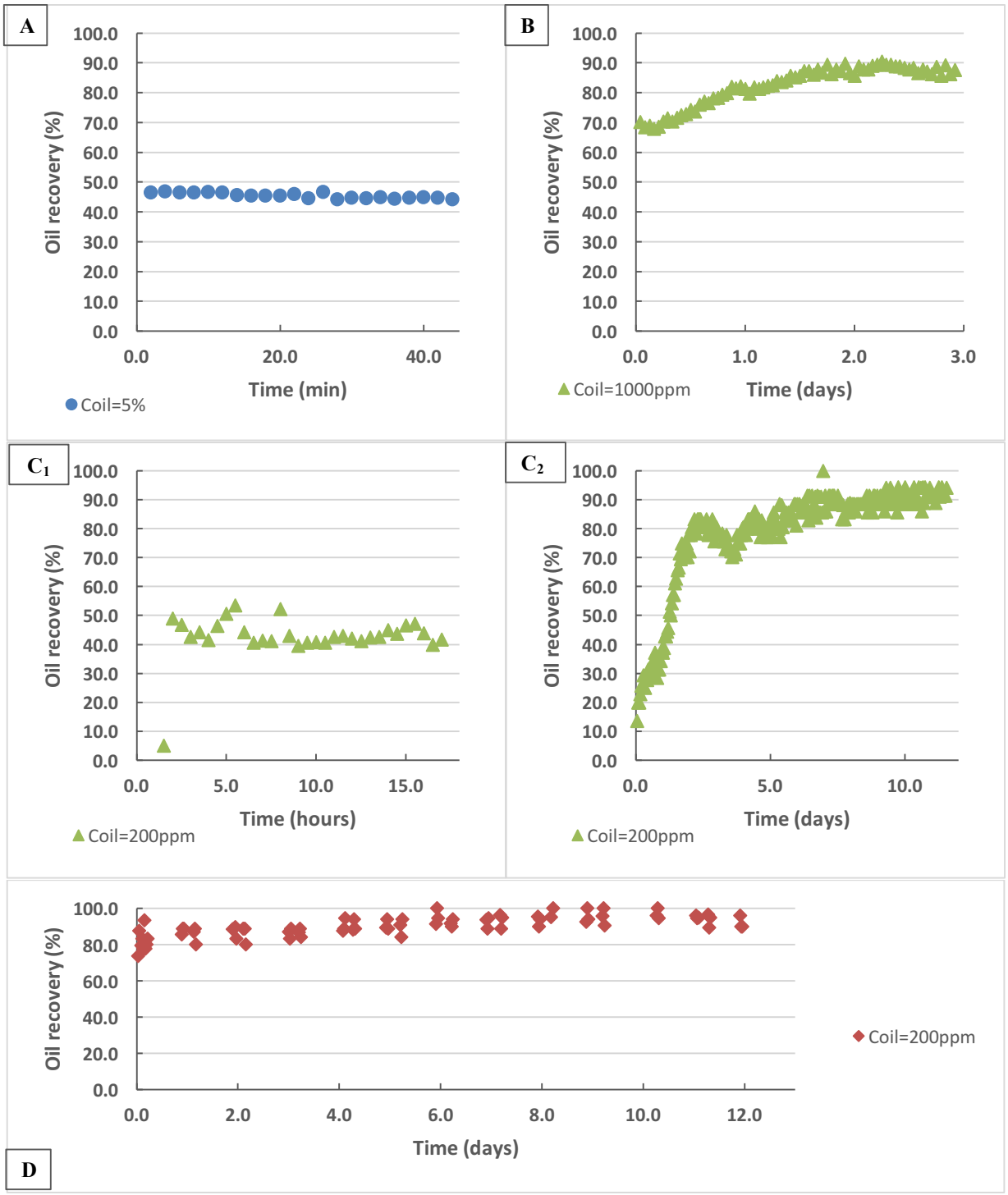

Figure 8-1: Oil-water experiments. Experimental conditions: 2.5-inch module, Isopar M, Influent flow rate = 3.8 L/min, TMP = 1.4 bar. A: C_{oil} = 5%, B: C_{oil} = 1000 ppmv, C: C_{oil} = 200 ppmv, C_1 Performance with brand new membrane, C_2: Performance after pure oil conditioning, D: C_{oil} = 200 ppmv performance after running multiple higher oil concentration experiments (80%-200 ppmv).

Therefore, maintaining the hydrophobicity of the membrane surface is critical either by rapidly building the oil film or coating the fibers with oil ahead of time.

At higher oil concentrations, the amount of oil in the feed is sufficient to achieve rapid, uniform fiber coating. For more dilute mixtures, the approach of employing pure oil conditioning before start-up may prove valuable for minimizing the transition phase to steady state. Pure oil conditioning involves running the membrane system with pure oil feed to permeate oil and wet the fibers completely inside and out. Permeating a minimum of 20 L of oil is recommended. Experiments conducted on the small 2.5-inch module showed that running pure oil through the membrane prior to conducting experiments allowed improvement in oil recoveries as seen in Figure 8-1(C_1-C_2). Moreover, conditioning the membrane in this way may help remove the contaminant that appear to leach out of the system at the beginning of the membrane life. An alternative approach would be to first use a brand new contactor with higher oil concentrations and then proceed to more dilute operations in the treatment line. The pure oil conditioning is recommended for brand new and chemically cleaned membrane contactors.

OPERATING CONFIGURATION

For all the experiments presented in this work, the membrane module was consistently operated vertically with oil overflowing out of the top tube side port as seen in Figure 8-2-A. Operating in this configuration was believed to prevent possible bypassing and allow complete wetting of the fibers from the inside to avoid fiber compression and facilitate oil film build-up on the shell-side. Experiments were conducted to compare two other module configurations and determine the potential for short circuiting that might impair system performance The first alternative configuration tested was operating the membrane vertically with oil flowing from the bottom tube side

port (Figure 8-2-B). The second configuration consisted in switching the membrane module to a horizontal configuration (Figure 8-2-C).

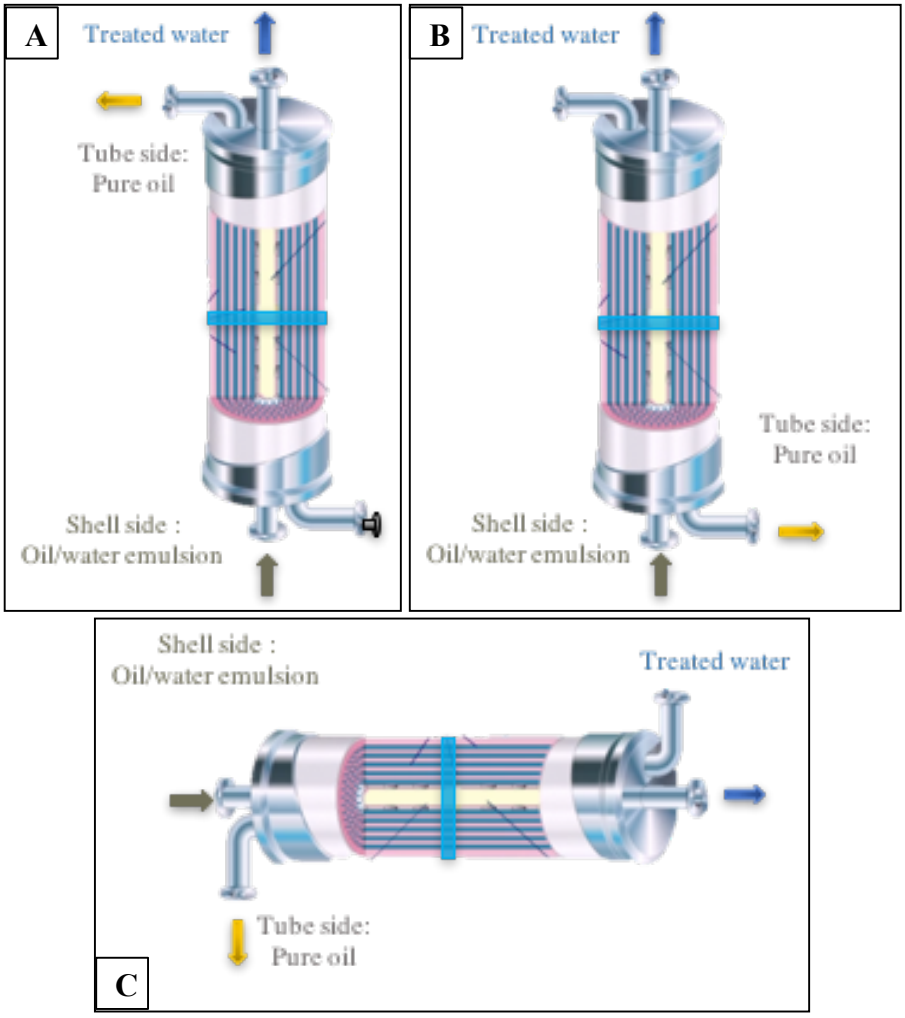

Figure 8-2: Module positioning, A: Vertical operation with oil overflow on top port B: Vertical operation with oil flow from bottom port, C: Horizontal operation

Figure 8-3 shows the results of the series of experiments conducted with each module configuration. After steady state was established at normal operation (Figure 8-3 day 2), a new experiment was initiated with oil flowing from the bottom port. No significant difference in oil recovery was observed in system performance. Similarly, after switching the module to a horizontal configuration, no significant change was

observed in performance. For steady state operation, the module configuration does not seem to impact membrane recovery performance.

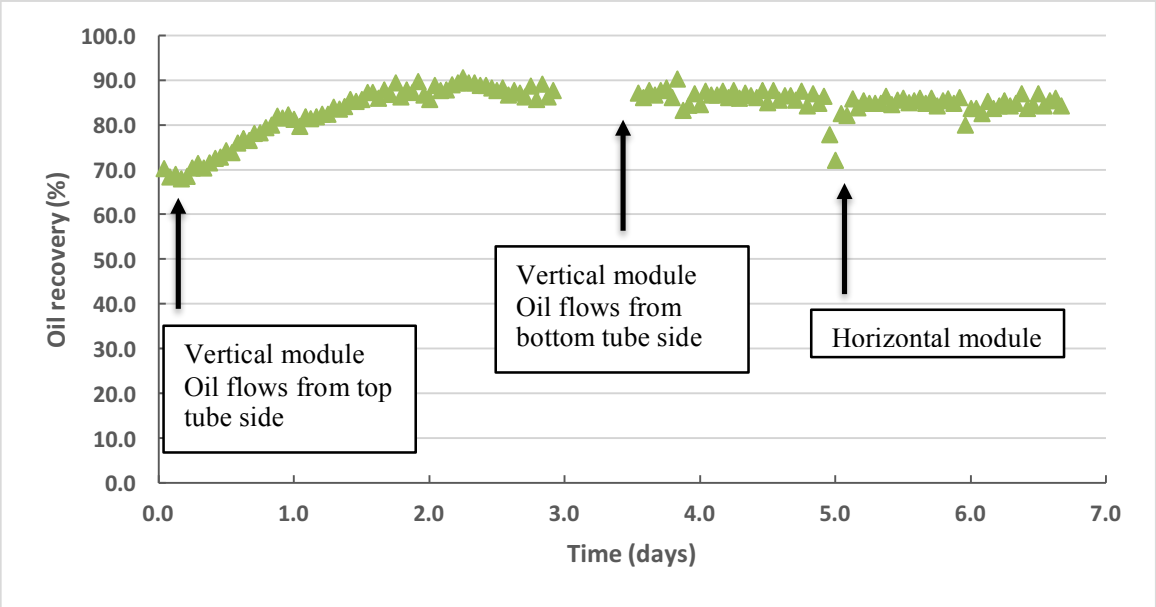

Figure 8-3: Oil-water experiments with various module configuration. Experimental conditions: C_{oil} = 1000 ppmv, Isopar M, Influent flow rate = 3.8 L/min, TMP = 1.4 bar.

Another process configuration thought to potentially improve oil permeation was the recirculation of oil on the tube side while an oil-water mixture is sent through the shell-side as shown in Figure 8-4. The recirculation of oil on the tube side was tested to determine whether recirculation would help keep the fibers well wetted from the inside-out and fully expanded. While the results shown in Figure 8-5 suggest that oil recirculation did not improve steady state performance, recirculation may still be useful for reducing the time to reach steady state recoveries when operating the membrane system with very dilute mixtures. However, conditioning the module with pure oil ahead of time would have the same benefits and is easier to implement on a larger scale system.

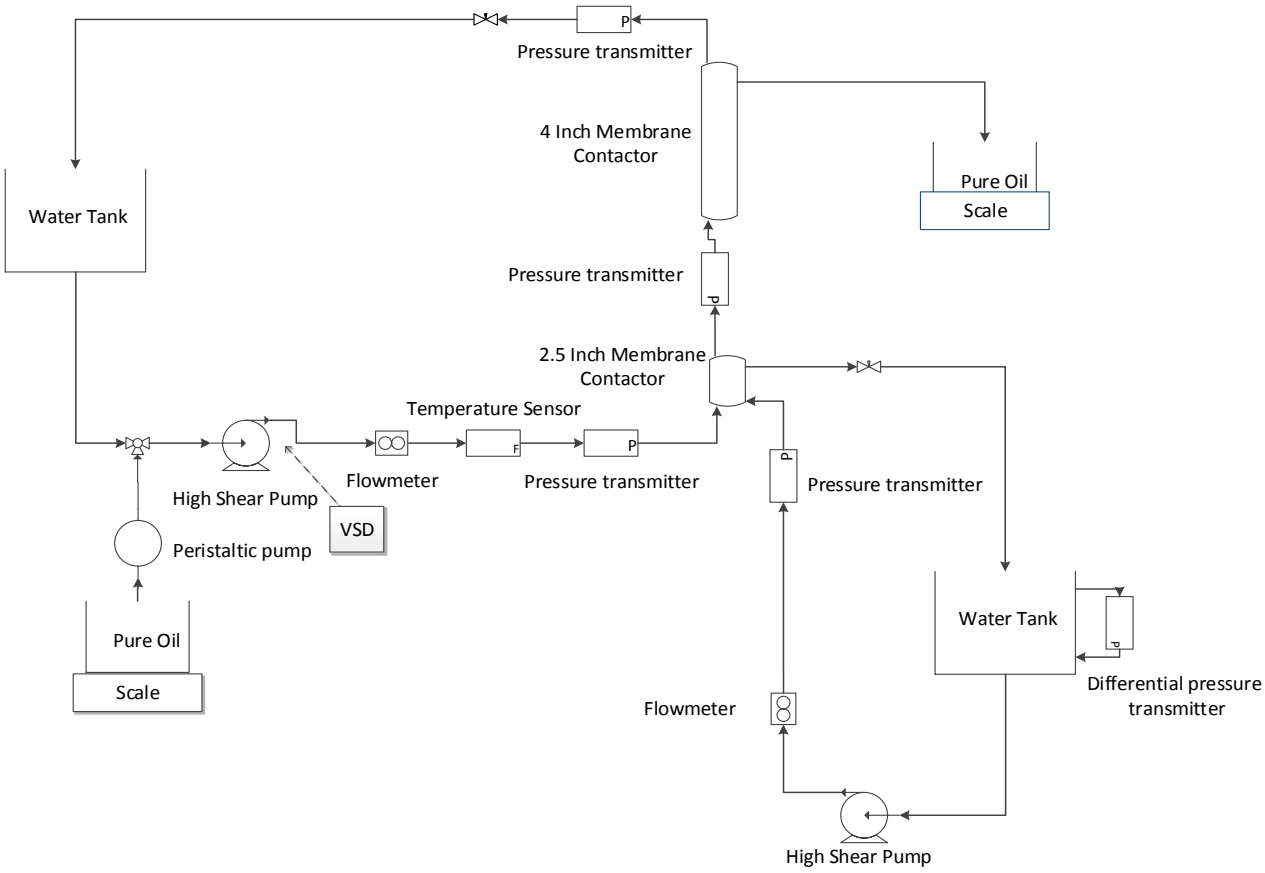

Figure 8-4: Oil recirculation system schematic.

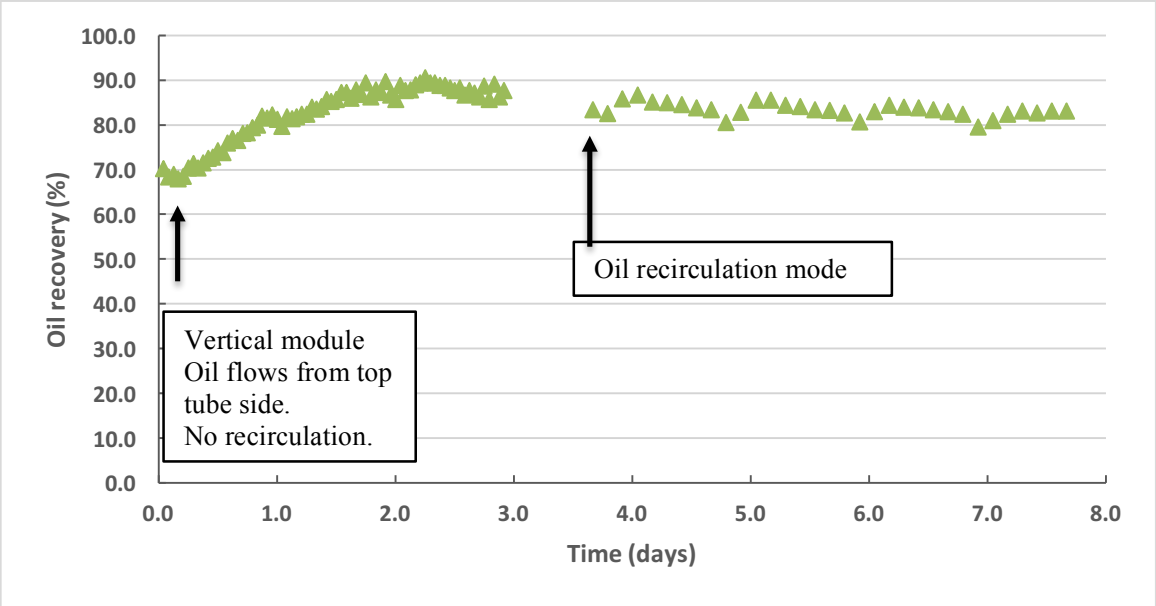

Figure 8-5: Oil-water experiments with and without oil recirculation. Experimental conditions: C_{oil} = 1000 ppmv, Isopar M, Influent flow rate = 3.8 L/min, TMP = 1.4 bar.

CONCLUSIONS

Start-up experiments with various oil-water mixtures showed that transient periods of low recovery can be significant (up to a few days) before reaching steady state and maximum recovery. Prior to processing very dilute mixtures, higher oil concentration runs or pure oil conditioning is recommended on brand new or cleaned modules to reduce the time to steady-state recoveries. Three membrane configurations were compared and were shown to have no effect on steady state performance of the membrane system. However, operating vertically with oil overflowing from the top tube side may contribute to a faster start-up period (reduced time to steady-state) when pure oil conditioning is not implemented ahead of time. Finally, the recirculation of oil on the tube side was tested and did not improve steady state performance. Therefore, pure oil conditioning on brand new and cleaned modules is recommended to quickly reach steady state. Any membrane configuration can then be selected.

Chapter 9: Conclusions and Recommendations

This dissertation provides a comprehensive characterization of a hydrophobic hollow fiber membrane contactor for the recovery of insoluble oil from oil-water mixtures. The findings from this work are detailed below along with the original study objectives. Finally, recommendations are provided for future work and to enhance commercial implementation of the technology.

Objective 1: Characterize the effect of operating parameters such as oil concentration, viscosity, transmembrane pressure, and influent flow rate on membrane performance including oil permeation rate and recoveries.

Initial experiments with the hydrophobic membrane contactor were conducted with pure oil to establish the maximum flux as a function of influent flow rate, transmembrane pressure, and oil viscosity. For the pure oil feed conditions and the X50 fiber, the oil permeation rate through the hydrophobic hollow fiber membrane contactor was well described by the Ergun equation, a model commonly used for flow through packed columns. Under these conditions, increasing transmembrane pressure increased the oil permeation while viscosity linearly affected the oil flux as predicted by the Ergun equation.

Experiments with oil-water mixtures revealed some unexpected effects of operating parameters that impact the performance of the membrane contactor. In particular, the rate of oil transfer appears to be related to the effective surface area, which is believed to depend on the presence of an oil film on the membrane fibers. Indeed, pre-wetting of the modules with oil was found to reduce the time necessary to achieve high removals for dilute oil-water feeds.

Transmembrane pressure was shown to positively affect oil permeation at high oil feed concentrations consistent with the results from the pure oil experiments. However,

at oil concentrations below 2%, lower transmembrane pressure was proven to be more beneficial for oil permeation and recovery. The results suggest that for dilute oil-water mixtures and increasing transmembrane pressure, water blocks larger pores of the module which presumably reduces the effective surface area for mass transfer and, therefore, oil permeation. Thus, operating at lower transmembrane pressures should improve oil permeation and reduce energy input for dilute feed mixtures.

At high oil feed concentrations, higher viscosity oil was confirmed to reduce oil permeation, a phenomenon that was also observed in the pure oil feed experiments. Thus, operating at a higher temperature may be advantageous under these conditions. However, for very dilute mixtures (e.g., 200 ppmv oil) viscosity was shown to improve oil flux. Higher viscosity may contribute to the growth of a more stable oil film on the fibers by reducing the instantaneous permeation of the oil. A more stable film would yield a larger effective surface area on the membrane and ultimately a higher flux. These results suggest that lowering temperature to increase the viscosity of the oil is advantageous for dilute mixtures.

The experimental results obtained in this study highlight the need for different operating protocols in the field depending on the oil concentration in the feed. For instance, a 40% oil-water feed mixture that is generated from an oil and gas operation should be passed through a hydrophobic membrane contactor at a higher transmembrane pressure and higher temperature. In contrast, a 200 ppmv oil mixture feed (representative of a wastewater exiting a gravity separator, for example) should be operated at reduced transmembrane pressure and lower temperature. In addition, prior wetting of a new module with pure oil should be considered to reduce the start-up time required.

Objective 2: Understand the effect of membrane characteristics such as surface area, module size, porosity and wall thickness on membrane performance

Membrane characteristics were found to affect process performance in multiple ways. As expected, increasing membrane surface area led to a higher recovery of oil. However, the spacing of the fibers also impacted the permeation of oil. Results suggested that wider spacing between fibers led to more efficient use of the membrane surface area. Additional experiments with varying fiber spacing would be required to confirm these initial results.

In addition, the pure oil feed experiments with different hydrophobic membrane module sizes demonstrated that surface area was not the only factor influencing oil permeation. Fiber length and module geometry also need to be taken into consideration. Shorter fibers and a narrower module diameter proved to be more efficient for oil permeation. Additional testing with larger modules would be useful to confirm this behavior for a range of membrane contractor geometries treating oil-water mixtures. Porosity and wall thickness were also shown to affect oil permeation. Comparison of the experiments conducted with two different fibers (X40 and X50) indicates that a higher oil flux was obtained through the X50 fibers (higher porosity and thinner wall). Since no water breakthrough was observed in the working range of transmembrane pressures (up to 4.1 bar), the X50 fiber type is recommended for future use to separate insoluble oil and water mixtures with the membrane contactor.

Objective 3: Assess the potential of the system for oil-removal over time

The hydrophobic membrane contactor achieved very high levels of oil-water separation, that approached 99% oil recovery when adequate membrane surface area was provided. The performance of the system was proven to be stable over periods of up to two weeks in the current study. Over this timeframe, there was no apparent sign of the viscous fouling that is typically observed within minutes in hydrophilic systems treating

oil-water mixtures. Start-up operations proved to be important to the efficiency of oil recovery in the system. Use of a brand new module with dilute mixtures (oil concentrations <2%) led to a slow approach to steady state. Pre-conditioning of a new module with pure oil permeation is recommended to wet the fibers with oil and enhance the effective surface area of the membrane. Such conditioning will reduce the duration of the startup period and allow flushing of possible contaminants that may initially leach from the module. Moreover, biological fouling was shown to be a potential factor that can significantly reduce the performance of the membrane contactor. As with any type of membrane systems, regular preventive disinfection is recommended to avoid biofilm growth at the membrane surface. In this study, after biological fouling of the experimental modules was identified, cleaning and disinfection were able to restore some of the available surface area of the membrane contactor and, therefore, the capacity of the module to treat lower oil concentration mixtures. Finally, membrane orientation did not seem to impact membrane performance. Therefore, the results indicate that the membrane modules can be operated vertically or horizontally during steady state operation.

Objective 4: Develop a model for preliminary assessment and engineering design of a membrane contactor system

A semi-empirical model was developed to predict oil flux as a function of operating parameters (transmembrane pressure and influent flow rate), membrane characteristics (porosity and wall thickness) and influent feed conditions (oil viscosity and concentration). The model can be used to define the operating conditions and membrane surface area required to achieve a desired oil-water separation efficiency. The model is a valuable tool for design and implementation of the membrane contactor technology for the treatment of oily wastewaters.

Recommendations for Future Work

Additional work would be beneficial to further anticipate application of the technology into the field. Initial studies performed by the Separations Research Program and OpenAlgae LLC demonstrated that the application of the microporous hollow fiber membrane for oil-water separation were promising. The results of the research presented in this dissertation highlight the need to develop fundamentally-based modeling approaches that capture the range of conditions expected in the field. Future work is needed to address the impact of typical oily wastewater contaminants such as solids and surfactants on the performance of the system. Identification of wastewater components such as solids that may require pretreatment prior to introduction of the feed into the membrane contactor system is a necessary next step. The presence of surfactants in the feed may also impact membrane performance by changing the hydrophobicity of the oil droplets surface and the interfacial tension with water. Incorporating the effect of interfacial tension on system performance into the existing model should be developed at the lab scale and validated in the field for a range of oily mixtures. The knowledge acquired during this dissertation will lay the foundation necessary to improve the design, and on-site implementation of the technology at the field scale.

Appendices

APPENDIX A: PURE OIL EXPERIMENTAL RAW DATA

- X50 fiber, 2.5-inch module

	Experimental Flux	TMP	Influent flow	Viscosity	SA
	m^3/s	Pa	(m^3/s)	cP	m^2
Flux vs viscosity study	8.79E-06	1.38E+05	6.30E-05	1.45	1.4
	8.26E-06	1.38E+05	6.30E-05	1.47	1.4
	8.47E-06	1.38E+05	6.30E-05	1.45	1.4
	3.96E-06	1.38E+05	6.30E-05	3.23	1.4
	3.64E-06	1.38E+05	6.30E-05	3.45	1.4
	4.09E-06	1.38E+05	6.30E-05	3.03	1.4
	1.51E-06	1.38E+05	6.30E-05	8.33	1.4
	1.74E-06	1.38E+05	6.30E-05	7.69	1.4
	1.75E-06	1.38E+05	6.30E-05	7.69	1.4
	1.79E-05	2.76E+05	6.30E-05	1.41	1.4
	1.76E-05	2.76E+05	6.30E-05	1.39	1.4
	1.68E-05	2.76E+05	6.30E-05	1.43	1.4
	9.03E-06	2.76E+05	6.30E-05	2.86	1.4
	8.15E-06	2.76E+05	6.30E-05	3.03	1.4
	8.47E-06	2.76E+05	6.30E-05	2.94	1.4
	3.36E-06	2.76E+05	6.30E-05	8.33	1.4
	3.58E-06	2.76E+05	6.30E-05	7.69	1.4
	3.75E-06	2.76E+05	6.30E-05	7.14	1.4
	2.52E-05	4.14E+05	6.30E-05	1.45	1.4
	2.56E-05	4.14E+05	6.30E-05	1.39	1.4
	2.39E-05	4.14E+05	6.30E-05	1.45	1.4
	1.21E-05	4.14E+05	6.30E-05	3.03	1.4
	1.35E-05	4.14E+05	6.30E-05	2.78	1.4
	1.21E-05	4.14E+05	6.30E-05	2.94	1.4
	4.83E-06	4.14E+05	6.30E-05	8.33	1.4
	5.26E-06	4.14E+05	6.30E-05	7.69	1.4
	5.54E-06	4.14E+05	6.30E-05	7.14	1.4
Flux vs TMP study	1.88E-06	6.89E+04	6.30E-05	3.46	1.4

	3.90E-06	1.38E+05	6.30E-05	3.22	1.4
	6.21E-06	2.07E+05	6.30E-05	3.04	1.4
	8.55E-06	2.76E+05	6.30E-05	2.93	1.4
	1.09E-05	3.45E+05	6.30E-05	2.86	1.4
	1.23E-05	4.14E+05	6.30E-05	2.95	1.4
Flux vs influent flow rate study	3.83E-06	1.38E+05	3.15E-05	3.26	1.4
	8.04E-06	2.76E+05	3.15E-05	3.05	1.4
	1.29E-05	4.14E+05	3.15E-05	2.82	1.4
	3.90E-06	1.38E+05	6.30E-05	3.22	1.4
	8.55E-06	2.76E+05	6.30E-05	2.93	1.4
	1.25E-05	4.14E+05	6.30E-05	2.90	1.4
	4.14E-06	1.38E+05	9.45E-05	3.16	1.4
	8.60E-06	2.76E+05	9.45E-05	2.91	1.4
	1.28E-05	4.14E+05	9.45E-05	2.83	1.4
Flux vs TMP, Surface area study	9.84E-07	6.89E+04	6.30E-05	3.31	0.7
	1.92E-06	1.38E+05	6.30E-05	3.21	0.7
	2.87E-06	2.07E+05	6.30E-05	3.14	0.7
	3.82E-06	2.76E+05	6.30E-05	3.09	0.7
	4.71E-06	3.45E+05	6.30E-05	3.11	0.7
	5.36E-06	4.14E+05	6.30E-05	3.23	0.7
Flux vs Influent flow rate, Surface area study	1.76E-06	1.38E+05	3.15E-05	3.39	0.7
	3.62E-06	2.76E+05	3.15E-05	3.23	0.7
	5.70E-06	4.14E+05	3.15E-05	3.01	0.7
	1.92E-06	1.38E+05	6.30E-05	3.21	0.7
	3.82E-06	2.76E+05	6.30E-05	3.09	0.7
	5.36E-06	4.14E+05	6.30E-05	3.23	0.7
	1.76E-06	1.38E+05	9.45E-05	3.51	0.7
	3.47E-06	2.76E+05	9.45E-05	3.34	0.7
	5.51E-06	4.14E+05	9.45E-05	3.13	0.7
Flux vs viscosity, Surface area study	3.66E-06	1.38E+05	6.30E-05	1.49	0.7
	3.91E-06	1.38E+05	6.30E-05	1.45	0.7
	3.88E-06	1.38E+05	6.30E-05	1.43	0.7
	1.95E-06	1.38E+05	6.30E-05	3.23	0.7
	1.96E-06	1.38E+05	6.30E-05	3.13	0.7
	1.85E-06	1.38E+05	6.30E-05	3.23	0.7
	6.27E-07	1.38E+05	6.30E-05	9.09	0.7
	6.82E-07	1.38E+05	6.30E-05	8.33	0.7
	7.14E-07	1.38E+05	6.30E-05	8.33	0.7
	7.21E-06	2.76E+05	6.30E-05	1.47	0.7

	7.56E-06	2.76E+05	6.30E-05	1.43	0.7
	7.70E-06	2.76E+05	6.30E-05	1.39	0.7
	3.90E-06	2.76E+05	6.30E-05	3.03	0.7
	3.96E-06	2.76E+05	6.30E-05	3.03	0.7
	3.62E-06	2.76E+05	6.30E-05	3.23	0.7
	1.27E-06	2.76E+05	6.30E-05	9.09	0.7
	1.37E-06	2.76E+05	6.30E-05	8.33	0.7
	1.48E-06	2.76E+05	6.30E-05	7.69	0.7
	1.05E-05	4.14E+05	6.30E-05	1.47	0.7
	1.10E-05	4.14E+05	6.30E-05	1.41	0.7
	1.12E-05	4.14E+05	6.30E-05	1.39	0.7
	5.58E-06	4.14E+05	6.30E-05	3.23	0.7
	5.70E-06	4.14E+05	6.30E-05	3.03	0.7
	4.82E-06	4.14E+05	6.30E-05	3.45	0.7
	1.77E-06	4.14E+05	6.30E-05	9.09	0.7
	2.05E-06	4.14E+05	6.30E-05	8.33	0.7
	2.18E-06	4.14E+05	6.30E-05	7.69	0.7

- X40 fiber, 2.5-inch module

	Flux	TMP	Influent flow	Viscosity	SA
	m^3/s	Pa	(m^3/S)	cP	m^2
Flux vs viscosity study	7.02E-07	1.38E+05	6.30E-05	3.35	1.40
	7.32E-07	1.38E+05	6.30E-05	3.10	1.40
	7.35E-07	1.38E+05	6.30E-05	3.17	1.40
	1.55E-06	2.76E+05	6.30E-05	2.83	1.40
	1.57E-06	2.76E+05	6.30E-05	2.84	1.40
	1.55E-06	2.76E+05	6.30E-05	2.85	1.40
	2.29E-06	4.14E+05	6.30E-05	2.79	1.40
	2.08E-06	4.14E+05	6.30E-05	2.97	1.40
	2.14E-06	4.14E+05	6.30E-05	2.91	1.40
Flux vs TMP study	3.50E-07	6.89E+04	6.30E-05	3.38	1.40
	7.23E-07	1.38E+05	6.30E-05	3.14	1.40
	1.14E-06	2.07E+05	6.30E-05	2.93	1.40
	1.56E-06	2.76E+05	6.30E-05	2.84	1.40
	1.94E-06	3.45E+05	6.30E-05	2.78	1.40
	2.17E-06	4.14E+05	6.30E-05	2.89	1.40
Flux vs influent flow rate study	6.98E-07	1.38E+05	3.15E-05	3.18	1.40
	1.58E-06	2.76E+05	3.15E-05	2.81	1.40
	2.37E-06	4.14E+05	3.15E-05	2.73	1.40
	7.23E-07	1.38E+05	6.30E-05	3.14	1.40
	1.56E-06	2.76E+05	6.30E-05	2.84	1.40
	2.17E-06	4.14E+05	6.30E-05	2.89	1.40
	7.43E-07	1.38E+05	9.45E-05	3.18	1.40
	1.59E-06	2.76E+05	9.45E-05	2.82	1.40
	2.27E-06	4.14E+05	9.45E-05	2.82	1.40

- X50 fiber, 4-inch module

TMP (bar)	0.7	1.4	2.1	2.8	3.4	4.1	Influent flow rate (L/h)
Oil flux x Viscosity (m^3-cP/s-m^2)	4.16E-06	7.42E-06	1.06E-05	1.41E-05	1.73E-05	2.01E-05	680
	-	8.10E-06	-	1.44E-05	-	2.09E-05	1134
	-	9.32E-06	-	1.50E-05	-	2.09E-05	1588

APPENDIX B: OIL-WATER EXPERIMENTAL RAW DATA

- X50 fiber, 2.5-inch module, SA = 1.4 m^2

Flux	Coil	TMP	Viscosity	Influent flow
L/h-m^2	Volume fraction	(bar)	cP	L/h
5.66E+00	7.99E-01	1.38	3.76	226.8
5.56E+00	5.91E-01	1.38	3.73	226.8
5.94E+00	4.05E-01	1.38	3.65	226.8
5.38E+00	2.10E-01	1.38	3.54	226.8
4.83E+00	1.06E-01	1.38	3.50	226.8
3.70E+00	5.00E-02	1.38	3.49	226.8
1.91E+00	2.03E-02	1.38	3.50	226.8
9.63E-01	1.02E-02	1.38	3.53	226.8
5.08E-01	5.02E-03	1.38	3.55	226.8
2.65E-01	2.51E-03	1.38	3.79	226.8
1.10E-01	9.82E-04	1.38	3.86	226.8
5.46E-02	4.72E-04	1.38	3.83	226.8
2.38E-02	1.94E-04	1.38	3.69	226.8
1.38E+01	9.00E-01	2.76	3.75	226.8
1.34E+01	7.92E-01	2.76	3.69	226.8
1.26E+01	5.94E-01	2.76	3.68	226.8
1.24E+01	4.14E-01	2.76	3.61	226.8
1.10E+01	2.08E-01	2.76	3.65	226.8
9.48E+00	1.04E-01	2.76	3.43	226.8
5.60E+00	5.51E-02	2.76	3.62	226.8
1.48E+00	2.18E-02	2.76	3.69	226.8
1.26E+00	1.02E-02	1.38	3.82	226.8
6.31E-01	5.03E-03	1.38	3.69	226.8
3.15E-01	2.43E-03	1.38	3.65	226.8
1.33E-01	1.01E-03	1.38	3.65	226.8
6.96E-02	5.16E-04	1.38	3.66	226.8
2.94E-02	2.01E-04	1.38	3.59	226.8
6.37E+00	4.06E-01	1.38	3.72	226.8
1.99E+00	2.07E-02	1.38	3.69	226.8
1.63E+00	2.33E-02	4.14	3.63	226.8
1.70E+01	4.08E-01	4.14	3.68	226.8
1.16E+01	4.05E-01	2.76	3.58	113.4

7.89E-01	1.94E-02	2.76	3.58	113.4
1.22E+01	3.89E-01	2.76	3.65	340.2
1.84E+00	2.24E-02	2.76	3.52	340.2
1.31E+00	2.04E-02	2.76	3.76	226.8
1.99E+00	2.07E-02	1.38	3.69	226.8
1.26E+00	2.05E-02	4.14	3.48	226.8
1.05E+00	2.05E-02	1.38	3.67	113.4
2.77E+00	1.95E-02	1.38	3.68	340.2
1.54E+00	2.06E-02	2.76	3.55	226.8
1.33E+00	2.00E-02	2.76	3.61	226.8
1.31E+00	2.00E-02	2.76	3.59	226.8
1.36E+00	2.03E-02	2.76	3.64	226.8
2.21E+00	2.01E-02	1.38	3.82	226.8
2.27E+00	2.03E-02	1.38	3.69	226.8
2.29E+00	2.03E-02	1.38	3.58	226.8
1.27E+00	2.03E-02	4.14	3.70	226.8
1.17E+00	2.06E-02	1.38	3.64	113.4
2.65E-02	2.08E-04	1.38	1.54	226.8
3.00E-02	1.97E-04	1.38	11.45	226.8
1.09E+01	2.04E-01	1.38	1.59	226.8
1.68E+00	1.98E-01	1.38	12.06	226.8
1.18E+01	7.92E-01	1.38	1.57	226.8
1.87E+00	7.77E-01	1.38	12.06	226.8
2.17E+00	1.99E-02	0.69	3.70	226.8
2.01E+00	2.04E-02	0.69	3.71	226.8
1.99E+00	2.03E-02	0.69	3.73	226.8

- X50 fiber, 2.5-inch module, SA = 0.7 m^2, C_{oil} = 2%, Influent flow rate = 3.8 L/min

	SA=0.7m2	
TMP (bar)	2.8	1.4
Oil Flux (m^3/s-m^2)	5.39E-07	9.57E-07
Viscosity (cP)	3.7	3.6

- Example of experimental raw data over time :
  Experiment conditions : X50 fiber, 2.5-inch module, SA = 1.4 m^2, C_{oil} = 200 ppmv, Influent flow rate = 3.8 L/min, TMP = 1.4 bar

							Oil in Feed					Oil out of 2.5 inch module				
Influent flow rate	P_{in}	P_{out}	TMP	T°	μ	Time	Initial mass	Final mass	Total mass	Flow rate	C_{oil}	Initial mass	Final mass	Total mass	Flow rate	Oil recovery
gpm	psi	psi	psi	°C	cP	min	g	g	g	ml/ min	%	g	g	g	ml/ min	%
1.0	21.0	19.0	20.0	24.2	3.55	30	10531	10512	19	0.805	0.0213	4	18	14	0.593	%
1.0	21.0	19.0	20.0	23.8	3.58	60	10512	10496	16	0.68	0.0179	18	32	14	0.593	73.7
1.0	21.0	19.0	20.0	23.9	3.57	120	10496	10462	34	0.72	0.0190	32	59	27	0.572	87.5
1.0	21.0	19.0	20.0	23.9	3.57	150	10462	10444	18	0.76	0.0202	59	74	15	0.635	79.4
1.0	21.0	19.0	20.0	23.7	3.59	180	10444	10426	18	0.76	0.0202	74	88	14	0.593	83.3
1.0	21.0	19.0	20.0	23.3	3.62	210	10426	10411	15	0.64	0.0168	88	102	14	0.593	77.8
1.0	21.0	19.0	20.0	23.6	3.59	240	10411	10393	18	0.76	0.0202	102	116	14	0.593	93.3
1.0	21.0	19.0	20.0	23.9	3.57	270	10393	10373	20	0.85	0.0224	116	132	16	0.678	77.8
1.0	21.0	19.0	20.0	23.6	3.59	300	10373	10355	18	0.76	0.0202	132	147	15	0.635	80.0
1.0	21.0	19.0	20.0	23.4	3.61	1282	10355	9797	558	0.72	0.0191	147	625	478	0.618	83.3
1.0	21.0	19.0	20.0	23.6	3.59	1312	9797	9779	18	0.76	0.0200	625	641	16	0.672	85.7
1.0	21.0	19.0	20.0	23.5	3.60	1342	9779	9761	18	0.77	0.0203	641	657	16	0.683	88.9
1.0	21.0	19.0	20.0	23.3	3.62	1624	9761	9590	171	0.77	0.0204	657	806	149	0.671	88.9
1.0	21.0	19.0	20.0	23.6	3.59	1654	9590	9572	18	0.76	0.0202	806	822	16	0.678	87.1
1.0	21.0	19.0	20.0	23.2	3.62	1685	9572	9552	20	0.82	0.0217	822	838	16	0.656	88.9
1.0	21.0	19.0	20.0	23.4	3.61	2719	9552	8938	614	0.75	0.0200	838	1381	543	0.667	80.0
1.0	21.0	19.0	20.0	23.2	3.62	2801	8938	8889	49	0.76	0.0201	1381	1425	44	0.682	88.4
1.0	21.0	19.0	20.0	23.2	3.62	2832	8889	8871	18	0.74	0.0195	1425	1440	15	0.615	89.8
1.0	21.0	19.0	20.0	23.2	3.62	3028	8871	8755	116	0.75	0.0199	1440	1543	103	0.668	83.3
1.0	21.0	19.0	20.0	23.5	3.60	3060	8755	8737	18	0.71	0.0189	1543	1559	16	0.635	88.8
1.0	21.0	19.0	20.0	23.5	3.60	3090	8737	8717	20	0.85	0.0224	1559	1575	16	0.678	88.9
1.0	21.0	19.0	20.0	24.9	3.50	4319	8717	7999	718	0.74	0.0196	1575	2200	625	0.646	80.0
1.0	21.0	19.0	20.0	24.7	3.52	4349	7999	7981	18	0.76	0.0202	2200	2215	15	0.635	87.0
1.0	21.0	19.0	20.0	25	3.49	4379	7981	7963	18	0.76	0.0202	2215	2231	16	0.678	83.3
1.0	21.0	19.0	20.0	25	3.49	4606	7963	7827	136	0.76	0.0201	2231	2349	118	0.660	88.9
1.0	21.0	19.0	20.0	24.9	3.50	4636	7827	7809	18	0.76	0.0202	2349	2365	16	0.678	86.8
1.0	21.0	19.0	20.0	24.5	3.53	4667	7809	7790	19	0.78	0.0206	2365	2381	16	0.656	88.9
1.0	21.0	19.0	20.0	24.3	3.54	5865	7790	7071	719	0.76	0.0202	2381	3012	631	0.669	84.2
1.0	21.0	19.0	20.0	24.3	3.54	5895	7071	7053	18	0.76	0.0202	3012	3028	16	0.678	87.8
1.0	21.0	19.0	20.0	24.6	3.52	5925	7053	7035	18	0.76	0.0202	3028	3045	17	0.720	88.9
1.0	21.0	19.0	20.0	24.5	3.53	6149	7035	6898	137	0.78	0.0206	3045	3166	121	0.686	94.4
1.0	21.0	19.0	20.0	24.8	3.51	6179	6898	6881	17	0.72	0.0190	3166	3182	16	0.676	88.3

1.0	21.0	19.0	20.0	24.6	3.52	6209	6881	6863	18	0.76	0.0202	3182	3198	16	0.679	94.1
1.0	21.0	19.0	20.0	23.8	3.58	7076	6863	6348	515	0.75	0.0200	3198	3659	461	0.675	88.9
1.0	21.0	19.0	20.0	23.6	3.59	7106	6348	6331	17	0.72	0.0190	3659	3675	16	0.678	89.5
1.0	21.0	19.0	20.0	23.9	3.57	7136	6331	6313	18	0.76	0.0202	3675	3691	16	0.678	94.1
1.0	21.0	19.0	20.0	24.3	3.54	7487	6313	6106	207	0.75	0.0198	3691	3879	188	0.680	88.9
1.0	21.0	19.0	20.0	24	3.57	7517	6106	6087	19	0.80	0.0213	3879	3895	16	0.678	90.8
1.0	21.0	19.0	20.0	24.4	3.54	7547	6087	6070	17	0.72	0.0190	3895	3911	16	0.678	84.2
1.0	21.0	19.0	20.0	23.9	3.57	8502	6070	5507	563	0.75	0.0198	3911	4425	514	0.684	94.1
1.0	21.0	19.0	20.0	24.2	3.55	8532	5507	5490	17	0.72	0.0190	4425	4442	17	0.720	91.3
1.0	21.0	19.0	20.0	24.2	3.55	8563	5490	5472	18	0.74	0.0195	4442	4459	17	0.697	100.0
1.0	21.0	19.0	20.0	24.2	3.55	8914	5472	5270	202	0.73	0.0193	4459	4644	185	0.670	94.4
1.0	21.0	19.0	20.0	24	3.57	8944	5270	5250	20	0.85	0.0224	4644	4662	18	0.762	91.6
1.0	21.0	19.0	20.0	24	3.57	8974	5250	5233	17	0.72	0.0190	4662	4678	16	0.678	90.0
1.0	21.0	19.0	20.0	24.2	3.55	9941	5233	4664	569	0.75	0.0198	4678	5211	533	0.700	94.1
1.0	21.0	19.0	20.0	23.8	3.58	9971	4664	4646	18	0.76	0.0202	5211	5227	16	0.678	93.7
1.0	21.0	19.0	20.0	23.1	3.63	10001	4646	4628	18	0.76	0.0202	5227	5244	17	0.720	88.9
1.0	21.0	19.0	20.0	23.2	3.62	10318	4628	4442	186	0.75	0.0197	5244	5423	179	0.717	94.4
1.0	21.0	19.0	20.0	23	3.64	10348	4442	4424	18	0.76	0.0202	5423	5439	16	0.678	96.2
1.0	21.0	19.0	20.0	23.2	3.62	10382	4424	4404	20	0.75	0.0198	5439	5458	19	0.710	88.9
1.0	21.0	19.0	20.0	23.2	3.62	11395	4404	3819	585	0.73	0.0194	5458	6017	559	0.701	95.0
1.0	21.0	19.0	20.0	23.1	3.63	11427	3819	3799	20	0.79	0.0210	6017	6035	18	0.715	95.6
1.0	21.0	19.0	20.0	23.1	3.63	11455	3799	3782	17	0.77	0.0204	6035	6051	16	0.726	90.0
1.0	21.0	19.0	20.0	22.3	3.69	11775	3782	3592	190	0.75	0.0200	6051	6232	181	0.719	94.1
1.0	21.0	19.0	20.0	22.6	3.67	11805	3592	3575	17	0.72	0.0190	6232	6250	18	0.762	95.3
1.0	21.0	19.0	20.0	22.8	3.65	11835	3575	3558	17	0.72	0.0190	6250	6267	17	0.720	105.9
1.0	21.0	19.0	20.0	23	3.64	12769	9462	8891	571	0.78	0.0205	0	528	528	0.718	100.0
1.0	21.0	19.0	20.0	22.9	3.64	12799	8891	8874	17	0.72	0.0190	528	545	17	0.720	92.5
1.0	21.0	19.0	20.0	23.1	3.63	12829	8874	8857	17	0.72	0.0190	545	561	16	0.678	100.0
1.0	21.0	19.0	20.0	22.7	3.66	13230	8857	8623	234	0.74	0.0196	561	785	224	0.710	94.1
1.0	21.0	19.0	20.0	22.8	3.65	13260	8623	8607	16	0.68	0.0179	785	801	16	0.678	95.7
1.0	21.0	19.0	20.0	23	3.64	13293	8607	8586	21	0.81	0.0214	801	820	19	0.731	100.0
1.0	21.0	19.0	20.0	22.9	3.64	14771	8586	7678	908	0.78	0.0206	820	1693	873	0.750	90.5
1.0	21.0	19.0	20.0	22.8	3.65	14801	7678	7660	18	0.76	0.0202	1693	1711	18	0.762	96.1
1.0	21.0	19.0	20.0	23.1	3.63	14832	7660	7642	18	0.74	0.0195	1711	1728	17	0.697	100.0
1.0	21.0	19.0	20.0	23	3.64	15899	7642	6987	655	0.78	0.0206	1728	2357	629	0.749	94.4
1.0	21.0	19.0	20.0	23.2	3.62	15929	6987	6969	18	0.76	0.0202	2357	2374	17	0.720	96.0
1.0	21.0	19.0	20.0	23.1	3.63	15959	6969	6949	20	0.85	0.0224	2374	2393	19	0.805	94.4
1.0	21.0	19.0	20.0	23.1	3.63	16240	6949	6774	175	0.79	0.0209	2393	2562	169	0.764	95.0
1.0	21.0	19.0	20.0	23	3.64	16270	6774	6755	19	0.80	0.0213	2562	2579	17	0.720	96.6

1.0	21.0	19.0	20.0	22.9	3.64	16300	6755	6736	19	0.80	0.0213	2579	2597	18	0.762	89.5
1.0	21.0	19.0	20.0	23.8	3.58	17141	6736	6216	520	0.79	0.0208	2597	3097	500	0.755	94.7
1.0	21.0	19.0	20.0	23.5	3.60	17171	6216	6196	20	0.85	0.0224	3097	3115	18	0.762	96.2
1.0	21.0	19.0	20.0	23.3	3.62	17201	6196	6176	20	0.85	0.0224	3115	3133	18	0.762	90.0

APPENDIX C: DATA ACQUISITION CODE

VBA Time Stamp Code

Used to keep record of time after the start of the experiment and collect data periodically.

```
Option Explicit

Dim DataTimestamp As Date

Sub Worksheet_Calculate()
    Dim CurrentTime As Date, waitTime As Date, CurrentHour As
Single, CurrentMinutes As Single, CurrentSeconds As Single,
DelayInterval As Single


    If Worksheets("Delta V").Range("P2").Value = "True" Then
        CurrentTime = Now()
        If RowNumber = 0 Then
            If CurrentTime >= DataTimestamp + (Worksheets("Delta
V").Range("A2").Value / 86400) Then
                CurrentHour = Hour(CurrentTime)
                CurrentMinutes = Minute(CurrentTime)
                CurrentSeconds = Second(CurrentTime)
                waitTime = TimeSerial(CurrentHour,
CurrentMinutes, CurrentSeconds + 5)
                Application.Wait waitTime
                DataTimestamp = CurrentTime
                Call FillColumns
            End If
        Else
            If CurrentTime >= DataTimestamp + (Worksheets("Delta
V").Range("Q2").Value / 1440) Then
                CurrentHour = Hour(CurrentTime)
                CurrentMinutes = Minute(CurrentTime)
                CurrentSeconds = Second(CurrentTime)
                waitTime = TimeSerial(CurrentHour,
CurrentMinutes, CurrentSeconds + 5)
                Application.Wait waitTime
                DataTimestamp = CurrentTime
                Call FillColumns
            End If
        End If
    Else
        DataTimestamp = CurrentTime
    End If
```

```
End Sub
```

VBA Column Filling Code

Code used to populate the columns of the EXCEL spreadsheet with the raw data displayed by the instruments.

```
Public RowNumber As Integer
Sub FillColumns()

            'Increment row number
            If RowNumber = 0 Then
            RowNumber = 16
            Else: RowNumber = RowNumber + 1
            End If

        'MsgBox "RowNumber is " & RowNumber


            If RowNumber = 16 Then

 ' Flow Rate column fill up
Worksheets("Data calc").Cells(RowNumber + 1, 1).Value =
Worksheets("Delta V").Range("B2").Value

' P1 column fill up
Worksheets("Data calc").Cells(RowNumber + 1, 2).Value =
Worksheets("Delta V").Range("C2").Value

' P2 column fill up
Worksheets("Data calc").Cells(RowNumber + 1, 3).Value =
Worksheets("Delta V").Range("D2").Value

' DP1 column fill up
Worksheets("Data calc").Cells(RowNumber + 1, 5).Value =
Worksheets("Delta V").Range("E2").Value

' P2' column fill up
Worksheets("Data calc").Cells(RowNumber + 1, 22).Value =
Worksheets("Delta V").Range("F2").Value

 'P3 column fill up
Worksheets("Data calc").Cells(RowNumber + 1, 23).Value =
Worksheets("Delta V").Range("G2").Value

'DP2 column fill up
Worksheets("Data calc").Cells(RowNumber + 1, 25).Value =
```

```
Worksheets("Delta V").Range("H2").Value

'P3' column fill up
Worksheets("Data calc").Cells(RowNumber + 1, 31).Value =
Worksheets("Delta V").Range("I2").Value

'P4 column fill up
Worksheets("Data calc").Cells(RowNumber + 1, 32).Value =
Worksheets("Delta V").Range("J2").Value

' Temperature column fill up
Worksheets("Data calc").Cells(RowNumber + 1, 6).Value =
Worksheets("Delta V").Range("K2").Value

' Pump feed Mass column fill up
Worksheets("Data calc").Cells(RowNumber + 1, 12).Value =
Worksheets("Delta V").Range("L2").Value

' Membrane 1 Mass column fill up
Worksheets("Data calc").Cells(RowNumber + 1, 17).Value =
Worksheets("Delta V").Range("M2").Value

' Membrane 2 Mass column fill up
Worksheets("Data calc").Cells(RowNumber + 1, 26).Value =
Worksheets("Delta V").Range("N2").Value

'Membrane 3 Mass column fill up
Worksheets("Data calc").Cells(RowNumber + 1, 34).Value =
Worksheets("Delta V").Range("O2").Value

'Sampling time fill up
Worksheets("Data calc").Cells(RowNumber + 1, 9).Value =
Worksheets("Delta V").Range("Q2").Value

           Else

' Flow Rate column fill up
Worksheets("Data calc").Cells(RowNumber, 1).Value =
Worksheets("Delta V").Range("B2").Value

' P1 column fill up
Worksheets("Data calc").Cells(RowNumber, 2).Value =
Worksheets("Delta V").Range("C2").Value

' P2 column fill up
Worksheets("Data calc").Cells(RowNumber, 3).Value =
Worksheets("Delta V").Range("D2").Value

' DP1 column fill up
Worksheets("Data calc").Cells(RowNumber, 5).Value =
```

```
Worksheets("Delta V").Range("E2").Value

' P2' column fill up
Worksheets("Data calc").Cells(RowNumber, 22).Value =
Worksheets("Delta V").Range("F2").Value

'P3 column fill up

Worksheets("Data calc").Cells(RowNumber, 23).Value =
Worksheets("Delta V").Range("G2").Value

'DP2 column fill up
Worksheets("Data calc").Cells(RowNumber, 25).Value =
Worksheets("Delta V").Range("H2").Value

'P3' column fill up
Worksheets("Data calc").Cells(RowNumber, 31).Value =
Worksheets("Delta V").Range("I2").Value

'P4 column fill up
Worksheets("Data calc").Cells(RowNumber, 32).Value =
Worksheets("Delta V").Range("J2").Value

' Temperature column fill up
Worksheets("Data calc").Cells(RowNumber, 7).Value =
Worksheets("Delta V").Range("K2").Value

' Pump feed Mass column fill up
Worksheets("Data calc").Cells(RowNumber, 13).Value =
Worksheets("Delta V").Range("L2").Value

' Membrane 1 Mass column fill up
Worksheets("Data calc").Cells(RowNumber, 18).Value =
Worksheets("Delta V").Range("M2").Value

' Membrane 2 Mass column fill up
Worksheets("Data calc").Cells(RowNumber, 27).Value =
Worksheets("Delta V").Range("N2").Value

'Membrane 3 Mass column fill up
Worksheets("Data calc").Cells(RowNumber, 35).Value =
Worksheets("Delta V").Range("O2").Value

'Sampling time fill up
Worksheets("Data calc").Cells(RowNumber, 9).Value =
Worksheets("Delta V").Range("Q2").Value

ActiveWorkbook.Save

                End If
```

```
End Sub
```

VBA Cell Clearing Code

Code used to clear cells before the start of a new experiment and reset the variables for the previous codes to populate the table at the right row number.

```
Sub Clearcells()
' Clearcells Macro

Range("A17:C652,E17:G652,I17:I652,L17,M17:M652,Q17,R17:R652,V17:W
652,Y17:Y652,Z17,AA17:AA652,AE17:AF652,AH17,AI17:AI652").ClearCon
tents
    RowNumber = 0

      End Sub
```

OPC Code to Import Weight Readings from Scale to Computer

```
using System;
using System.Collections.Generic;
using System.Linq;
using System.Text;
using OPCDotNetAutomation;
using System.Configuration;
using System.IO.Ports;
using System.Threading;
using System.Text.RegularExpressions;

namespace SerialToOPC
{
    public class Weighscale
    {
        private string ComPort { get; set; }
        private string OPCTag { get; set; }

        public Weighscale(string comPort = "COM1", string opcTag = "tag")
        {
            ComPort = comPort;
            OPCTag = opcTag;
        }

        // This method that will be called when the thread is started
        public void testScale()
        {
            while (true)
            {
                DateTime now = DateTime.Now;
                Console.WriteLine("Weighscale {0} is writing to {1} at: {2}",
ComPort, OPCTag, now);
                Thread.Sleep(2000);
            }
        }
```

```
        public void readScale()
        {
            var ports = SerialPort.GetPortNames();
            Console.WriteLine("Available Ports - {0}", String.Join(",", ports));

            OPCServer server = new OPCServer();
            string opcServer = ConfigurationManager.AppSettings["OPC.Server"];
            //string opcTag = ConfigurationManager.AppSettings["OPC.Tag"];
            string portName = ConfigurationManager.AppSettings["Port.Name"];
            string portSpeed = ConfigurationManager.AppSettings["Port.Speed"];
            string regEx = ConfigurationManager.AppSettings["RegEx"];
            int speed = 9600;
            Int32.TryParse(portSpeed, out speed);
            Console.WriteLine("OPC.Server = {0}, OPC.Tag = {1}", opcServer,
OPCTag);
            Console.WriteLine("Port.Name = {0}, Port.Speed = {1}", portName,
speed);
            Console.WriteLine("RegEx = {0}", regEx);
            //Regex re = new Regex(regEx);
            //Read -0.012 lb
            Regex re = new Regex(@"[-+ ]?[0-9]*\.[0-9]?");
            server.Connect(opcServer);
            OPCGroup group = server.OPCGroups.Add("SerialWriter");
            //            group.UpdateRate = 5000;
            group.UpdateRate = 500;
            OPCItem item = group.OPCItems.AddItem(OPCTag, 1);
            OPCItem item2 = group.OPCItems.AddItem("WS101_HB/INITIALIZATION.CV",
2);

            // should be com ports 5, 6, 7, 8
            var sport = new SerialPort(ComPort, 9600, Parity.None);
            sport.Open();
            sport.DtrEnable = true;
            float oldF = 0;
            while (true)
            {
                //float initialization = item2.Value;
                //Console.WriteLine("WS101_HB/INITIALIZATION.CV: {0}",
initialization);

                int count = sport.BytesToRead;
                //Console.WriteLine("Count= {0}", count);
                if (count > 0)
                {
                    string message = sport.ReadLine();
                    var matches = re.Matches(message);
                    Console.WriteLine("Read {0}", message);

                    if (matches.Count > 0)
                    {
                        string val = matches[0].Value;
//                        string val = matches[0];
//                        string val = match.Groups[1].Value;
                        float fVal = 0;
                        if (float.TryParse(val, out fVal))
                        {
                            if (fVal != oldF)
                            {
```

```
                                Console.WriteLine("Weigh Scale: {0}   {1}   {2}",
fVal, ComPort, OPCTag);
                                oldF = fVal;
                                item.Write(fVal);
                            }
                            //Console.WriteLine("Write {0}", fVal);
                        }
                        else
                        {
                            Console.WriteLine("Couldn't parse {0}", val);
                        }
                    }
                }
            }
        }
    };

    class Program
    {
        static void Main(string[] args)
        {
            Console.WriteLine("Weighscale reader starting up...");

            //Weighscale weighScale1 = new Weighscale("COM3",
"WS101_HB/NET_WT.CV");
            //Weighscale weighScale2 = new Weighscale("COM4",
"WS102_HB/NET_WT.CV");
            //Weighscale weighScale3 = new Weighscale("COM5",
"WS103_HB/NET_WT.CV");
            //Weighscale weighScale4 = new Weighscale("COM6",
"WS104_HB/NET_WT.CV");

            Weighscale weighScale1 = new Weighscale("COM3", "HI-BAY-TEST/W1.CV");
            Weighscale weighScale2 = new Weighscale("COM4", "HI-BAY-TEST/W2.CV");
            Weighscale weighScale3 = new Weighscale("COM5", "HI-BAY-TEST/W3.CV");
            Weighscale weighScale4 = new Weighscale("COM6", "HI-BAY-TEST/W4.CV");

            // Create the thread object, passing in the readScale method
            // via a ThreadStart delegate. This does not start the thread.
            //Thread w1Thread = new Thread(new
ThreadStart(weighScale1.testScale));
            //Thread w2Thread = new Thread(new
ThreadStart(weighScale2.testScale));
            //Thread w3Thread = new Thread(new
ThreadStart(weighScale3.testScale));
            //Thread w4Thread = new Thread(new
ThreadStart(weighScale4.testScale));

            Thread w1Thread = new Thread(new ThreadStart(weighScale1.readScale));
            Thread w2Thread = new Thread(new ThreadStart(weighScale2.readScale));
            Thread w3Thread = new Thread(new ThreadStart(weighScale3.readScale));
            Thread w4Thread = new Thread(new ThreadStart(weighScale4.readScale));

            // Start the thread
            w1Thread.Start();
            w2Thread.Start();
            w3Thread.Start();
            w4Thread.Start();
```

```
            // Spin for a while waiting for the started thread to become
            // alive:
            while ((!w1Thread.IsAlive) || (!w2Thread.IsAlive) ||
(!w3Thread.IsAlive) || (!w4Thread.IsAlive)) ;

            // Wait for a user input to stop the thread
            Console.ReadLine();

            // Request that oThread be stopped
            w1Thread.Abort();
            w2Thread.Abort();
            w3Thread.Abort();
            w4Thread.Abort();

            Console.WriteLine("Threads shutting down...");

            // Wait until threads have finished.
            w1Thread.Join();
            w2Thread.Join();
            w3Thread.Join();
            w4Thread.Join();

            Console.WriteLine("Weighscale reader shutdown");

        }
    }
}
```

References

1. C. Clark, J. Veil, "Produced water volumes and management practices in the United States," (Argonne National Laboratory (ANL), 2009).
2. S. Adham, paper presented at the AWWA/AMTA Membrane Technology conference and exposition, San Antonio, 2013.
3. A. F. Sayda, J. H. Taylor, in *American Control Conference, 2007. ACC '07.* (2007), pp. 4847-4853.
4. F. T. Tao *et al.*, 1993 1993.
5. R. Funston, R. Ganesh, L. Y. Leong, in *Ground Water Protection Council (GWPC) Meeting*. (2002).
6. G. F. Doran, F. H. Carini, D. A. Fruth, J. A. Drago, L. Y. C. Leong, 1997/1/1/ 1997.
7. P. Kipp, F. Seibert, R. Connelly. (US Patent 2012/0184759 A1. Non-Dispersive Process for Insoluble Oil Recovery From Aqueous Slurries, 2012).
8. M. K. Konishi, M.; Tamesui, N.; Omasa, T.; Shioya, S.; Ohtake, H., The separation of oil from an oil-water-bacteria mixture using a hydrophobic tubular membrane. *Biochemical Engineering Journal* **24**, 49-54 (2005).
9. M. Stewart, K. Arnold, *Produced water treatment field manual*. (Gulf Professional Publishing, 2011).
10. T. Frising, C. Noïk, C. Dalmazzone, The Liquid/Liquid Sedimentation Process: From Droplet Coalescence to Technologically Enhanced Water/Oil Emulsion Gravity Separators: A Review. *Journal of Dispersion Science & Technology* **27**, 1035-1057 (2006).
11. A. Cambiella *et al.*, Treatment of oil-in-water emulsions: Performance of a sawdust bed filter. *Journal of Hazardous Materials* **131**, 195-199 (2006).
12. J. Li, Y. Gu, Coalescence of oil-in-water emulsions in fibrous and granular beds. *Separation and Purification Technology* **42**, 1-13 (2005).
13. M. G. Hajra, K. Mehta, G. G. Chase, Effects of humidity, temperature, and nanofibers on drop coalescence in glass fiber media. *Separation and Purification Technology* **30**, 79-88 (2003).
14. C. Shin, G. G. Chase, The effect of wettability on drop attachment to glass rods. *J. Colloid Interface Sci.* **272**, 186-190 (2004).
15. F. Wiesler, How to Meet Today's Dissolved Oxygen Specifications with Degasification Membranes. *Ultrapure Water* **20**, 38-46 (2003).
16. P. Kipp *et al.* (US Patent 2012/0208247 A1. Non-Dispersive Process for Insoluble Oil Recovery from Aqueous Slurries, 2011).
17. F. Seibert, M. Poenie. (Google Patents, 2013).
18. P. B. Kipp, F. Seibert, R. Connelly. (Google Patents, 2013).
19. P. B. Kipp *et al.* (Google Patents, 2013).
20. F. Seibert, paper presented at the 2011 Annual AIChE Conference, Minneapolis, MN, Oct. 18 2011 2011.
21. U. EPA.
22. U. EPA.

23. J. G. Coca, G.; Benito, J. M., in *Water Purification and Management,* J. G. CocaPrados, G., Ed. (Springer, Dordrecht, 2011), pp. 1-55.
24. F. l.-R. Ahmadun *et al*., Review of technologies for oil and gas produced water treatment. *Journal of Hazardous Materials* **170**, 530-551 (2009).
25. J. P. Ray, F. R. Engelhardt. (Plenum Press, New York), vol. 46;46.;.
26. *A White Paper Describing Produced Water from Production of Crude Oil, Natural Gas and Coal Bed Methane* (2004 http://www.netl.doe.gov/publications/oil pubs/prodwaterpaper.pdf).
27. P. H. H. Duong, T. S. Chung, Application of thin film composite membranes with forward osmosis technology for the separation of emulsified oil-water. *Journal of Membrane Science* **452**, 117-126 (2014).
28. W. X. Kang, Bin; Wang, Yongjian; Li, Yuan; Shan, Xiuhua; An, Faquan; Liu, Jiaheng, Stability mechanism of W/O crude oil emulsion stabilized by polymer and surfactant. *Colloids and Surfaces A: Physicochemical and Engineering Aspects* **384**, 555-560 (2011).
29. T. E. Schultz, Get the most out of API separators. *Chemical Engineering*, (2005).
30. G. G. Aymong. (Google Patents, 1988), chap. a.
31. M. B. Schmit, R. T. McTighe. (Google Patents, 1989).
32. A. Cambiella, J. M. Benito, C. Pazos, J. Coca, Centrifugal Separation Efficiency in the Treatment of Waste Emulsified Oils. *Chemical Engineering Research and Design* **84**, 69-76 (2006).
33. G. R. Jackson. (Google Patents, 1994).
34. N. J. Miller. (Google Patents, 1992).
35. S. Amini, D. Mowla, M. Golkar, F. Esmaeilzadeh, Mathematical modelling of a hydrocyclone for the down-hole oil-water separation (DOWS). *Chemical Engineering Research and Design* **90**, 2186-2195 (2012).
36. W. S. Ltd, Oil/water separation: A centrifugal solution for troublesome oil. *Filtration & Separation* **46**, 42-43 (2009).
37. G. A. B. Young, W. D. Wakley, D. L. Taggart, S. L. Andrews, J. R. Worrell, Oil-water separation using hydrocyclones: An experimental search for optimum dimensions. *Journal of Petroleum Science and Engineering* **11**, 37-50 (1994).
38. R. Mastouri, S. M. Borghei, F. Nadim, E. Roayaei, The Effect of Temperature and Impeller Speed on Mechanically Induced Gas Flotation (IGF) Performance in Separation of Oil from Oilfield-Produced Water. *Pet. Sci. Technol.* **28**, 1415-1426 (2010).
39. A. A. Al-Shamrani, A. James, H. Xiao, Separation of oil from water by dissolved air flotation. *Colloids and Surfaces A: Physicochemical and Engineering Aspects* **209**, 15-26 (2002).
40. D. Feng, C. Aldrich, Removal of diesel from aqueous emulsions by flotation. *Sep. Sci. Technol.* **35**, 2159-2172 (2000).
41. G. N. V. Mathavan, T., Coalescence Filtration Of An Oil-In-Water Emulsion In A Peat Bed. *Water Res.* **26**, 91-98 (1992).
42. A. L. Ahmad, S. Sumathi, B. H. Hameed, Residual oil and suspended solid removal using natural adsorbents chitosan, bentonite and activated carbon: A comparative study. *Chemical Engineering Journal* **108**, 179-185 (2005).

43. S. E. Weschenfelder, A. C. C. Mello, C. P. Borges, J. C. Campos, Oilfield produced water treatment by ceramic membranes: Preliminary process cost estimation. *Desalination* **360**, 81-86 (2015).
44. S. Judd *et al*., The size and performance of offshore produced water oil-removal technologies for reinjection. *Separation and Purification Technology* **134**, 241-246 (2014).
45. S. W. Mondal, S. Ranil, Produced water treatment by nanofiltration and reverse osmosis membranes. *Journal of Membrane Science* **322**, 162-170 (2008).
46. E. N. Tummons, V. V. Tarabara, J. W. Chew, A. G. Fane, Behavior of oil droplets at the membrane surface during crossflow microfiltration of oil-water emulsions. *Journal of Membrane Science* **500**, 211-224 (2016).
47. V. Singh, M. K. Purkait, C. Das, Cross-Flow Microfiltration of Industrial Oily Wastewater: Experimental and Theoretical Consideration. *Sep. Sci. Technol.* **46**, 1213-1223 (2011).
48. T. Darvishzadeh, N. V. Priezjev, Effects of crossflow velocity and transmembrane pressure on microfiltration of oil-in-water emulsions. *Journal of Membrane Science* **423–424**, 468-476 (2012).
49. D. Vasanth, G. Pugazhenthi, R. Uppaluri, Performance of Low Cost Ceramic Microfiltration Membranes for the Treatment of Oil-in-water Emulsions. *Sep. Sci. Technol.* **48**, 849-858 (2013).
50. K. Masoudnia, A. Raisi, A. Aroujalian, M. Fathizadeh, Treatment of Oily Wastewaters Using the Microfiltration Process: Effect of Operating Parameters and Membrane Fouling Study. *Sep. Sci. Technol.* **48**, 1544-1555 (2013).
51. B. S. Hu, K., Microfiltration of water in oil emulsions and evaluation of fouling mechanism. *Chemical Engineering Journal* **136**, 210-220 (2008).
52. J. K. Milic, I. Petrinic, A. Gorsek, M. Simonic, Ultrafiltration of oil-in-water emulsion by using ceramic membrane: Taguchi experimental design approach. *Central European Journal of Chemistry* **12**, 242-249 (2014).
53. X. S. Y. Yi, S. L.; Shi, W. X.; Sun, N.; Jin, L. M.; Wang, S.; Zhang, B.; Ma, C.; Sun, L. P., The influence of important factors on ultrafiltration of oil/water emulsion using PVDF membrane modified by nano-sized TiO2/Al2O3. *Desalination* **281**, 179-184 (2011).
54. A. A. Salahi, Mohsen; Mohammadi, Toraj, Permeate flux decline during UF of oily wastewater: Experimental and modeling. *Desalination* **251**, 153-160 (2010).
55. Y. Liu, Y. Su, Y. Li, X. Zhao, Z. Jiang, Improved antifouling property of PVDF membranes by incorporating an amphiphilic block-like copolymer for oil/water emulsion separation. *RSC Advances* **5**, 21349-21359 (2015).
56. A. G. Ezzati, Elham; Mohammadi, Toraj, Separation of water in oil emulsions using microfiltration. *Desalination* **185**, 371-382 (2005).
57. K. J. Scott, R. J.; Hall, D., Crossflow microfiltration of water-in-oil emulsions using corrugated membranes. *Separation and Purification Technology* **22-3**, 431-441 (2001).
58. L. Wu, J. P. Zhang, B. C. Li, A. Q. Wang, Mechanical- and oil-durable superhydrophobic polyester materials for selective oil absorption and oil/water separation. *J. Colloid Interface Sci.* **413**, 112-117 (2014).

59. N. P. R. Tirmizi, Bhavani; Wiencek, John, Demulsification of water/oil/solid emulsions by hollow-fiber membranes. *Aiche J.* **42**, 1263-1276 (1996).
60. S. N. Hoffmann, W., Membrane Coalescence for Phase Separation of Oil-in-Water Emulsions Stabilized by Surfactants and Dispersed into Smallest Droplets. *Chemical Engineering & Technology* **24**, 22-27 (2001).
61. J. C. Mueller, Yanwei; Davis, Robert H., Crossflow microfiltration of oily water. *Journal of Membrane Science* **129**, 221-235 (1997).
62. S. S. Madaeni, M. K. Yeganeh, Microfiltration of Emulsified Oil Wastewater. *Journal of Porous Materials* **10**, 131-138 (2003).
63. B. Chakrabarty, A. K. Ghoshal, M. K. Purkait, Ultrafiltration of stable oil-in-water emulsion by polysulfone membrane. *Journal of Membrane Science* **325**, 427-437 (2008).
64. kozzini *et al.*, Membrane technology enhancement in oil–water separation. A review. *Desalination* **357**, 197-207 (2015).
65. S. R. H. S. Abadi, Mohammad Reza; Hemati, Mahmood; Rekabdar, Fatemeh; Mohammadi, Toraj, Ceramic membrane performance in microfiltration of oily wastewater. *Desalination* **265**, 222-228 (2011).
66. Q. Huang, H. G. Gomaa, N. Hashem, Flux Characteristics of Oil Separation from O/W Emulsions using Highly Hydrophilic UF Membrane in Narrow Channel. *Sep. Sci. Technol.* **49**, 12-21 (2014).
67. Y. Zhu, D. Wang, L. Jiang, J. Jin, Recent progress in developing advanced membranes for emulsified oil/water separation. *NPG Asia Mater* **6**, e101 (2014).
68. D. J. Miller, S. Kasemset, L. Wang, D. R. Paul, B. D. Freeman, Constant flux crossflow filtration evaluation of surface-modified fouling-resistant membranes. *Journal of Membrane Science* **452**, 171-183 (2014).
69. P. J. Srijaroonrat, E.; Aurelle, Y., Unstable secondary oil/water emulsion treatment using ultrafiltration: fouling control by backflushing. *Journal of Membrane Science* **159**, 11-20 (1999).
70. K. T. S. Tompkins, Jerome S;Owsenek, Brian L;Tomlinson, Lawrence W;Gavin, Joseph A. (Google Patents, 1999).
71. R. G. Holdich, I. W. Cumming, I. D. Smith, Crossflow microfiltration of oil in water dispersions using surface filtration with imposed fluid rotation. *Journal of Membrane Science* **143**, 263-274 (1998).
72. A. Ullah, R. G. Holdich, M. Naeem, V. M. Starov, Shear enhanced microfiltration and rejection of crude oil drops through a slotted pore membrane including migration velocities. *Journal of Membrane Science* **421,Äì422**, 69-74 (2012).
73. M. Y. Jaffrin, Dynamic shear-enhanced membrane filtration: A review of rotating disks, rotating membranes and vibrating systems. *Journal of Membrane Science* **324**, 7-25 (2008).
74. W. B. Zhang *et al.*, Superhydrophobic and Superoleophilic PVDF Membranes for Effective Separation of Water-in-Oil Emulsions with High Flux. *Adv. Mater.* **25**, 2071-2076 (2013).
75. I. W. Cumming, R. G. Holdich, I. D. Smith, The rejection of oil by microfiltration of a stabilised kerosene/water emulsion. *Journal of Membrane Science* **169**, 147-155 (2000).

76. F. F. Nazzal, M. R. Wiesner, Microfiltration of oil-in-water emulsions. *Water Environment Research* **68**, 1187-1191 (1996).
77. T. P. Darvishzadeh, Nikolai V., Effects of crossflow velocity and transmembrane pressure on microfiltration of oil-in-water emulsions. *Journal of Membrane Science* **423,Äì424**, 468-476 (2012).
78. R. H. Davis, Modeling of Fouling of Crossflow Microfiltration Membranes. *Separation & Purification Reviews* **21**, 75-126 (1992).
79. E. S. Gorouhi, Mohtada; Mohammadi, Toraj, Microfiltration of oily wastewater using PP hydrophobic membrane. *Desalination* **200**, 319-321 (2006).
80. H. S. Unno, H.; Akehata, T., Oil Separation From Oil-Water Mixture By A Porous Poly(Tetrafluoroethylene) (PTFE) Membrane. *J. Chem. Eng. Jpn.* **19**, 281-286 (1986).
81. K. F. Ueyama, K.; Furusaki, S., Oil-Phase Permeation Behavior Of O/W Emulsion Through A Porous Polytetrafluoroethylene Membrane. *J. Chem. Eng. Jpn.* **20**, 618-622 (1987).
82. D. Z. D. Sun, X. D.; Li, W. X.; Zhou, D., Demulsification of water-in-oil emulsion by using porous glass membrane. *Journal of Membrane Science* **146**, 65-72 (1998).
83. N. M. T. Kocherginsky, C. L.; Lu, W. F., Demulsification of water-in-oil emulsions via filtration through a hydrophilic polymer membrane. *Journal of Membrane Science* **220**, 117-128 (2003).
84. M. Kukizaki, M. Goto, Demulsification of water-in-oil emulsions by permeation through Shirasu-porous-glass (SPG) membranes. *Journal of Membrane Science* **322**, 196-203 (2008).
85. J. Fukushima *et al.*, Possibility of coalescence of water droplets in W/O emulsions by means of surface processes. *Colloids and Surfaces A: Physicochemical and Engineering Aspects* **333**, 53-58 (2009).
86. T. B. Kawakatsu, R. M.; Nabetani, H.; Kikuchi, Y.; Nakajima, M., Emulsion breakdown: Mechanisms and development of multilayer membrane. *Aiche J.* **45**, 967-975 (1999).
87. U. N. Daiminger, W.; Plucinski, P.; Hoffmann, S., Novel Techniques for Oil-Water Separation *Journal of Membrane Science* **99**, 197-203 (1995).
88. M. Hlavacek, Break-Up Of Oil-In-Water Emulsions Induced By Permeation Through A Microfiltration Membrane. *Journal of Membrane Science* **102**, 1-7 (1995).
89. A. F. Hong, A. G.; Burford, R., Factors affecting membrane coalescence of stable oil-in-water emulsions. *Journal of Membrane Science* **222**, 19-39 (2003).
90. F. Seibert, X. Py, M. Mshewa, J. R. Fair, Hydraulics And Mass-Transfer Efficiency Of A Commercial-Scale Membrane Extractor. *Sep. Sci. Technol.* **28**, 343-359 (1993).
91. C. J. Seeton, Viscosity–temperature correlation for liquids. *Tribology Letters* **22**, 67-78 (2006).
92. F. T. Tao *et al.*, paper presented at the SPE/EPA Exploration and Production Environmental Conference, San Antonio, 1993.
93. A. Hussain, J. Minier-Matar, S. Gharfeh, A. Janson, S. Adham, 2014/3/25/.

94. A. Amelio *et al*., Purification of biodiesel using a membrane contactor: Liquid-liquid extraction. *Fuel Processing Technology* **142**, 352-360 (2016).
95. R. Nagel, T. Will, Membrane processes for water treatment in the semiconductor industry. *Ultrapure Water* **16**, 35-41 (1999).
96. M. Cheryan, I. NetLibrary, *Ultrafiltration and microfiltration handbook*. (Technomic Pub. Co, Lancaster, Pa, 1998).
97. I. F. Macdonald, M. S. El-Sayed, K. Mow, F. A. L. Dullien, Flow through Porous Media-the Ergun Equation Revisited. *Industrial & Engineering Chemistry Fundamentals* **18**, 199-208 (1979).
98. H. E. Pacella, H. J. Eash, W. J. Federspiel, Darcy Permeability of Hollow Fiber Bundles Used in Blood Oxygenation Devices. *Journal of membrane science* **382**, 238-242 (2011).
99. L. K. Wang, J. P. Chen, Y.-T. Hung, N. K. Shammas, *Membrane and desalination technologies*. (Springer, 2011).
100. S. P. Madhani, B. D. D'Aloiso, B. Frankowski, W. J. Federspiel, Darcy permeability of hollow fiber membrane bundles made from Membrana(R) Polymethylpentene (PMP) fibers used in respiratory assist devices. *ASAIO journal (American Society for Artificial Internal Organs : 1992)*, (2016).
101. S. F. Chang, A. G.; Waite, T. D.; Yeo, A., Unstable filtration behavior with submerged hollow fiber membranes. *Journal of Membrane Science* **308**, 107-114 (2008).
102. D.-Q. Cao, E. Iritani, N. Katagiri, Properties of Filter Cake Formed during Dead-End Microfiltration of O/W Emulsion. *J. Chem. Eng. Jpn.* **46**, 593-600 (2013).
103. X. L. Xu, Jianxin; Xu, Nini; Hou, Yanlin; Lin, Jiebin, Visualization of fouling and diffusion behaviors during hollow fiber microfiltration of oily wastewater by ultrasonic reflectometry and wavelet analysis. *Journal of Membrane Science* **341**, 195-202 (2009).
104. S. C. Yao, M.; Fane, A. G.; Pope, J. M., Non-invasive observation of flow profiles and polarisation layers in hollow fibre membrane filtration modules using NMR micro-imaging. *Journal of Membrane Science* **99**, 207-216 (1995).
105. X. A. Chen, H. F. Lu, W. Jiang, L. Y. Chu, B. Liang, De-emulsification of Kerosene/Water Emulsions with Plate-Type Microchannels. *Industrial & Engineering Chemistry Research* **49**, 9279-9288 (2010).
106. D. A. V. J. Masciola, Roger C.; Reed, Brian E., Tubular ultrafiltration flux prediction for oil-in-water emulsions: analysis of series resistances. *Journal of Membrane Science* **184**, 197-208 (2001).
107. J. Marchese, N. A. Ochoa, C. Pagliero, C. Almandoz, Pilot-scale ultrafiltration of an emulsified oil wastewater. *Environmental Science & Technology* **34**, 2990-2996 (2000).
108. Liqui-Cel, 3M, Membrana. (http://www.liquicel.com/product-information/data-sheets.cfm).
109. X. Y. Zhu, W. T. Tu, K. H. Wee, R. B. Bai, Effective and low fouling oil/water separation by a novel hollow fiber membrane with both hydrophilic and oleophobic surface properties. *Journal of Membrane Science* **466**, 36-44 (2014).

110. H. S. Shokrkar, A.; Kasiri, N.; Mohammadi, T., Prediction of permeation flux decline during MF of oily wastewater using genetic programming. *Chemical Engineering Research and Design* **90**, 846-853 (2012).
111. A. Ullah, R. G. Holdich, M. Naeem, V. M. Starov, Stability and deformation of oil droplets during microfiltration on a slotted pore membrane. *Journal of Membrane Science* **401,Äì402**, 118-124 (2012).
112. C. Wang, M. Perry, F. Seibert, G. Rochelle, Packing Characterization for Post Combustion CO2 Capture: Mass Transfer Model Development. *Energy Procedia* **63**, 1727-1744 (2014).
113. M. DuBois, K. A. Gilles, J. K. Hamilton, P. A. Rebers, F. Smith, Colorimetric Method for Determination of Sugars and Related Substances. *Anal. Chem.* **28**, 350-356 (1956).
114. T. Masuko *et al.*, Carbohydrate analysis by a phenol-sulfuric acid method in microplate format. *Analytical biochemistry* **339**, 69-72 (2005).
115. R. S. Rengasamy, D. Das, C. P. Karan, Study of oil sorption behavior of filled and structured fiber assemblies made from polypropylene, kapok and milkweed fibers. *Journal of Hazardous Materials* **186**, 526-532 (2011).
116. S. Y. Chang, Adrian; Fane, Anthony; Cholewa, Marian; Ping, Yang; Moser, Herbert, Observation of flow characteristics in a hollow fiber lumen using non-invasive X-ray microimaging (XMI). *Journal of Membrane Science* **304**, 181-189 (2007).

Permanent email: aurore.mercelat@gmail.com

This dissertation was typed by Aurore Yvonne Joelle Mercelat.